筑　波　大　学

博 士 （医 学） 学 位 論 文

Immune Regulation by Transforming Growth Factor-β Superfamily Cytokines

(TGF-β スーパーファミリーサイトカインによる免疫系制御)

２０１６

筑波大学

尹　晶煥

Table of Contents

I. Introduction ---------- 2

II. Phosphorylation status determines the opposing functions of ---------- 9
Smad2/Smad3 as STAT3 cofactors in Th17 differentiation
（リン酸化状態が STAT3 転写共役因子としての Smad2/Smad3 相反作用を規定する）

Materials and Methods ---------- 10

Results ---------- 17

Summary ---------- 52

Discussion ---------- 53

III. Activin receptor-like kinase5 inhibition suppresses mouse ------ 56
melanoma by ubiquitin degradation of Smad4, thereby derepressing
eomesodermin in cytotoxic T lymphocytes
(TGF-β I 型受容体阻害は、細胞障害性 T リンパ球に発現する Smad4 ユビキチン分解による eomesodermin 抑制解除を誘導しマウス悪性黒色腫を抑制する)

Materials and Methods ---------- 57

Results ---------- 63

Summary ---------- 94

Discussion ---------- 95

IV. Conclusion ---------- 98

V. References ---------- 99

Introduction

1. TGF-β superfamily cytokines and signal transduction pathways

Transforming growth factor-β (TGF-β) superfamily cytokines are the evolutionary conserved pleiotropic secreted cytokines, which consist of TGF-β, Activins, Nodals, Bone Morphogenetic Protein (BMP), Myostatins, Growth and Differentiation Factors (GDF), Anti-Muellerian Hormones (AMH) and others (over 30 members) (Massague J et al, 2005). Individual family cytokines have crucial roles in multiple processes throughout development and in the maintenance of tissue homeostasis. Subversion of signaling by TGF-β superfamily members has been implicated in many human diseases, including cancer, fibrosis, inflammation, autoimmune and vascular diseases (Dijke P et al. 2007). Among them, TGF-β is produced from many kinds of cells, tissues and organs, and plays important roles in regulating cell proliferation, differentiation, homeostasis and death (Massague J et al, 2012).

The active form of TGF-β initiates its signal transduction by binding to specific serine/threonine kinase transmembrane type I and type II receptors (Heldin CH et al, 2012; Massague J et al, 2003). Upon ligand-induced heteromeric complex formation, the TGF-β type II receptor transphosphorylates and activates TGF-β type I receptor (Activin receptor-like kinase (ALK)5). Activated TGF-β type I receptor phosphorylates TGF-β-specific receptor regulated SMAD (R-Smad): Smad2 and Smad3 at the C-terminal two serine residues of Mad homology (MH)-2 domain. Activated Smad2 and Smad3 form heteromeric complexes with common-mediator SMAD: Smad4 to regulate transcription of the target genes (Massague J et al, 2005; Heldin CH et al, 2012). Besides SMAD pathway, various kinds of protein kinases mediate non-SMAD pathway. TGF-β type I receptor phosphorylates various protein kinases including phosphoinositide 3 kinase (PI3K), mitogen-activated protein kinases (MAPKs): extracellular signal-regulated kinase (ERK), c-Jun N-terminal kinase (JNK), and p38 MAPK (p38), which then phosphorylate the variable linker regions of receptor regulated SMADs (Massague J et al, 2003; Wrighton KH et al, 2009; Matsuzaki K et al, 2013) (**Background Fig. 1**).

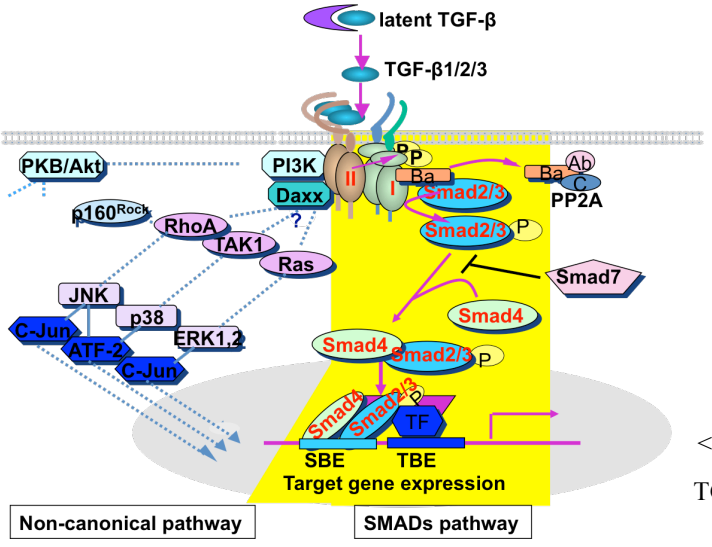

<**Background Figure 1**>
TGF-β signaling pathways

TGF-β R-Smads: Smad2 and Smad3 are highly homologous in their structure. They contain 2 conserved polypeptide segments, MH1 and MH2 domain, and connected by linker domain (**Background Fig. 2 left**). The MH1 domain is involved in DNA binding and nuclear transport, whereas the MH2 domain is involved in receptor-mediated Smad C-terminal phosphorylation, Smad-Smad interaction and binding with many different transcriptional regulators (Gaarenstroom T et al, 2014). MH1 domain has a DNA binding site, which recognizes Smad binding elements (SBE, 5'-CAGA-3') and regulates transcriptions of the genes. However, Smad2 cannot bind directly to DNA, it regulates transcriptions of target by interacting with other related molecules (Matsuzaki K, 2012). C-terminal serine residues, SSXS motif in MH2 domain are phosphorylated by TGF-β type I receptor, whereas various kinds of phosphorylation sites of linker domain are phosphorylated by protein kinases including MAPK. TGF-β type I receptor and various kinds of protein kinases differentially regulate Smad2 and Smad3 phosphorylations in a context-dependent manner (Matsuzaki K et al, 2013) (**Background Fig. 2 right**). Linker phosphorylated R-SMADs through Ras-MAPK antagonize C-terminally phosphorylated R-SMADs. Ras-MAPK mediated Smad3 linker phosphorylation enhances cell growth and proliferation by upregulating mitogenic signal genes such as c-Myc gene in normal epithelial cells. By contrast, TGF-β type I receptor regulated Smad3 C-terminal phosphorylation is involved in cell growth inhibition by inducing growth inhibition genes such as p15, p21 and p27 in normal epithelial cells (Matsuzaki K, 2012 and 2013). However, precise roles and regulatory mechanisms of linker-phosphorylated or C-terminal-phosphorylated R-SMADs remain largely undetermined in immune regulation.

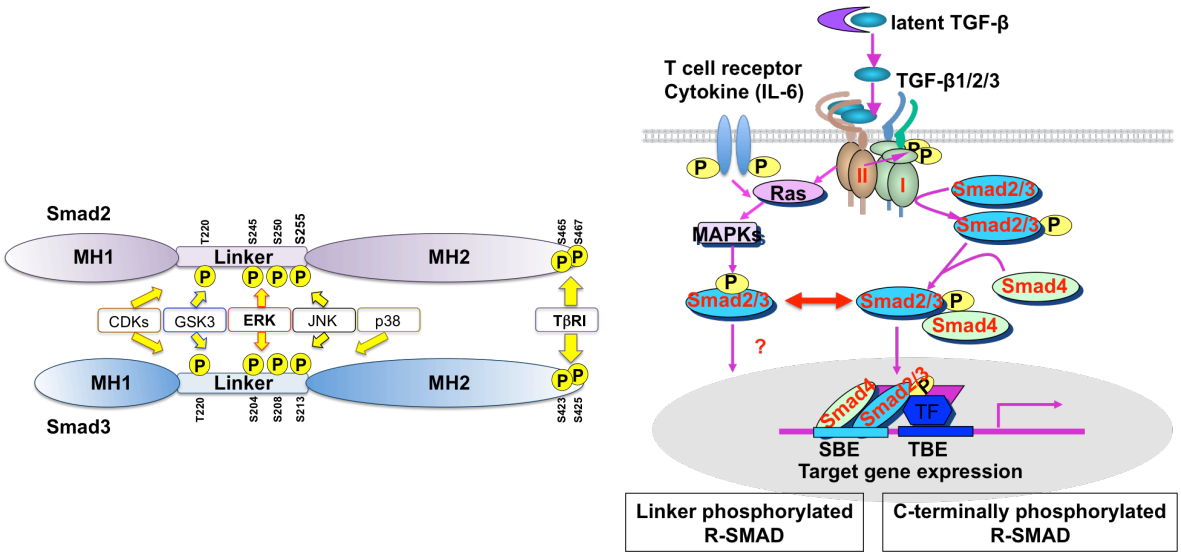

<**Background Figure 2**> Structure of receptor regulated SMAD (R-Smad) and TGF-β signaling pathways via linker phosphorylated R-SMAD and C-terminally phosphorylated R-SMAD

2. Role of TGF-β on immune system

TGF-β has been recognized as the most potent immunosuppressive cytokine, suppressing the differentiation and function of effector immune cells and inducing suppressor immune cells in immune system (Li MO et al, 2006; Travis MA et al, 2014). TGF-β inhibits differentiation, activation and immunogenic function of innate immune cells such as immunogenic dendritic cells (DC), macrophages and NK cells and immune responses of adaptive effector immune cells (Flavell RA et al, 2010). TGF-β directly suppresses the development, differentiation and immunogenic functions and activities of various effector T cell subsets such as $CD4^+$ T lymphocytes Th1 (cellular immunity), Th2 (allergic diseases and humoral immunity), cytotoxic $CD8^+$ T lymphocytes (CTL) (cytotoxic immunity and anti-tumor immunity) and IL-17 producing $CD4^+$ T cells: Th17 (autoimmunity). In addition to direct immune suppression, TGF-β indirectly suppresses effector immune cells by inducing differentiation and function of $CD4^+Foxp3^+$ regulatory T cells: Treg (immune surveillance) (Li MO et al, 2006 and Korn T et al, 2009) (**Background Fig. 3**).

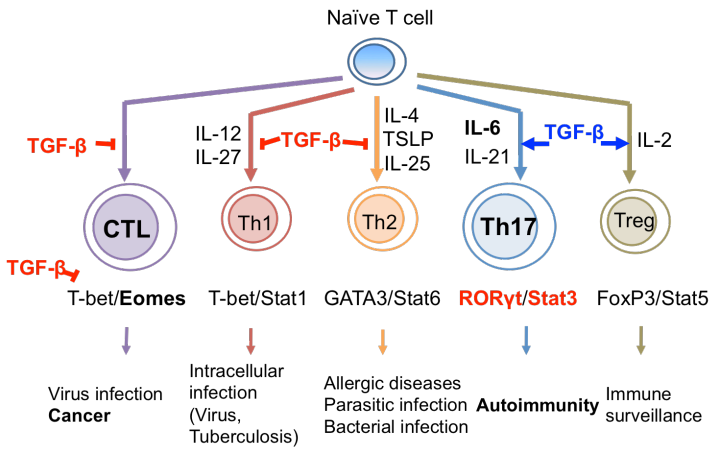

< **Background Figure 3**> Effects of TGF-β on effector T cell differentiation

Although TGF-β is abundantly produced and activated in inflammation and tumor microenvironment, however, precise molecular mechanisms how TGF-β signaling regulates effector immune cell responses in immune diseases and cancer still remain largely unknown.

In my doctoral dissertation, I report the novel TGF-β signaling mechanisms for Th17 cells in rheumatoid arthritis which is the representative autoimmune disease, and TGF-β signaling mechanisms for suppressing CTL in melanoma, which is a prototypical immunogenic tumor expressing melanoma -associated antigens.

3. Role of TGF-β signaling on Th17 in rheumatoid arthritis

Rheumatoid arthritis is one of autoimmune diseases, in which infiltration of the joint synovium membrane leads to bone and cartilage destruction. Th17 plays the pathogenic role in rheumatoid arthritis. IL-17A produced by Th17 enhances arthritogenic symptoms, such as inflammation, cartilage damage,

thrombosis and bone erosion (Korn T et al, 2009 and Pierre M et al, 2012). TGF-β had been appreciated as the most potent immunosuppressive cytokine, suppressing the differentiation and functions of effector immune cells as inducing suppressor immune cells (Li MO et al, 2006; Travis MA et al, 2014). However, since identified as the requisite cytokine in combination with IL-6 for the differentiation of Th17 through inducing a master transcription factor, RORγt and IL-17 (Veldhoen M et al, 2006; Manel N et al, 2008), context-dependent multidirectional roles of TGF-β have been highlighted in immune regulation, similarly with its roles in carcinogenesis and cancer progression (Massague J et al, 2012). Th17 is a crucial effector $CD4^+$ T cell subset in inflammation, protective mechanisms against infections, tumor immunity, and autoimmune responses (Korn T et al, 2009; Iwakura Y et al, 2011). Crucial pathogenic role of Th17 in rheumatoid arthritis has been well demonstrated by numerous studies including the pioneer work showing the attenuation of collagen-induced arthritis (CIA) in the mice deficient in IL-17A (Nakae S et al, 2003).

Activated TGF-β type I receptor through TGF-β signal phosphorylates not only C-termini of R-Smads, but also activates various protein kinases including mitogen-activated protein kinases (MAPKs) (**Background Fig. 1**). TCR, IL-6 and TGF-beta share Ras-MAPK pathways, which induce linker phosphorylation of TGF-β receptor-regulated SMADs, Smad2 and Smad3. However, phosphorylation status of Smad2/Smad3, C-terminal and linker phosphorylation or unphosphorylation during Th17 differentiation remains undetermined (Neurath MF et al, 2011; Liu H et al, 2013) (**Backgrund Fig. 2 right**).

Several reports have been published regarding TGF-β signaling in Th17 differentiation as listed in Background Table 1. However, there are points of controversy in theses reports. Lu L et al. concluded that JNK and p38-mediated TGF-β signaling pathways are required for Th17 differentiation based on the similar inhibitory effect of inhibitors against TβRI, JNK and p38 on Th17 differentiation. However, effect similarity of inhibitors with TβRI/TβRII inhibition on Th17 cannot demonstrate that each targeted enzyme is downstream of TβRI for Th17 differentiation (Hasan M et al, 2015). Lu L et al. also addressed that Smad2 and Smad3 were not involved in Th17 differentiation both in vitro and in vivo using murine experimental encephalomyelitis (EAE) model, which is inconsistent with the other reports by Matinez GJ et al. and Malhorta N et al, in which they showed that Smad2 deficiency suppressed, whereas Smad3 deficiency enhanced Th17 differentiation and EAE. Martinez GJ et al. reported that Smad3 interacted with RORγt to decrease, whereas Smad2 interacted with RORγt to enhance RORγt-induced Th17 differentiation. However, mechanisms how Smad2 and Smad3 oppositely regulate RORγt-induced Th17 differentiation were not addressed. Malhorta N et al. reported that Smad2 was essential for Th17 differentiation by modulating IL-6 receptor (IL-6R) expression, which was not observed in my system (**Fig. 9**). Takimoto T et al. reported that TGF-β-mediated induction of RORγt was independent of both Smad2 and Smad3 and Ichiyama K et al. reported that the suppression of Eomesodermin by TGF-β via the JNK pathway is an important mechanism for Smad-independent Th17 cell differentiation using Smad2/3 double knockout mice, in which it is impossible to distinguish the distinct effects of Smad2 and

Smad3. Xial S et al. reported that TGF-β-driven Smad3 signaling enhanced by retinoic acid inhibited Th17 differentiation. Collectively, Smad2 seems to be an inducer, whereas Smad3 seems to be a suppressor of Th17, thus far. MAPK signaling pathways, which phosphorylate linker regions of R-Smads, play crucial roles in differentiation and functions of effector T cells (Li MO et al, 2006; Travis MA et al, 2014; Dong C et al, 2002). Chang X et al reported that the kinases MEKK2/3 induced linker phosphorylation of Smad2/3, which antagonized their C-terminal phosphorylation and inhibited Th17 differentiation, although inhibition of Smad3 C-terminal phosphorylation in MEKK2/3 double knockout T cells determined by CAGA-luc reporter assay and Western blotting did not seem to be significant, moreover, they did not examine Smad2 linker phosphorylation. However whether diverse phosphorylation status of R-Smads, such as linker phosphorylation or unphosphorylation affects Th17 differentiation remains largely undetermined.

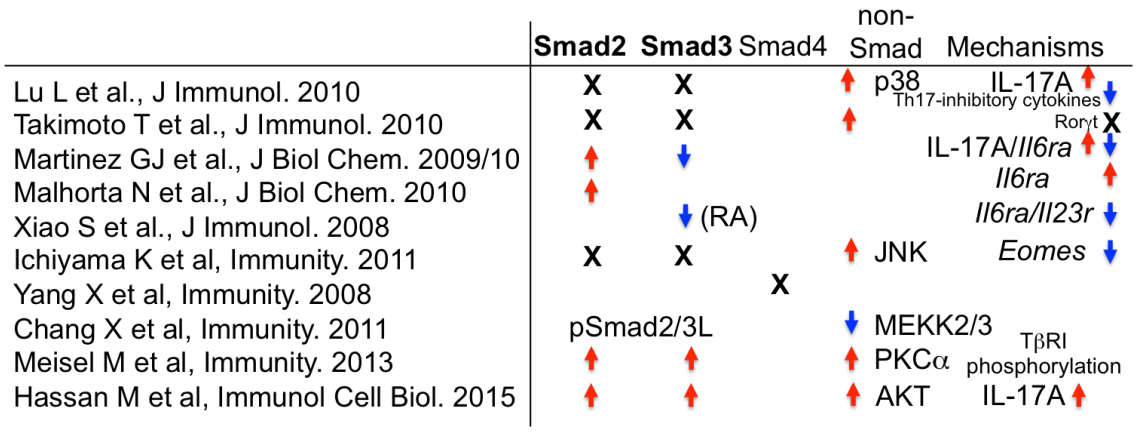

<**Background Table 1**> Reported roles of TGF-β signaling in Th17 differentiation

IL-6 and other cytokines such as IL-21 and IL-23 that induce and maintain Th17 activate STAT3, a critical transcription factor for Th17 differentiation and the pathogenesis of autoimmune diseases including RA (Hirahara K et al, 2010). In contrast to the established essential roles of STAT3-mediated IL-6 signaling in Th17 differentiation, molecular mechanisms by which R-Smads regulate Th17 differentiation still remain under debate. Despite their high amino acid sequence homology, Smad2 and Smad3 exert both redundant and distinct functions in TGF-β signaling depending on the context (Brown KA et al, 2007).

Therefore, I sought to determine the mechanisms whereby R-Smads regulate Th17 differentiation. I investigated the molecular mechanisms how Smad2 and Smad3 regulate the transcription of the essential genes for Th17 and examined the pathophysiological roles of R-Smads in Th17-related inflammatory disease by applying a CIA model to Smad2-deficient (*Smad2*$^{-/-}$), Smad3-deficient (*Smad3*$^{-/-}$), and control wild-type mice. I discovered the opposing functions of Smad2 and Smad3 as transcription cofactors of STAT3 in Th17 differentiation independently of Smad4: the canonical partner of C-terminally phosphorylated R-Smads. Mechanistic studies showed that phosphorylation status of R-Smads

distinctively modulated STAT3-induced transcription of the *Rorc* and *Il17a* genes. Linker-phosphorylated Smad2 (pSmad2L) at the residue Ser255 via ERK served as a STAT3 coactivator in cooperation with p300, whereas C-terminally unphosphorylated Smad3 (unphosphorylated Smad3C) served as a STAT3 corepressor in cooperation with protein inhibitor of activated STAT3 (PIAS3), the negative regulator of STAT3 signaling.

4. Role of TGF-β signaling on CTL in melanoma

Tumor cells and stromal cells in the tumor microenvironment produce and activate TGF-β abundantly for suppressing anti-tumor immunity (Bierie et al, 2006; Flavell RA et al, 2010). TGF-β suppresses anti-tumor immunity by directly inhibiting the differentiation and functions of various effector cells, such as DC, NK, Th1, and cytotoxic T lymphocytes (CTLs) (Li MO et al, 2006). In addition to direct immune suppression, TGF-β indirectly suppresses anti-tumor immunity by inducing suppressor immune cell subsets, such as Foxp3^{+} regulatory T cells (Treg) and myeloid-derived suppressor cells (Flavell RA et al, 2010) (**Background Fig. 4**).

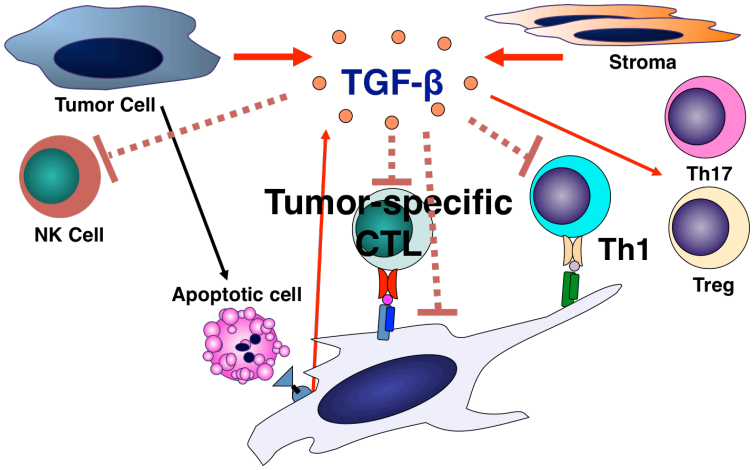

<**Background Figure 4**> Inhibition of Anti-tumor Immune Responses by TGF-β

Varieties of TGF-β antagonists have been developed to intervene with excessive TGF-β signaling activity in cancer (Hata A et al, 2012). TGF-β type I receptor: activin receptor-like kinase5 (ALK5) inhibitors are the small molecule inhibitors, which block phosphorylation of TGF-β receptor-activated Smads (R-Smads) by occupying the ATP binding site of TβRI domain (Jin et al, 2011). On the basis of a selective, imidazole-based ALK5 inhibitor, 4-(4-(benzo[*d*][1,3]dioxol-5-yl)-5-(pyridin-2-yl)-1*H*-imidazol-2-yl) benzamide, SB-431542 (Callahan et al, 2002) as a lead compound, we designed and synthesized an orally bioavailable ALK5 inhibitor, *N*-((4-([1,2,4]triazolo[1,5-*a*]pyridin-6-yl)-5-(6-methylpyridin-2-yl)-1*H*-imidazol-2-yl)methyl)-2-fluoroaniline, EW-7197 (Kim et al, 2011) <**Background Fig. 5**>.

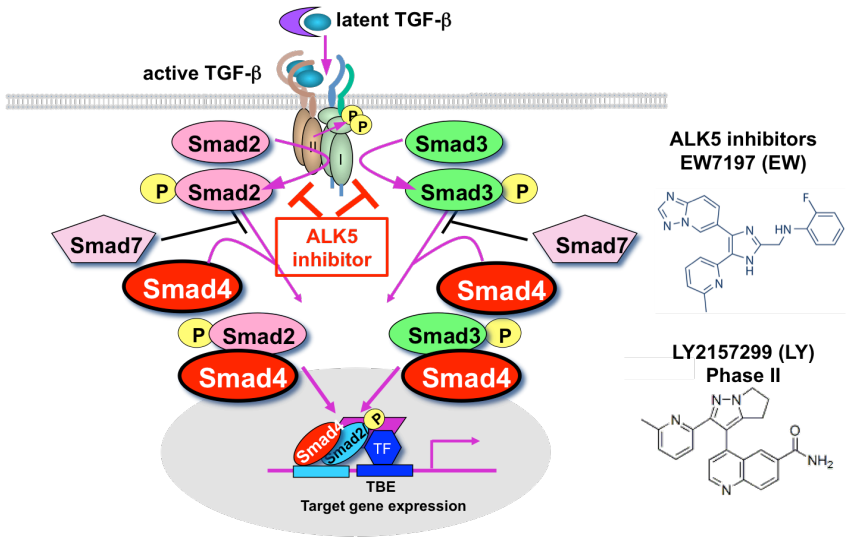

< **Background Figure 5**> ALK5 inhibitors (EW7197 and LY2157299) and TGF-β signaling pathway

Melanoma is a prototypical immunogenic tumor expressing melanoma-associated antigens, which are targeted by CTLs (Thomson et al, 1988). CTLs lyse the target tumor cells with the cytolytic molecules (Russell et al, 2002). The T-box transcription factors, T-bet and Eomes are crucial for the differentiation and effector functions of CTLs (Glimcher et al, 2004; Intlekofer et al, 2005; Pearce et al, 2003), which are required for anti-tumor immune responses (Zhu et al, 2010). Thus, intensive efforts have focused on developing immunotherapies to activate anti-melanoma T cell responses (Kirkwood et al, 2008). However, melanoma cells produce high amounts of TGF-β, which limit the success of immunotherapy by rendering the host immune response tolerant to tumor-associated antigens (Javelaud et al, 2008).

Therfore, I report the cellular and molecular mechanisms how EW-7197 and a representative ALK5 inhibitor,4-(2-(6-methylpyridin-2-yl)-5,6-dihydro-4H-pyrrolo[1,2-b]pyrazol-3-yl)quinolone-6-carboxamide, LY-2157299 (Calvo-Aller et al, 2008) exert a therapeutic effect on a mouse model of B16 melanoma. Oral treatment with a novel ALK5 inhibitor, EW-7197 (2.5 mg/kg daily) or a representative ALK5 inhibitor, LY-2157299 (75 mg/kg bid) suppressed the progression of melanoma with enhanced CTL responses. Notably, ALK5 inhibitors not only blocked R-Smads phosphorylation, but also induced ubiquitin-mediated degradation of the Smad4 mainly in $CD8^+$ T cells in melanoma-bearing mice. Accordingly, T-cell specific deletion of Smad4 was sufficient to suppress the progression of melanoma. I further identified eomesodermin (Eomes), the T-box transcription factor regulating CTL functions, as a specific target repressed by TGF-β via Smad4 and Smad3 in $CD8^+$ T cells. Thus, ALK5 inhibition enhances anti-melanoma CTL responses through ubiquitin-mediated degradation of Smad4 in addition to the direct inhibitory effect on R-Smad phosphorylation.

Phosphorylation status determines the opposing functions of Smad2/Smad3 as STAT3 cofactors in Th17 differentiation

（リン酸化状態が **STAT3** 転写共役因子としての **Smad2 /Smad3** 相反作用を規定する）

Materials and Methods

Mice

Smad2$^{3loxp/3loxp}$ mice targeting exons 9 and 10 (Liu Y et al, 2004), *Smad3*$^{ex8/ex8}$ mice targeting exon 8 (Yang X et al, 1999) were generated as described on Sv129 x C57BL/6J background and backcrossed to C57BL/6J mice (Nihon SLC) for eight generations. For *in vitro* experiments, *Smad3*$^{ex8/ex8}$ mice were backcrossed to C57BL/6J background for four generations. I used *Smad3*$^{+/-}$ mice because *Smad3*$^{-/-}$ mice develop osteoarthritis, bone malformation (Yang X et al, 2001), and impaired mucosal immunity (Yang X et al, 1999), and the embryonic lethality of *Smad3*$^{-/-}$ mice in C57BL/6 background was extremely high, similarly with *Tgf-β1*$^{-/-}$ mice (Bonyadi M et al, 1997). *Cd4Cre* transgenic mice (Lee PP et al, 2001) were purchased from Jackson laboratories. *Mx-1Cre* transgenic mice (Kuhn R et al, 1995) were kindly provided by Dr. Masayuki Yamamoto (Tohoku University, Japan). For *Mx-1Cre* mice, gene deletion was induced by *i.p.* injection of polyI:C at 2-3 weeks of age as described previously (Campbell IK et al, 2000). For immunophenotyping, spleens and superficial lymph nodes (cervical, axillary, brachial, and inguinal) from the female mice aged between 12-16 weeks were used (age and sex matched, no randomized). All animals were maintained and used for experiments according to the ethical guidelines for animal experiments and the safety guidelines for gene manipulation experiments at Konkuk University, Korea, University of Tsukuba, Japan, Tokyo Medical University, Japan under approved animal study protocols.

Collagen Induced-Arthritis (CIA)

For induction of collagen-induced arthritis, I used immunization protocol for C57BL/6 strain (H-2b) (Campbell IK et al, 2000). Briefly, 100 μg of type II chick collagen (Sigma-Aldrich, Cat. #C9301) was dissolved in 10 mM acetic acid (2 mg/ml) by stirring overnight at 4°C. I dissolved 250 μg of heat-killed *mycobacterium tuberculosis* (Difco Laboratories) in incomplete Freund adjuvant (GIBCO). Type II chick collagen mixture gently emulsified in complete Freund adjuvant by 1:1 ratio on ice for 1 hr (100 μg of type II chick collagen emulsified in 100 μl of incomplete adjuvant with 250 μg of heat-killed *mycobacterium tuberculosis*). Mice aged between 8-10 weeks were injected *i.d.* (100 μl of emulsion) at several sites into the base of the tail and back that is near hind leg areas by using 26 G needle on day -21, and the same injection was repeated on day 0. Arthritis development in each paw was scored by macroscopic evaluation (Rosloiec EF et al, 2010) as: (0) no change, (1) erythema and mild swelling confined to the ankle, (2) erythema and mild swelling from the ankle to mid-foot, (3) moderate swelling (4) severe swelling. The maximum score per mouse is 16. Ten to twenty mice/genotype were used (Figure 1 legend and Supplementary figure 2 legend). Mice were dissected 2 weeks after the second immunization to evaluate the draining lymph nodes (popliteal, inguinal, axillary, and brachial).

Histological analysis

Paws from collagen-immunized mice were harvested, fixed in 10% neutral-buffered formalin, decalcified, dehydrated with 70% ethanol, embedded in paraffin, and sectioned at 3 μm. Sections were stained with hematoxylin and eosin (H&E), toluidine blue, or safranin O. For immunohistochemistry, sections were incubated in the 60°C for overnight. Incubated sections were deparaffinized and hydrated by xylene and graded alcohol series (Xylene for 15 min, and 100%, 95%, 90%, 85%, 80% and 70% of EtOH for 5 min). After deparaffinization and hydration, tissue sections were rinsed in tap water for 10 min. Tissue sections were added by 3% hydrogen peroxide solution in room temperature for 30 min for peroxidase quenching, and washed in PBS for 5 min. After peroxidase quenching, added one or two drops of blocking solution (Dako, Cat.# x0590) in 37°C for 30 min. After blocking, tissue sections were incubated with rat anti-CD4 (Abcam, Cat.# ab25475), rabbit anti-RORγt (Abcam, Cat.# ab78007), rabbit anti-IL-17A (Abcam, Cat. #ab79056) antibodies in 4°C for overnight, and washed in PBS for 5 min. Incubated sections from primary antibodies were incubated by diluted biotinlated secondary antibody in 37°C for 30 min, and washed in PBS for 5 min. After secondary antibody incubation, the sections were incubated with VETA STAIN R.T.U Elite ABC Reagent (Vector) in 37°C for 30 min, and washed in PBS for 5 min. The tissue sections were treated DAB solution for 5 min (according to samples), and washed in PBS for 5 min. After DAB exposure step, the tissue sections were incubated in hematoxylene for 1 min, and washed in tap water for 30 min. After counterstain step, dehydrated and mounted. Slides were observed using an optical microscope, DM5000B (Leica).

Flow cytometry analyses

Fluorophore-conjugated antibodies were purchased from BD Pharmingen and eBioscience (APC-Cy7-anti-CD4, Pacific blue-anti-CD8, APC-anti-CD25, FITC-anti-CD103, PE-anti-RORγt, PE-anti-T-bet, PE-Cy7-anti-Foxp3, APC-anti-IL-17A, PE-anti-IL-6, FITC-anti-TNFa, PE-Cy7-anti-IFN-γ, APC-anti-phospho ERK1/2, PE-anti-phospho JNK, FITC-anti-phospho p38 were used). CD16/32 were blocked by Fc-Block (BD Pharmingen, Cat. #553142) and isotype-matched control antibodies were used in each experiment. For cytokine intracellular staining, cultured Th17 cells or freshly isolated cells from CIA mice were treated with 5 ng/ml of phorbol-12-myristate 13-acetate (PMA) (Sigma Aldrich) and 500 ng/ml of ionomycin (Sigma Aldrich) in the presence of GolgiPlug (BD Pharmingen) for the last 4 hours of culture. For intracellular staining, cultured cells were fixed by Cytoperm/Cytofix kit (BD Pharmingen). For Foxp3 staining, Foxp3 staining kit (eBioscience, Cat. #00-5523-00) was used. Stained cells were acquired and analyzed using LSR II (BD) and FlowJo software (Tree Star Inc.).

T cell stimulation *in vitro*.

Cell suspensions were prepared from spleens and superficial lymph nodes (cervical, brachial, axillary and inguinal and popliteal lymph nodes) by filtering through Cell Strainers (pore size: 40-μm diameter) (BD

Falcon). Erythrocytes were lysed using RBC Lysis Buffer (Rhoche) and cells were washed in PBS containing 2% FBS (Hyclone Laboratories). Viable cells were counted by hemacytometer using trypan blue exclusion. $CD4^+$ T cells were purified to >90% by magnetic activated cell separation purification using $CD4^+$ (L3T4) Microbeads (Miltenyi Biotec). In some experiments, $CD44^{low}CD62L^{high}CD4^+$ T cells were sorted by FACS Aria (BD) and the purity was >98%. Purified $CD4^+$ T cells were stimulated by plate-coated anti-CD3 (2.0 μg/ml; BD Pharmingen, Cat. #553057) and soluble anti-CD28 antibodies (5.0 μg/ml; BD Pharmingen, Cat. #553294) with mIL-6 (50 ng/ml), TGF-β1 (1 ng/ml; Peprotech), anti-mouse IL-4 (10 μg/ml; Biolegend, Cat. #504108) and anti-mouse IFN-γ antibodies (10 μg/ml; BioLegend, Cat. #505812) in 10% FCS RPMI 1640 media supplemented with penicillin and streptmycin (HyClone) for Th17 differentiation for 3-4 days as previously described (Veldhoen M et al, 2006). In some experiments, Purified $CD4^+$ T cells were stimulated by the indicated doses of plate-coated anti-CD3, TGF-β1, and mIL-6, or by plate-coated anti-CD3 (10.0 μg/ml; BD Pharmingen, Cat. #553057), soluble anti-CD28 antibodies (5.0 μg/ml; BD Pharmingen, Cat. #553294), IL-1β (10 ng/ml; Peprotech), IL-23 (10 ng/ml; Peprotech), and the neutralizing antibodies described above, or by the indicated doses of various small molecule inhibitors: EW-7197 (ALK5 inhibitor) from Dr. Dae-Kee Kim, PD98059 (MEK inhibitor), SP600125 (JNK inhibitor), and SB203580 (p38 inhibitor) (Sigma Aldrich). STAT3 siRNA (Dharmacon), PIAS3 siRNA (Santa Cruz), DNA constructs: Smad2, Smad2 (S255A), Smad3, Smad3 (3S-A), and Smad3 (MH1+L) from Dr. Koichi Matsuzaki and Dr. Takeshi Imamura, PIAS3 (Addgene, submitted by Shuai), and pcDNA or control RNA were transfected to purified $CD4^+$ T cells using 4D-Nucleofector™ and Amaxa® Mouse T cell nucleofactor® kit (Lonza) prior to the cell culture.

RNA isolation and quantitation of mRNA by real-time RT-PCR

Total RNA was extracted using Trizol according to the manufacturer's instructions (Invitrogen). RNA was reverse transcribed with cDNA reverse transcription kit (Invitrogen). Amount of cDNA was quantitated by SYBR green (Applied Biosystems) real time PCR using ABI 7900 and ABI 7300 machines (Applied Biosystems). The primers are described in Table 1.

Table 1 Primer sequences for quantitative RT-PCR

Gene	Sense primer	Antisense primer
Gapdh	TGGTGAAGGTCGGTGTGAAC	CCATGTAGTTGAGGTCAATGAAGG
Il17a	CTCCAGAAGGCCCTCAGACTAC	AGCTTTCCCTCCGCATTGACACAG
Rorc	CCGCTGAGAGGGCTTCAC	TGCAGGAGTAGGCCACATTACA
Batf	CCCAAAGCAGCGAGATGT	GGTTCTAATCTTCCGGGCTC
Il6	GAGGATACCACTCCCAACAGACC	AAGTGCATCATCGTTGTTCATACA
Il6ra	GCACGTGGTCCAGGTCCGTG	GGGGCGAGGACACTCGTTGC
Il23r	GTCCACCAAACTTCCCAAGA	ACATGATGGCCAAGAAGACC
Il21	CGCCTCCTGATTAGACTTCG	TGTTTCTTTCCTCCCCTCCT
Il21r	ATGGCTATCCAGCCATGAAC	GGGTCCTTCATCAGTCTCCA
Il2	CCCACTTCAAGCTCCACTTC	ATCCTGGGGAGTTTCAGGTT
Il2ra	AGAACACCACCGATTTCTGG	AGCTGGCCACTGCTACCTTA
Tbet	GCCAGGGAACCGCTTATATG	GACGATCATCTGGGTCACATTGT
Eomes	TGAATGAACCTTCCAAGACTCAGA	GGCTTGAGGCAAAGTGTTGACA
Pias3	GGACGTGTCCTGTGTGTGAC	CTCTGATGCCTCCTTCTTGG

Western blotting and immunoprecipitation

293T cells (ATCC-CRL-3216) were transfected using PEI with STAT3 (Addgene, submitted by J. Darnell), FLAG-tagged Smad2 (full length, MH1, MH1+Linker, MH2+Linker, MH2, Y220V, S245A, S250A, S255A) and FLAG-tagged Smad3 (full length, MH1, MH1+Linker, MH2+Linker, MH2, 3S-A) from Dr. Koichi Matsuzaki and Dr. Takeshi Imamura. Cells were lysed with lysis buffer (PBS containing 0.5% Triton X-100, 20 mM HEPES (pH 7.4), 150 mM NaCl, 12.5 mM β-glycerol phosphate, 1.5 mM MgCl2, 10 mM NaF, 2 mM DTT, 1 mM NaOV, 2 mM EGTA, 1 mM PMSF, and protease inhibitor cock-tail) were electrophoresed on 10% SDS-polyacrylamide gel and transferred to PVDF membrane, and probed with antibodies against phospho-Smad2 (Abcam, Cat. #ab53100), phospho-Smad3 (Abcam, Cat. #ab51451), Smad2 (Santa Cruz, Cat. #sc-101153), Smad3 (Santa Cruz, Cat. #sc-101154), Smad4 (Santa Cruz, Cat. #sc-7966) and β-actin (Santa Cruz, Cat. #sc-7210). Blots were visualized using an electrochemiluminescence kit (GE Healthcare).

For immunoprecipitation, the lysates were cleared by centrifugation at 16,000 *g* for 10 min, incubated with protein A/G agarose beads and with anti-STAT3 antibody (Santa Cruz, Cat. # sc-7179) at 4°C for 12-16 h. The beads were washed three times with lysis buffer and immunoprecipitates were separated from the beads by adding 2× sample buffer and boiled. SDS–PAGE-separated immunoprecipitates were transferred onto PVDF membranes. The membranes were denatured with denaturation buffer containing 6 M guanidine chloride, 20 mM Tris (pH 7.5), 100 mM PMSF, and 5 mM β-mercaptoethanol at 4°C for 30 min and washed three times with TBST. The membranes were blocked with 5 % BSA and incubated with anti-FLAG antibody (Biomol, Cat. #ADI-SAB-410-0100). 293T cells (ATCC-CRL-3216) were confirmed to be mycoplasma negative using e-Myco plus Mycoplasma PCR Detection Kit (iNtRON

Biotechnology, Cat. #25237).

Immunocytochemistry: Proximity Ligation Assay (PLA)

$CD4^+$ T cells cultured in Th17 condition for 3-5 days or 293T cells (ATCC-CRL-3216) transfected with various constructs were fixed on the slides by 3.7 % formaldehyde in PBS. The slides were washed, permeabilized by 0.1 % Triton X-100 in TBS and blocked by 0.5 % bovine serum albumin. PLA was performed using the Duolink II Fluorescence kit (OLINK) as previously described using the rabbit antibodies against: STAT3 (Cell Signaling Technology, Cat. #12640), phospho-STAT3 Y705 (Cell Signaling Technology, Cat. #9145), phospho-STAT3 S727 (Cell Signaling Technology, Cat. #9134), Smad2 (Cell Signaling Technology, Cat. #5339), phospho-Smad2C S465/467 (Cell Signaling Technology, Cat. #3101), phospho-Smad2L S245/250/255 (Cell Signaling Technology, Cat. #3104), Smad3 (Cell Signaling Technology, Cat. #9523), phospho-Smad3C S423/425 (Cell Signaling Technology, Cat. #9520), RORγt (Abcam, Cat. #ab78007), PIAS3 (Santa Cruz, Cat. #sc-14017), Flag (Biomol, Cat. #ADI-SAB-410-0100) and phospho-Smad3L S208/213 (IBL, Cat. #JP28029), mouse antibodies against: Smad2/3 (Santa Cruz, Cat. #sc-133098), Smad4 (Santa Cruz, Cat. #sc-7966), STAT3 (Santa Cruz, Cat. #sc-8019), and p300 (Santa Cruz, Cat. #sc-48343). Target specific rabbit primary antibodies and the secondary antibodies conjugated with oligonucleotides: PLA probe anti-rabbit PLUS (Sigma-Aldrich, Cat. #DUO92002) and PLA probe anti-rabbit MINUS (Sigma-Aldrich, Cat. #DUO92005) or PLA probe anti-mouse PLUS (Sigma-Aldrich, Cat. #DUO92001) and PLA probe anti-mouse MINUS (Sigma-Aldrich, Cat. #DUO92004) were used for single recognitions. Two primary antibodies raised in different species and the secondary antibodies conjugated with oligonucleotides: PLA probe anti-rabbit PLUS and PLA probe anti-mouse MINUS were used for double recognitions. After incubation of the slides with Blocking Solution for 30 min at 37°C, they were incubated with primary antibodies diluted in the Antibody Diluent overnight at 4°C, in PLA probe solution for 1 h at 37°C and in Ligation-Ligase solution for 30 min at 37°C with washing with Wash Buffer A (0.01 M Tris, 0.15 M NaCl and 0.05% Tween 20, filtered in a 0.22 μm) in the interim of each step. The slides were incubated in Amplification-Polymerase solution for 100 min at 37°C and then washed in Wash Buffer B. Nucleus was stained with DAPI. Then, the slides were dried at room temperature in the dark. Slides were observed using a confocal microscope, LSM700 (Carl Zeiss). PLA signals were quantified using BlobFinder software (Centre for Image Analysis, Uppsala University).

Luciferase assay

The 2000 bp promoter region of RORγt was generated by PCR from genomic C57BL/6 DNA using primers described in Table 2. Products were verified by sequencing and were subcloned into pGL4 firefly luciferase construct (Promega) using NheI, EcoRV sites and XhoI, HindIII sites respectively. The pGL4 mIL-17 2kb promoter construct was from Addgene (submitted by W. Strober). The promoter constructs

in various combination with Flag-tagged STAT3 (Addgene, submitted by J. Darnell), Flag-tagged Smads, Flag-tagged Smad mutants, HA-tagged p300, Flag-tagged PIAS3 (Addgene, submitted by Shuai), or empty pcDNA3 plasmid were co-transfected with control TK-pRL *Renilla* plasmid using PEI for 293T cells or using 4D-Nucleofector™ and Amaxa® Mouse T cell nucleofactor® kit (Lonza) for Th17 cells. Six hours after transfection, 293T cells (ATCC-CRL-3216) were lysed for the measurement by luminometer. $CD4^+$ T cells were transfected in prior to the cell culture under Th17 polarizing condition for 4 days.

Table 2 Primer sequences for the proximal promoter regions

the *Rorc* promoter	Sense primer	Antisense primer
-2.0 kb	AAAGCTAGCTTGGTGTTCATCTCTGTG GT	AAAGATATCGACTGAGAACTTGGCTCCC T

the *Il17a* promoter	Sense primer	Antisense primer
-2.0 kb	AAACTCGAGTAACAACAACAACAAC AAAAG	AAAAAGCTTGTTTGCGCGTCCTGATCAG CTG

ChIP

Chromatin was prepared from $1x10^7$ $CD4^+$ T cells isolated from C57BL/6 mice, *Cd4Cre;Smad2*$^{fl/fl}$ mice, *Smad3*$^{-/-}$ mice and the littermate control mice under Th17 polarizing condition for 3-4 days. Immunoprecipitation was performed with antibodies against Smad2 (Cell Signaling Technology, Cat. #5339), Smad3 (Cell Signaling Technology, Cat. #9523), phospho-Smad3C S423/425 (Cell Signaling Technology, Cat. #9520), Smad4 (Santa Cruz, Cat. #sc-7966), STAT3 (Santa Cruz, Cat. #sc-7179), tri-methyl histone H3 Lys4 (Cell Signaling Technology, Cat. #9751), tri-methyl histone H3 Lys27 (Cell Signaling Technology, Cat. #9733), acetyl histone H3 Lys23 (Millipore, Cat. #17-10112), and PIAS3 (Santa Cruz) using ChIP kit (Cell Signaling) according to the manufacturer's protocol. Immunoprecipitated DNA released from the cross-linked proteins was quantitated by real time PCR using the primers (Table 3) and was normalized to input DNA.

Table 3 Primer sequences for ChIP

the *Rorc* promoter	Sense primer	Antisense primer
-1499 to -1304	AGTCTCAACAATGGGGTCGT	CGTGTGAGTGTGCATGTCTG
-1331 to -1170	ATCCTCCACAGACATGCACA	GTTCTTAGCCCCAGGGAGAC
-1071 to -853	CAACGGTGGAGAATGGAATG	TTCCTGCTTACCCAACAACC
-230 to -44	AATCACTCGTGCCTGTAGGG	GAGGGGACTCAGGGAGAGAG

The *Il17a* promoter	Sense primer	Antisense primer
-1958 to -1795	CCCTATGCAGTTGGTACAAAGA	TCTCTCCAGCTCCATGGATTA
-1847 to -1731	GCCACATACCAAAGAGACAAATGA	TGGTTTCTGGGAATTGAACTCA
-279 to -112	GCAGCAGCTTCAGATATGTCC	TGAGGTCAGCACAGAACCAC
-184 to -10	AACTTCTGCCCTTCCCATCT	GCTCCTTTCTCTCTTTTTATACGG
+4 to +59	CACCTCACACGAGGCACAAG	ATGTTTGCGCGTCCTGATC

Statistical analyses

Statistical analysis was performed using analysis tools on the VassarStats Statistical Computation site (http://vassarstats.net/) and Excel. Data were analyzed using the parametric unpaired Student t-test, or two-way ANOVA test for CIA scoring.

Results

Opposing roles of Smad2 and Smad3 in the pathogenesis of CIA

To examine the pathophysiological roles of R-Smads in Th17-mediated inflammatory disease, I applied a CIA model to T cell-specific (*Cd4Cre;Smad2*$^{+/+,\ +/fl,\ fl/fl}$), inducible systemic (*Mx-1Cre;Smad2*$^{+/+,\ +/fl,\ fl/fl}$) Smad2 conditional knockout mice, and Smad3 heterozygote (*Smad3*$^{+/+,\ +/-}$) mice. They showed normal immune phenotypes with C57BL/6 background in a specific pathogen free environment (**Fig. 1**), indicating that R-Smads are dispensable for immune homeostasis. T cell-specific and systemic deletion of Smad2 ameliorated, whereas Smad3 heterozygosity exacerbated CIA (**Fig. 2a** and **3a**). Because both systemic and T cell-specific deletion of Smad2 showed the same phenotype (**Fig. 3a** and **3b)**, I used *Cd4Cre;Smad2*$^{+/+,+/fl.\ fl/fl}$ mice for further study. *Cd4Cre;Smad2*$^{fl/fl}$ mice showed significant amelioration in joint lesions, whereas *Smad3*$^{+/-}$ mice showed proliferative detritic synovitis with mononuclear cell infiltration and joint destruction (**Fig. 2b**, upper). Evaluation of proteoglycan and mucopolysaccharide of cartilage by staining with toluidine blue and Safranin O showed the significant maintenance of cartilages in *Cd4Cre;Smad2*$^{fl/fl}$ mice and marked destruction of cartilages in *Smad3*$^{+/-}$ mice (**Fig. 2b**, lower). Accumulation of $CD4^+$, $ROR\gamma t^+$, and $IL\text{-}17A^+$ cells in the joint lesions was ameliorated in *Cd4Cre;Smad2*$^{fl/fl}$ mice, whereas it was exacerbated in *Smad3*$^{+/-}$ mice (**Fig. 4-6**). Consistent with the joint lesions, $IL\text{-}17A^+$, $ROR\gamma t^+$, $IL\text{-}17A^+TNF\text{-}\alpha^+$ and $IL\text{-}17A^+ROR\gamma t^+$ $CD4^+$ T cells decreased in the draining lymph nodes of the arthritic joints of *Cd4Cre;Smad2*$^{fl/fl}$ mice and *Mx-1Cre;Smad2*$^{fl/fl}$ mice, whereas they increased significantly in those of *Smad3*$^{+/-}$ mice (**Fig. 2c** and **3b**). Smad genotypes did not affect other effector T cell subsets, such as $IL\text{-}6^+CD4^+$, $TNF\text{-}\alpha^+CD4^+$, Th1 ($T\text{-}bet^+IFN\text{-}\gamma^+CD4^+$), natural and inducible Treg cells ($CD103^-Foxp3^+CD4^+$, $CD103^+Foxp3^+CD4^+$), naïve and memory $CD4^+$ and $CD8^+$ T cells ($CD44^{low}CD62L^{high}$, $CD44^{high}CD62L^{low}$) in the draining lymph nodes of the arthritic joints (**Fig. 7**). Thus, Smad2 and Smad3 have the opposing roles in Th17 differentiation in the pathogenesis of CIA.

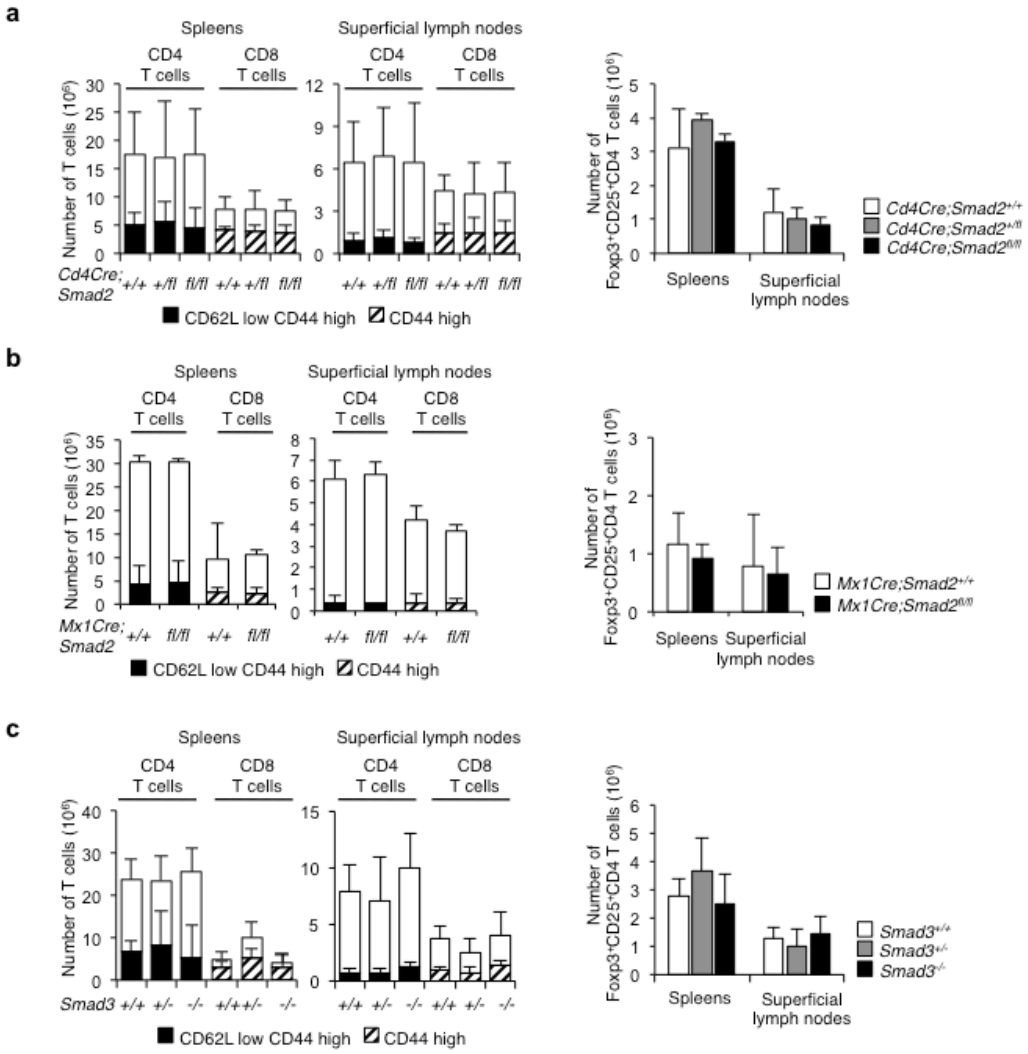

Figure 1 Smad2 and Smad3 are not essential for T cell homeostasis.

Numbers of naïve/memory $CD4^+$ T cells, naïve/memory $CD8^+$ T cells, and $Foxp3^+$ Tregs in spleens and superficial lymphnodes from (**a**) *Cd4Cre;Smad2*$^{+/+,\ +/fl,\ fl/fl}$ mice, (**b**) *Mx-1Cre;Smad2*$^{+/+,\ fl/fl}$ mice, and (**c**) *Smad3*$^{+/+,\ +/-,\ -/-}$ mice (12-16 weeks of age, *Cd4Cre;Smad2* and *Smad3*, n = 10/genotype, *Mx-1Cre;Smad2*, n = 5 genotype). Data are from one experiment representative of seven independent experiments. Data are mean + s.d.

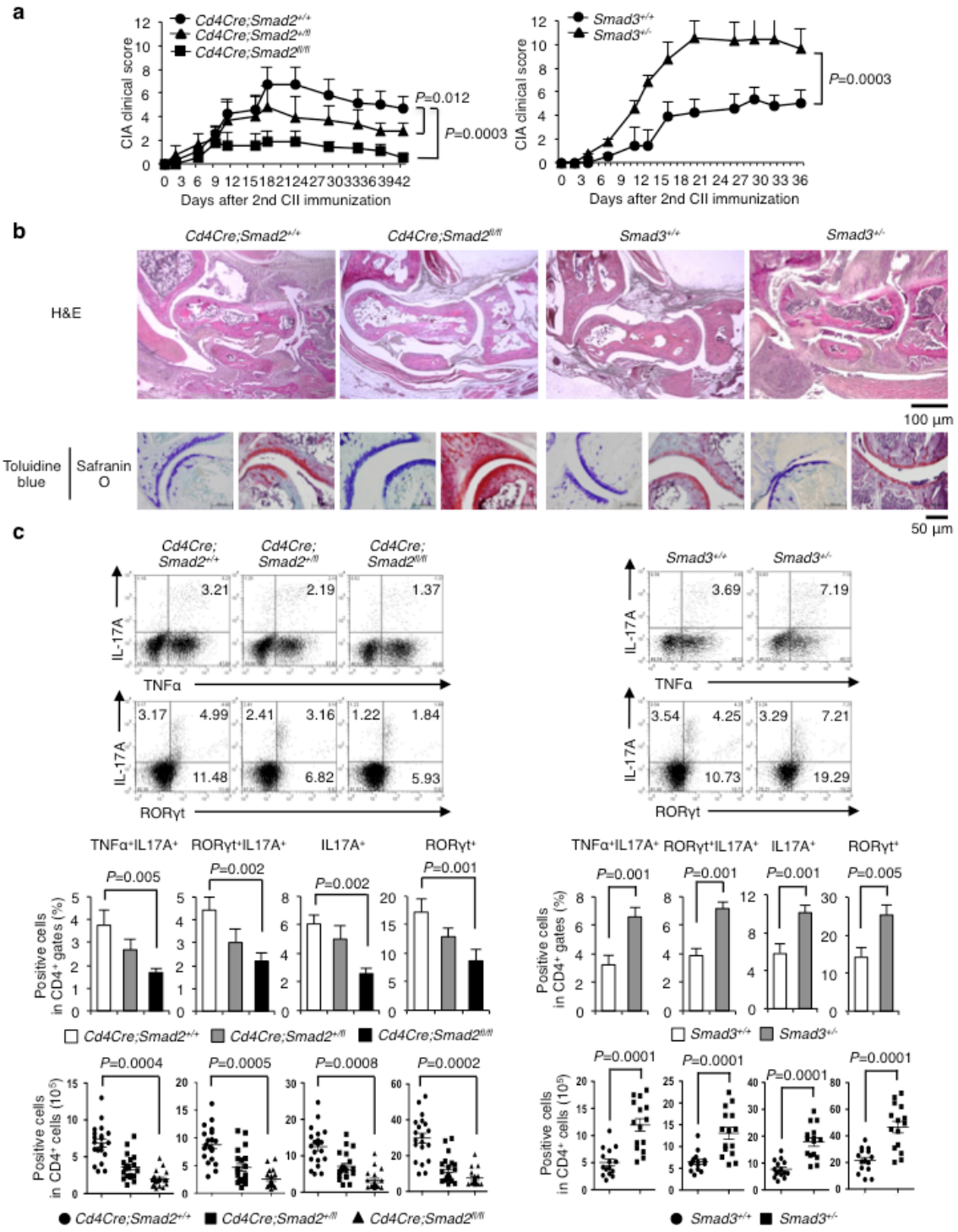

Figure 2 Opposing effects of Smad2 and Smad3 on Th17 response in CIA.

Cd4Cre;Smad2$^{+/+,\ +/fl,\ fl/fl}$ and *Smad3*$^{+/+,\ +/-}$ mice were immunized with type II collagen emulsified in complete Freund adjuvant twice in 3 weeks interval to induce CIA. (**a**) CIA scoring courses of *Cd4Cre;Smad2*$^{+/+}$, *Cd4Cre;Smad2*$^{+/fl}$, *Cd4Cre;Smad2*$^{fl/fl}$ mice (left, *n* = 11/*Cd4Cre;Smad2* genotype) and

Smad3$^{+/+}$, *Smad3*$^{+/-}$ mice (right, n = 13/*Smad3* genotype) with P values (two-way ANOVA test). (**b**) Pathological analyses of the joint sections (haematoxylin and eosin: HE, magnification, ×40, scale bar: 100 μm, toluidine blue and safranin O, magnification, ×200, scale bar: 50 μm). (**c**) Flow cytometry analyses of IL-17A^{+}TNF-α^{+} CD4^{+} T cells and RORγt^{+}IL-17A^{+} CD4^{+} T cells in the draining lymph nodes of *Cd4Cre;Smad2*$^{+/+,+/fl,\ fl/fl}$ (n = 20/*Cd4Cre;Smad2* genotype) and *Smad3*$^{+/+,+/-}$ mice (n = 15/*Smad3* genotype) on day 14 after second immunization. Graphs show the percentages and cell numbers of IL-17A^{+}, RORγt^{+}, IL-17A^{+}TNF-α^{+} and IL-17A^{+}RORγt^{+} in CD4^{+} gates in the draining lymph nodes. Data are from one experiment representative of seven (**a**, **b**), four (**c**, *Cd4Cre;Smad2*) or three (**c**, *Smad3*) independent experiments. Graphs show mean + s.d. with P values (unpaired Student's t-test).

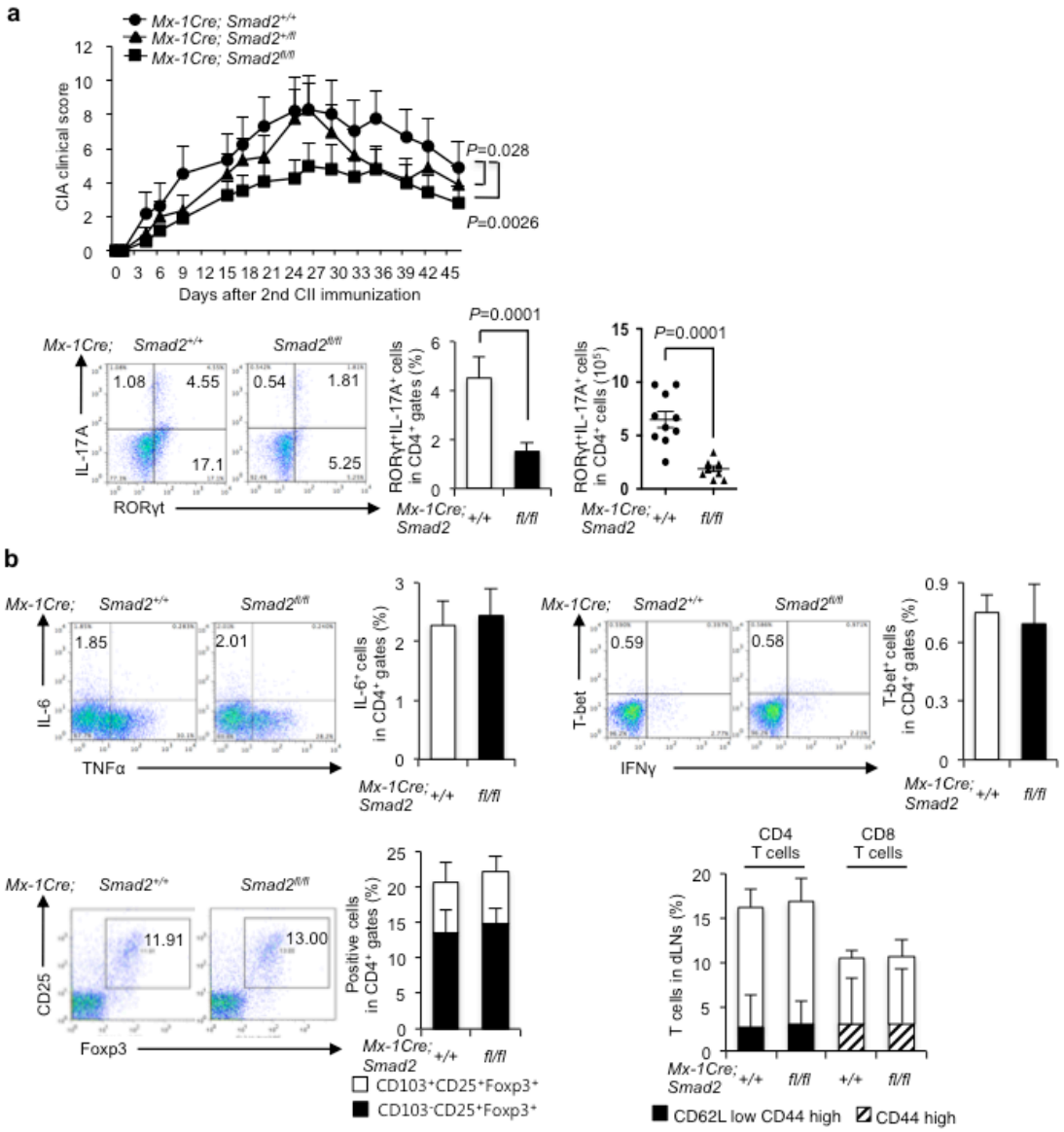

Figure 3 Inducible systemic disruption of the *Smad2* gene ameliorates CIA.

(**a**) CIA scoring courses of *Mx-1Cre;Smad2*$^{+/+,\ +/fl,\ fl/fl}$ mice (n = 10/genotype) are shown. Dot plots and graphs of the proportions and numbers of IL-17A^{+}RORγt^{+}CD4^{+} draining lymph node cells from *Mx-1Cre;Smad2*$^{+/+,fl/fl}$ mice are shown. (**b**) Dot plots and proportions of IL-6^{+}TNF-α^{+}CD4^{+}, T-bet^{+}IFN-γ^{+}CD4^{+}, CD25^{+}Foxp3^{+}CD4^{+}, CD62L^{high}CD44^{low}, CD62L^{low}CD44^{high} CD4^{+} T cells and CD44^{low},CD44^{high} CD8^{+} T cells in the draining lymph nodes from *Mx-1Cre;Smad2*$^{+/+,fl/fl}$ mice are shown. Data are from one experiment representative of two independent experiments. Data are mean + s.d. with P values (two-way ANOVA test).

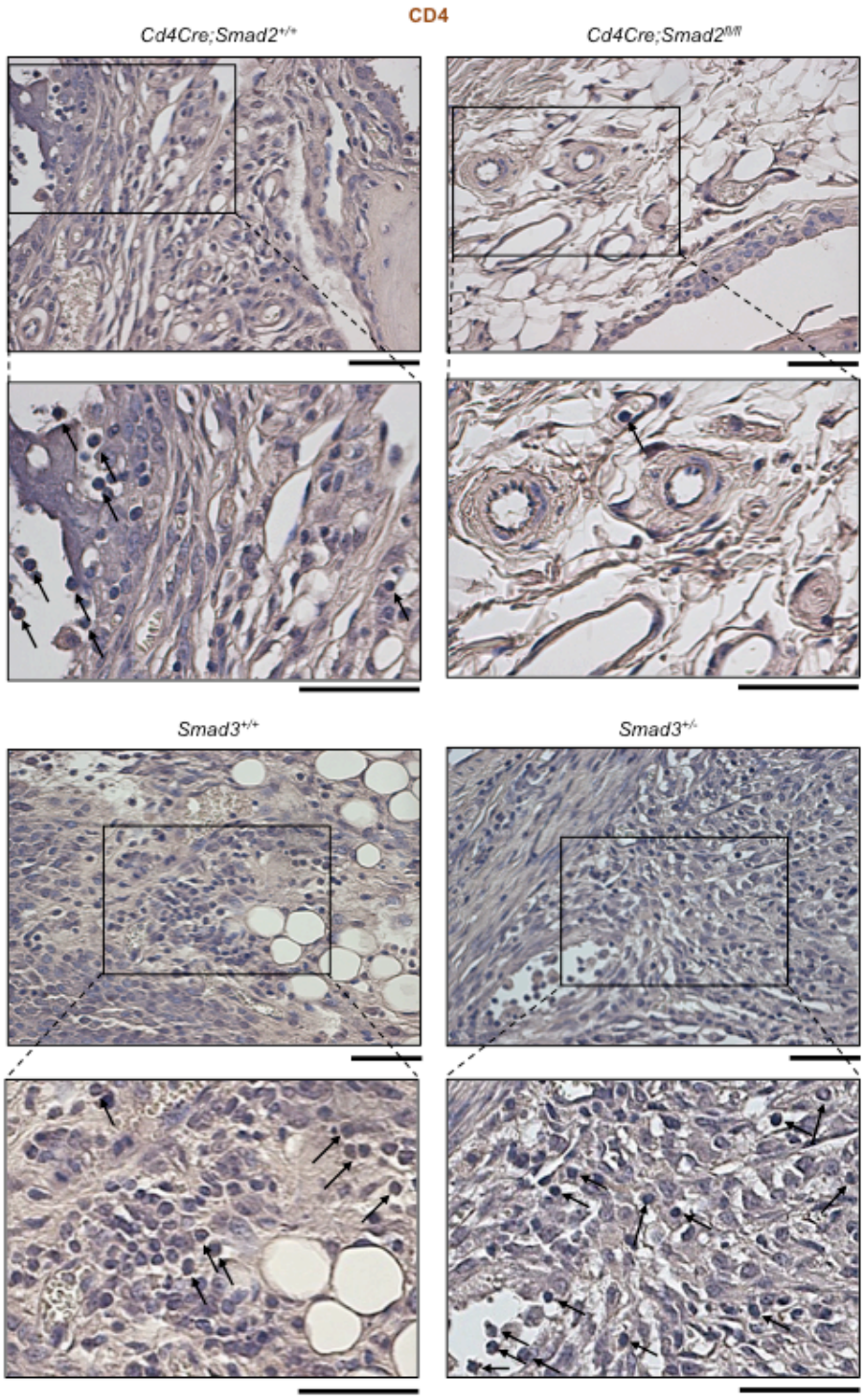

Figure 4 Accumulation of CD4$^+$ cells in the joint lesions was ameliorated in *Cd4Cre;Smad2$^{fl/fl}$* mice, whereas it was exacerbated in *Smad3$^{+/-}$* mice.

Immunohistochemistry staining of CD4$^+$ in the joint sections (magnification, ×400, scale bars: 50 μm). Data are from one experiment representative of two independent experiments (*Cd4Cre;Smad2* and *Smad3*, *n* = 10/genotype).

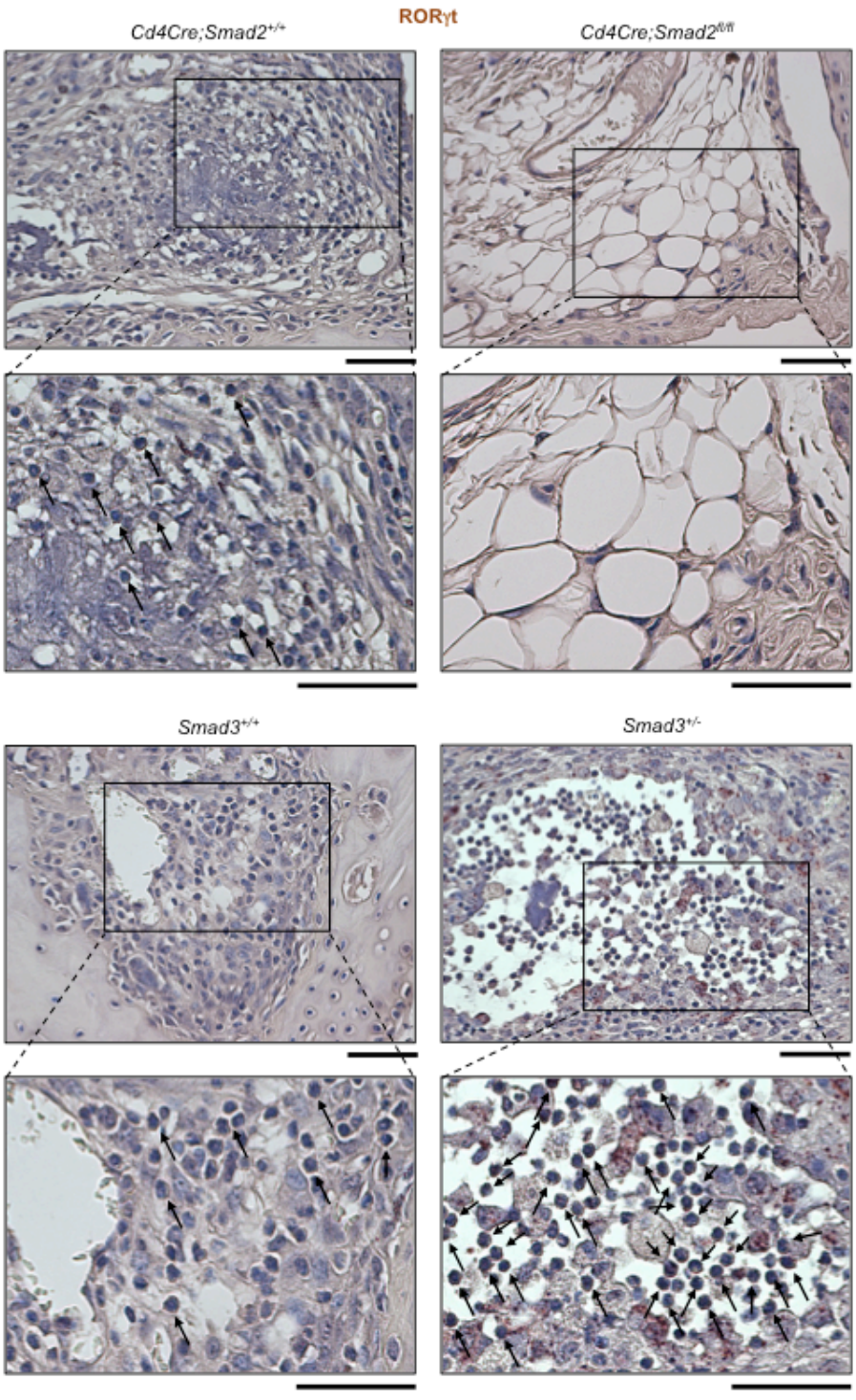

Figure 5 Accumulation of RORγt^{+} cells in the joint lesions was ameliorated in *Cd4Cre;Smad2$^{fl/fl}$* mice, whereas it was exacerbated in *Smad3$^{+/-}$* mice.

Immunohistochemistry staining of RORγt^{+} in the joint sections (magnification, ×400, scale bars: 50 μm). Data are from one experiment representative of two independent experiments (*Cd4Cre;Smad2* and *Smad3*, *n* = 10/genotype).

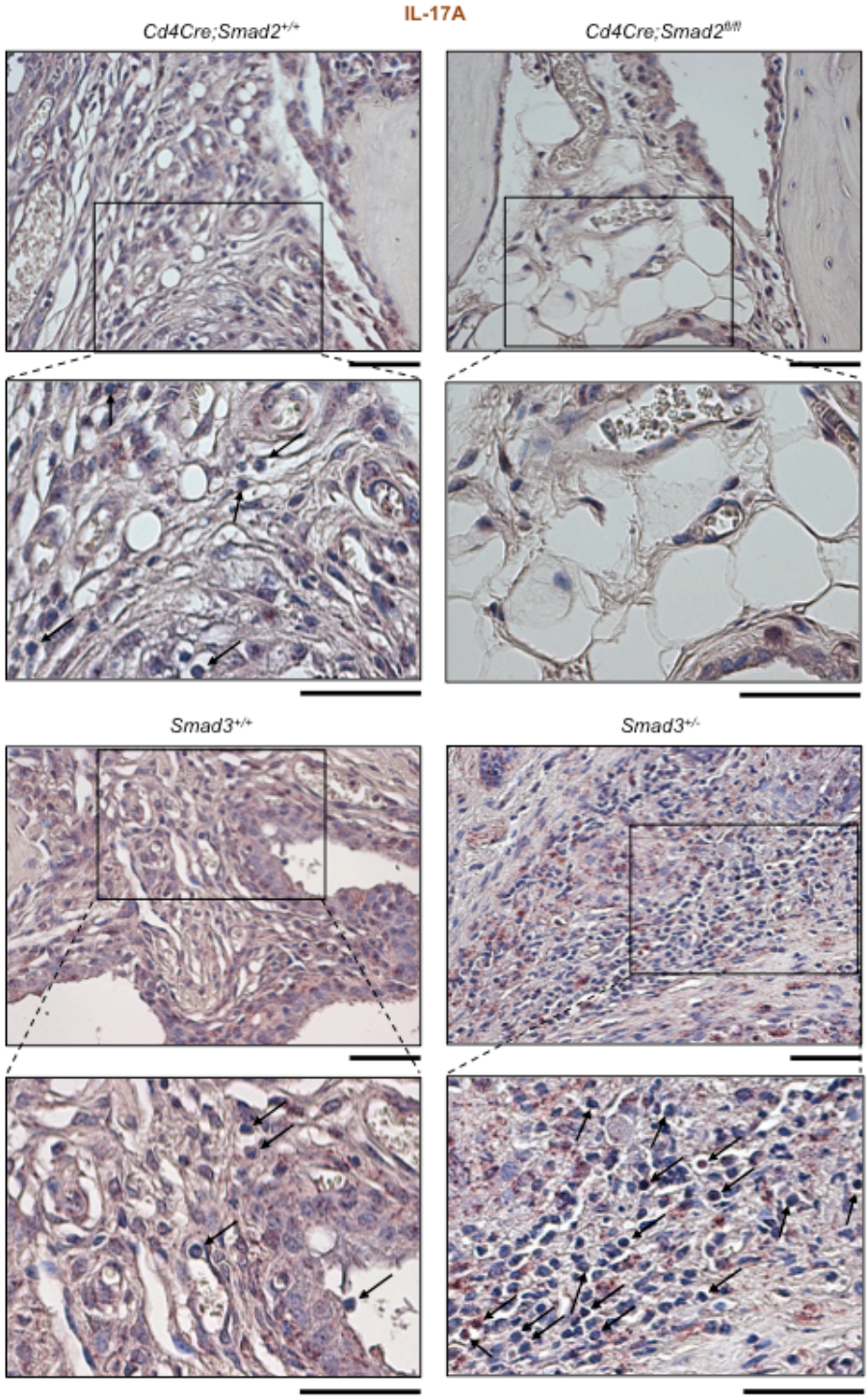

Figure 6 Accumulation of IL-17A^{+} cells in the joint lesions was ameliorated in *Cd4Cre;Smad2$^{fl/fl}$* mice, whereas it was exacerbated in *Smad3$^{+/-}$* mice.

Immunohistochemistry staining of IL-17A^{+} in the joint sections (magnification, ×400, scale bars: 50 μm). Data are from one experiment representative of two independent experiments (*Cd4Cre;Smad2* and *Smad3*, n = 10/genotype).

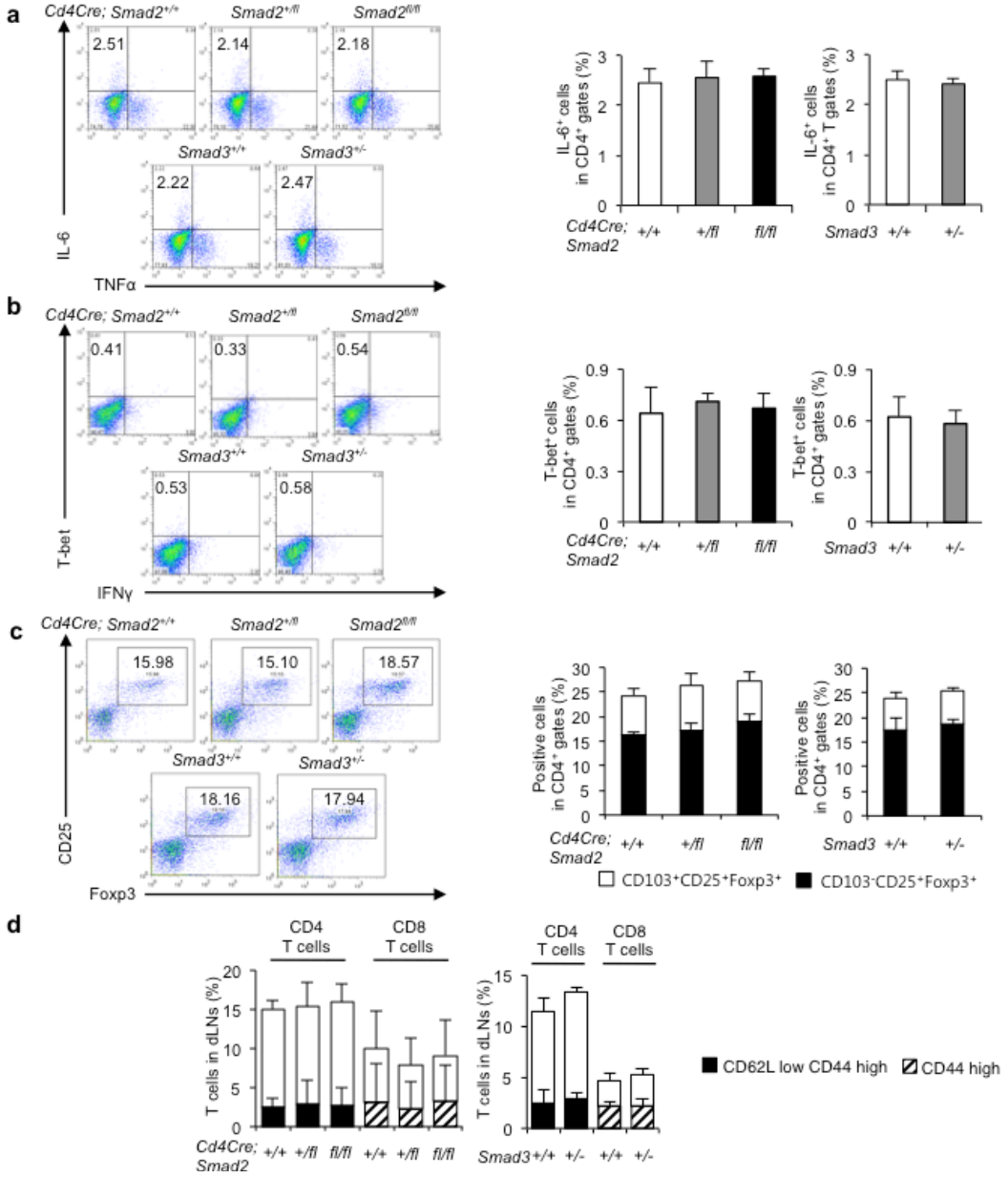

Figure 7 Disruption of Smad2 or Smad3 has no effect on effector T cell subsets except Th17 in CIA. Flow cytometry analyses of T cells in the draining lymph nodes of the arthritic joints from *Cd4Cre;Smad2*$^{+/+,\ +/fl,\ fl/fl}$ mice and *Smad3*$^{+/+,\ +/-}$ mice (**a**) IL-6^{+}TNF-α^{+} in CD4^{+} gates, (**b**) T-bet^{+}IFN-γ^{+} in CD4^{+} gates, (**c**) CD25^{+}Foxp3^{+} in CD4^{+} gates, CD103^{-}CD25^{+}Foxp3^{+} in CD4^{+} gates, CD103^{+}CD25^{+}Foxp3^{+} in CD4^{+} gates, (**d**) CD62L^{high}CD44^{low}, CD62L^{low}CD44^{high} CD4^{+} T cells and CD44^{low}, CD44^{high} CD8^{+} T cells (n = 10/genotype). Data are from one experiment representative of four (*Cd4Cre;Smad2*$^{+/+,\ fl/fl}$, n = 20/genotype, *Cd4Cre;Smad*$^{+/fl}$, n = 15) or three (*Smad3*, n = 15/genotype) independent experiments. Data are mean + s.d.

Opposing functions of Smad2 and Smad3 as STAT3 cofactors

IL-6 is the main arthritogenic cytokine and TGF-β is produced and activated in the inflammatory lesions (Li MO et al, 2006; Travis MA et al, 2014; Kimura A et al, 2010). Because IL-6 and TGF-β are the pivotal cytokines to induce Th17 differentiation, I cultured *Smad2*$^{-/-}$ or *Smad3*$^{-/-}$ CD4^{+} T cells under Th17-polarizing condition with IL-6 and TGF-β (Veldhoen M et al, 2006) to examine the mechanisms whereby R-Smads regulate Th17 differentiation. Expression levels of protein and mRNA of RORγt and IL-17A decreased in *Smad2*$^{-/-}$ CD4^{+} T cells, whereas those increased in *Smad3*$^{-/-}$ CD4^{+} T cells (**Fig. 8a**,**b**). The mRNA levels of Th17-inducing genes (*Batf*, *Il23r*, *Il6*, *Il6ra*, *Il21*, and *Il21r*) and Th17-suppressing genes (*Il2*, *Il2ra*, *Tbet*, and *Eomesodermin*) were unaffected in both *Smad2*$^{-/-}$ and *Smad3*$^{-/-}$ CD4^{+} T cells (**Fig. 9**), suggesting that R-Smads regulate Th17 differentiation by specifically targeting the *Rorc* and *Il17a* genes. Because IL-6 or TGF-β alone has little effect on Th17 differentiation (Veldhoen M et al, 2006) and STAT3-mediated IL-6 signaling is crucial for Th17 differentiation (Massague J et al, 2005), I examined whether R-Smads regulate STAT3-induced transcription of RORγt and IL-17A in CD4^{+} T cells cultured under Th17-polarizing condition by promoter assays with the luciferase reporters spanning 2 kilobase upstream of the first exons of the *Rorc* and *Il17a* genes (**Fig. 8c**). STAT3 or Smad2 alone induced their promoter activities, whereas Smad3 alone had no effect. Smad2 further enhanced, whereas Smad3 suppressed STAT3-induced reporter activation. Co-transfection of Smad4 with R-Smads and STAT3 did not show the additive effects. I next determined the binding of R-Smads to the proximal promoter regions of the *Rorc* and *Il17a* genes in Th17 cells by chromatin immunoprecipitation (ChIP) using the primers to detect the DNA-binding sequences of Smads and STAT3 (Heldin CH et al, 2012; Durant L et al, 2010; Yang XP et al, 2011). Smad2 and Smad3 were bound to the same sites in the *Rorc* promoter, whereas they were bound to the distinct sites in the *Il17a* promoter (**Fig. 8d**). Active promoters are characterized by histone acetylation and trimethylation of H3K4, whereas repressed inactive chromatin is marked by methylation of H3K27 and H3K9 (Gaarenstroom T et al, 2014). Smad2-binding sites in the *Il17a* promoter showed higher acetylation of histone H3 and trimethylation of histone H3K4, which correlate with transcriptionally active chromatin (**Fig. 10a**). By contrast, Smad3-binding sites in the *Il17a* promoter showed higher trimethylation of histone H3K27, which correlate with transcriptionally inactive chromatin (**Fig. 10b**). These data suggest that Smad2 and Smad3 have the opposing roles in STAT3-induced transcription of the *Rorc* and *Il17a* genes.

I next examined whether STAT3 was necessary for R-Smads to bind to these sites by STAT3 knockdown using siRNA in Th17 cells (**Fig. 11**). STAT3 knockdown completely abolished the binding of R-Smads to these sites (**Fig. 8e**). I then confirmed whether R-Smads are sufficient for STAT3 to bind to these sites using *Smad2*$^{-/-}$ and *Smad3*$^{-/-}$ Th17 cells. STAT3 bound to the Smad2/3-binding sites in the *Rorc* promoter or the Smad2-binding site in the *Il17a* promoter (**Fig. 8f**,**g**, white bars). Deficiency of Smad2 or Smad3 prevented STAT3 from binding to these sites (**Fig. 8f**,**g**, black bars). Thus, R-Smads and STAT3 are mutually required to bind to the proximal promoters of the *Rorc* and *Il17a* genes. Taken together,

Smad2 functions as a transcription coactivator, whereas Smad3 functions as a transcription corepressor of STAT3 in Th17 differentiation.

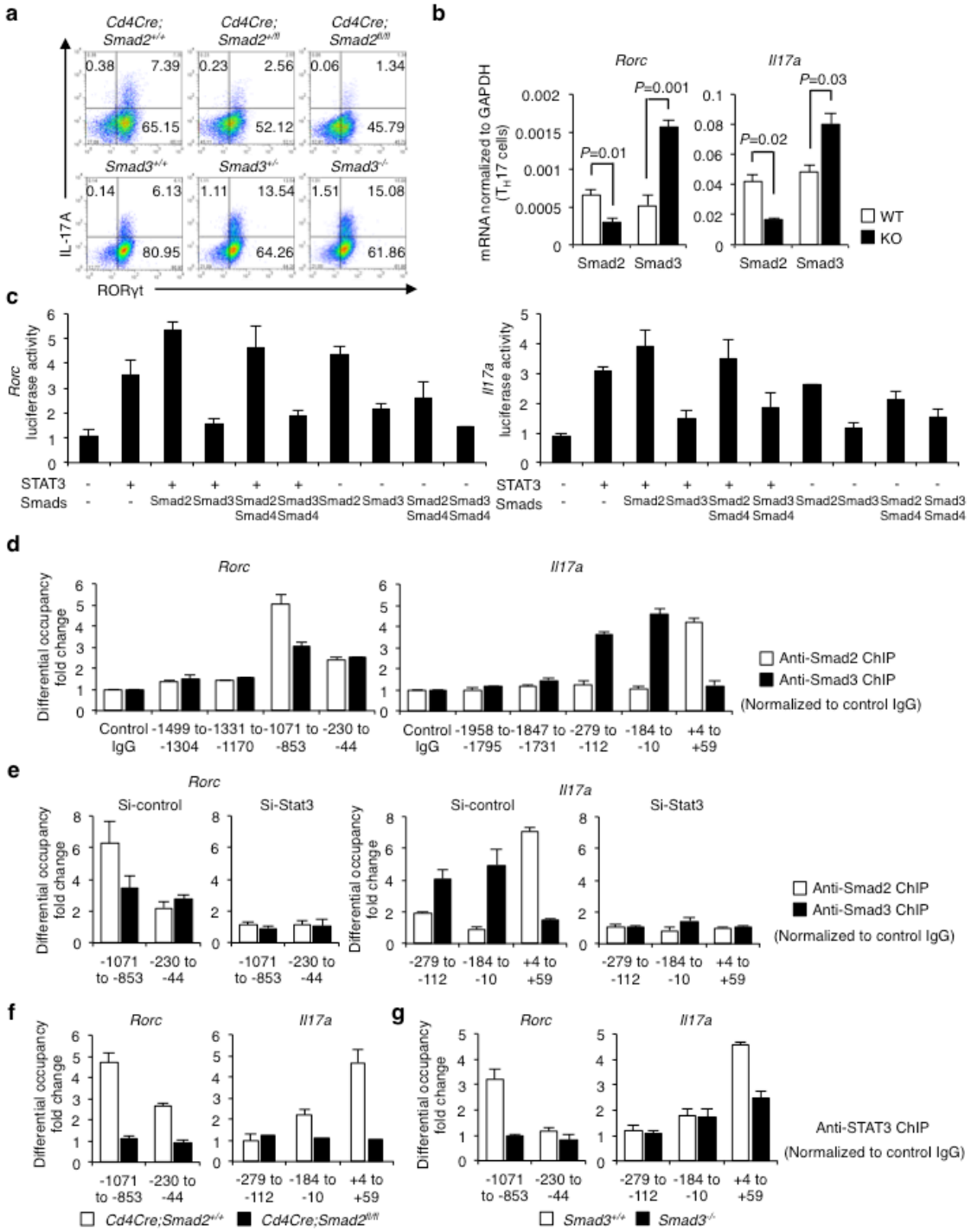

Figure 8 Opposing roles of Smad2 and Smad3 in STAT3-induced Th17 differentiation.

Purified $CD4^+$ T cells were activated under Th17-polarizing condition for 3 days. (**a**) Flow cytometry

analyses of IL-17A and RORγt in *Smad2*$^{+/+,+/-,\ -/-}$ and *Smad3*$^{+/+,+/-,\ -/-}$ CD4^{+} T cells. (**b**) Quantitative RT-PCR analysis of the *Il17a* and *Rorc* mRNA in *Smad2*$^{+/+,\ -/-}$ and *Smad3*$^{+/+,\ -/-}$ Th17 cells (n = 7). (**c**) Effects of Smads on STAT3-induced activation of the *Rorc* promoter and the *Il17a* promoter constructs transfected in Th17 cells were analyzed by luciferase assay. (**d**) Binding of Smad2 and Smad3 to the proximal promoter regions of the *Rorc* gene and the *Il17a* gene in Th17 cells was determined by ChIP. (**e**) Requirement of STAT3 for the binding of Smad2 and Smad3 to the proximal promoter regions of the *Rorc* gene and the *Il17a* gene was determined by ChIP using STAT3 knockdown Th17 cells. Requirement of Smad2 and Smad3 for the binding of STAT3 to the proximal promoter regions of the *Rorc* gene and the *Il17a* gene was determined by ChIP using (**f**) *Smad2*$^{-/-}$ or (**g**) *Smad3*$^{-/-}$ Th17 cells. ChIP data are shown as differential occupancy fold changes. Data are from one experiment representative of seven (**a**, **d**), three (**c**), two (**e**) or five (**f**, **g**) independent experiments or pooled from seven experiments (**b**). Each experiment (**a**-**g**) was performed in triplicate (n = 3). Data are mean + s.d. or mean + s.d. with P values (**b**, unpaired Student's t-test).

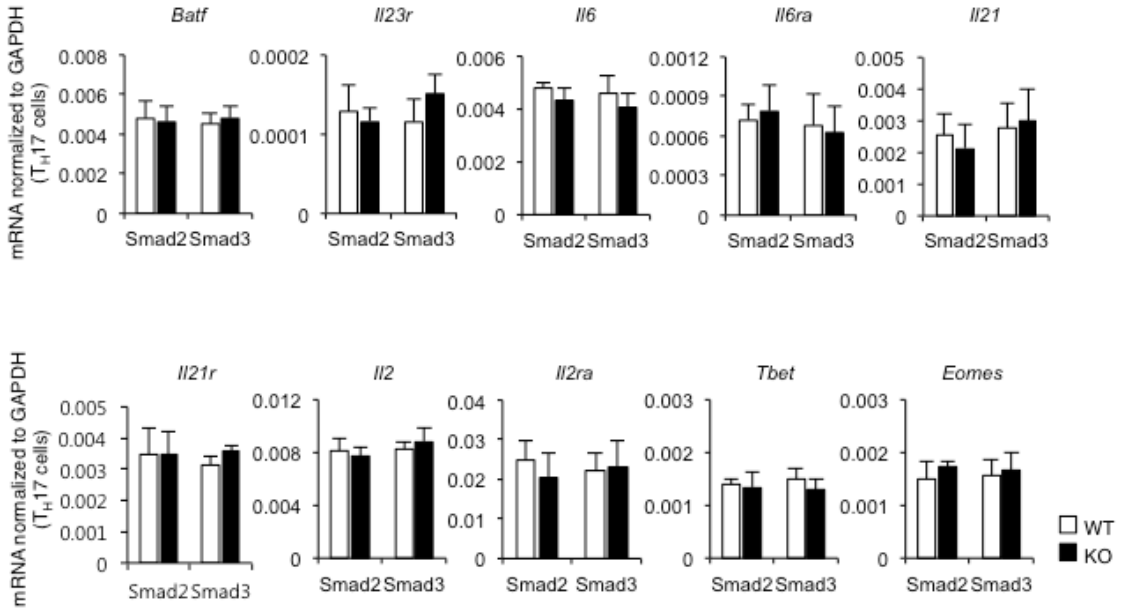

Figure 9 Disruption of Smad2 or Smad3 has no effect on Th17-related genes except the *Rorc* and *Il17a* genes.

Quantitative RT-PCR analysis of *Batf*, *Il23r*, *Il6*, *Il6ra*, *Il21*, *Il21r*, *Il2*, *Il2ra*, *Tbet*, *Eomes* to *Gapdh* in *Smad2*$^{+/+,\ -/-}$ and *Smad3*$^{+/+,\ \ -/-}$ Th17 cells. Data are pooled from three independent experiments. Each experiment was performed in triplicate (n = 3). Data are mean + s.d.

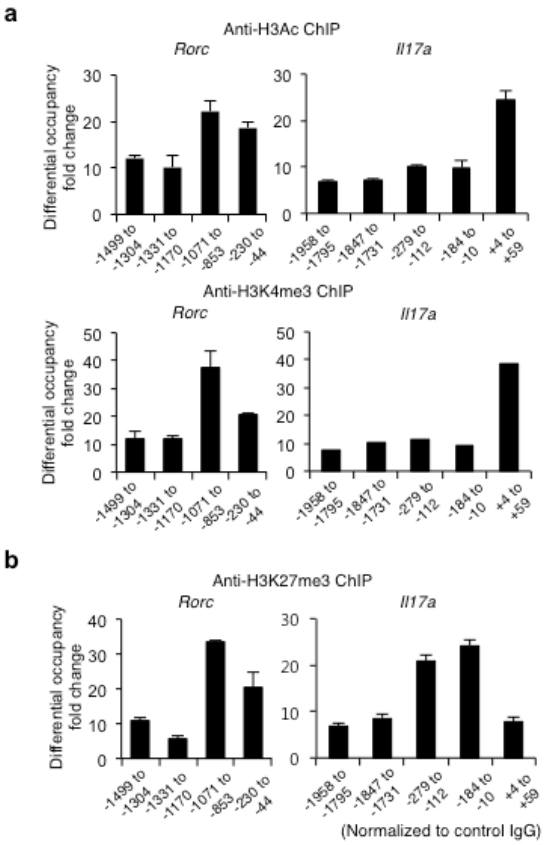

Figure 10 Smad2 binding sites are associated with active epigenetic marks, whereas Smad3 binding sites are associated with inactive epigenetic marks in the *Rorc* and *Il17a* promoter regions.

ChIP analysis of Th17 cells with antibodies against (**a**) acetylated histone H3 (H3Ac), trimethylated histone H3 Lys4 (H3K4me3), and (**b**) trimethylated histone H3 Lys 27 (H3K27me3). Data are from one experiment representative of two independent experiments. Each experiment was performed in triplicate (n = 3). Data are mean + s.d.

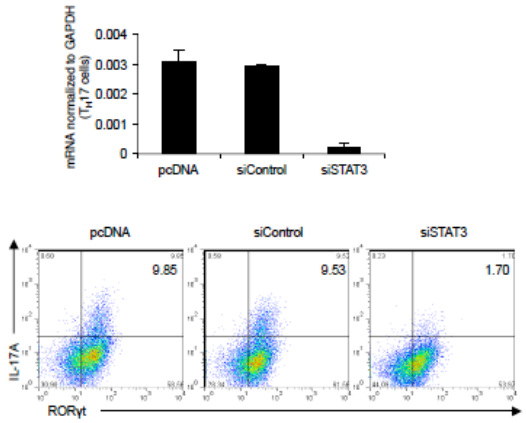

Figure 11 Knockdown of the *Stat3* gene using STAT3 siRNA in Th17 cells.

Stat3 mRNA levels in Th17 cells transduced with the controls or STAT3 siRNA were confirmed by quantitative RT-PCR. Flow cytometry analyses of IL-17A$^+$RORγt$^+$ in CD4$^+$ gates transduced with pcDNA, control siRNA or STAT3 siRNA in Th17-polarizing condition. Data are from one experiment representative of two independent experiments. Each experiment was performed in triplicate (n = 3). Data are mean + s.d.

Linker-phosphorylated Smad2 induces Th17 differentiation

I investigated the mechanism how Smad2 functions as a transcription coactivator of STAT3. Proximity ligation assays (PLA) confirmed the endogenous close proximity between Smad2 and STAT3 in Th17 cells (**Fig. 12a**, left). I found that pSmad2L had close proximity with STAT3 in Th17 cells (**Fig. 12a**, right). By contrast, C-terminally phosphorylated Smad2 (pSmad2C) did not show close proximity with STAT3 (**Fig. 12a**, middle). PLA and immunoprecipitation of 293T cells transfected with the various deletion mutants of Smad2 showed that Smad2 linker deletion mutants (MH1 and MH2) (Kawabata M et al, 1999) failed to bind with STAT3 (**Fig. 12b** and **13a**). Transfection of the linker variants of Smad2 showed that the mutant of the linker serine residue 255 to alanine: Smad2 (S255A) (Sekimoto G et al, 2007) failed to bind with STAT3 (**Fig. 12c** and **13b**). Luciferase reporter assays showed that Smad2 (S255A) failed to enhance STAT3-induced activation of the *Rorc* and *Il17* promoters (**Fig. 12d**). Overexpression of Smad2 (S255A) in $CD4^+$ T cells cultured under Th17-polarizing condition impaired Th17 differentiation (**Fig. 12e**). Therefore, pSmad2L (Ser255) is essential for Th17 differentiation.

The histone acetyl-transferase p300 is a crucial transcription coactivator of Smads (Massague J et al, 2005; Janknecht R et al, 1998). PLA showed that STAT3 and pSmad2L, but not pSmad2C, had the close proximity with p300 in Th17 cells (**Fig. 12f**). Luciferase reporter assays confirmed that p300 further enhanced Smad2/STAT3-induced activation of the *Rorc* and *Il17* promoters in 293T cells (**Fig. 12g**). Smad2, STAT3, and p300 bound to the same sites in the proximal promoters of the *Rorc* and *Il17a* genes in T_H17 cells (**Fig. 12h**). Thus, pSmad2L (Ser255) forms complex with p300 and STAT3 to bind to the proximal promoter of the *Rorc* and *Il17a* genes.

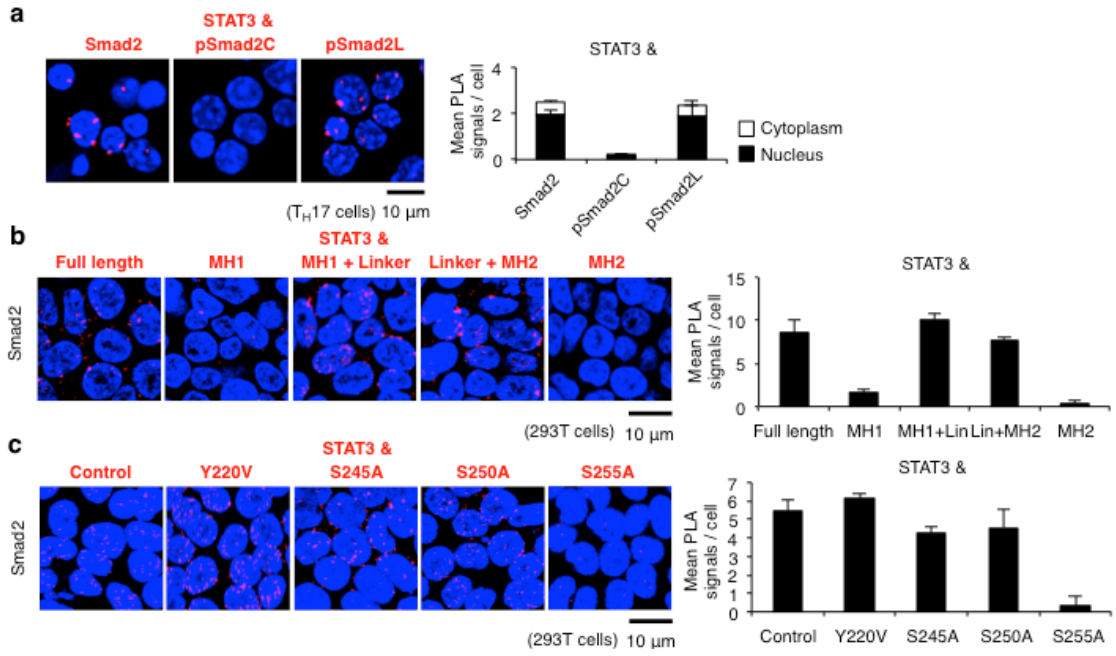

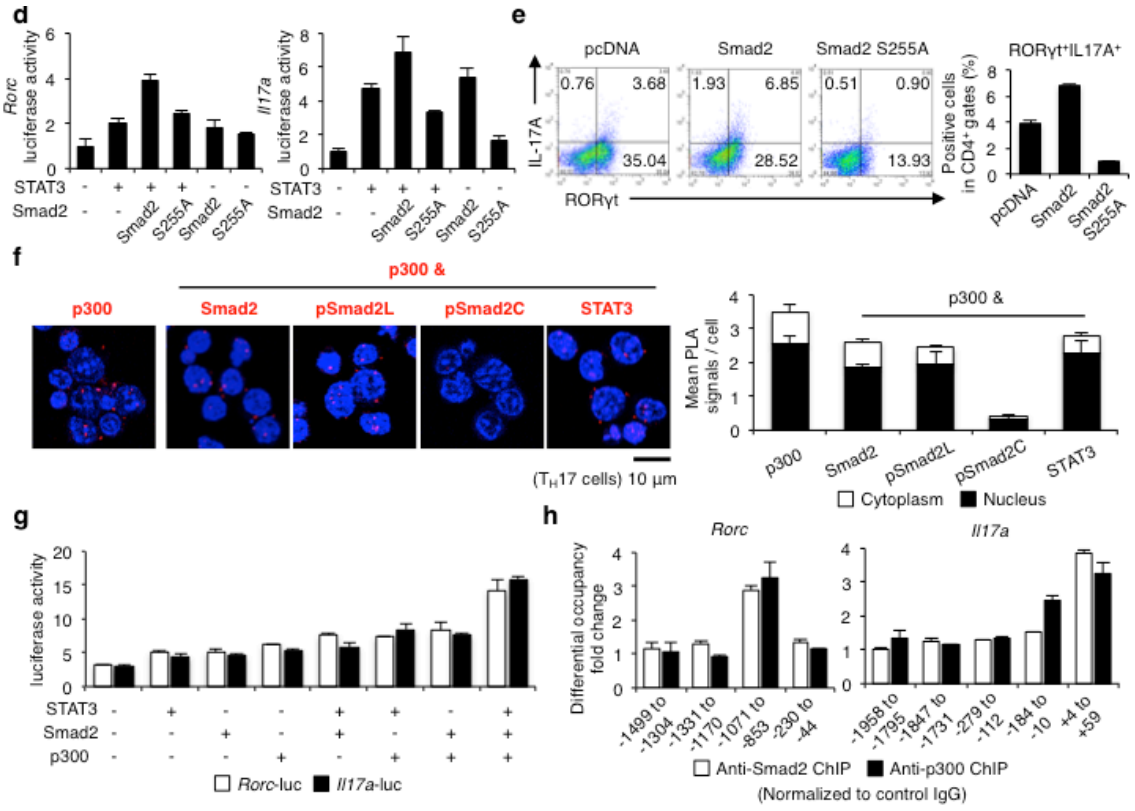

Figure 12 Linker-phosphorylated Smad2 (S255)-STAT3-p300 complex transactivates the *Rorc* and *Il17a*.

Interactions of endogenous proteins in Th17 cells and exogenous proteins in 293T cells were determined by proximity ligation assay (PLA). PLA signals (**a-c**, **f**) were quantified using BlobFinder software (scale bars: 10 μm, nucleus: black, cytoplasm: white, *n* = 10 fields). (**a**) Endogenous interaction between Smad2 and STAT3 in Th17 cells. (**b**) Effects of truncated mutations in Smad2 on the interaction with STAT3 in 293T cells. (**c**) Effects of linker domain variations in Smad2 on the interaction with STAT3 in 293T cells. (**d**) Effects of Smad2 (S255A) on STAT3-induced activation of the *Rorc* promoter and the *Il17a* promoter constructs transfected in Th17 cells were analyzed by luciferase assay. (**e**) Flow cytometry analyses of IL-17A$^+$RORγt$^+$CD4$^+$ T cells transduced with the indicated DNA constructs using Nucleofector (n = 2). (**f**) Endogenous interactions between p300 and Smad2 or STAT3 in Th17 cells were determined by PLA. (**g**) Effects of p300 on Smad2/STAT3-induced activation of the *Rorc* promoter (white) and the *Il17a* promoter (black) constructs transfected in 293T cells were analyzed by luciferase assay. (**h**) Binding of Smad2 (white) and p300 (black) to the proximal promoter regions of the *Rorc* gene and the *Il17a* gene in Th17 cells was determined by ChIP. ChIP data are shown as differential occupancy fold changes. Data are from one experiment representative of six (**a**), three (**b-d**) or two (**e-h**) independent experiments. Each experiment (**d**, **g**, **h**) was performed in triplicate (*n* = 3). Data are mean + s.d.

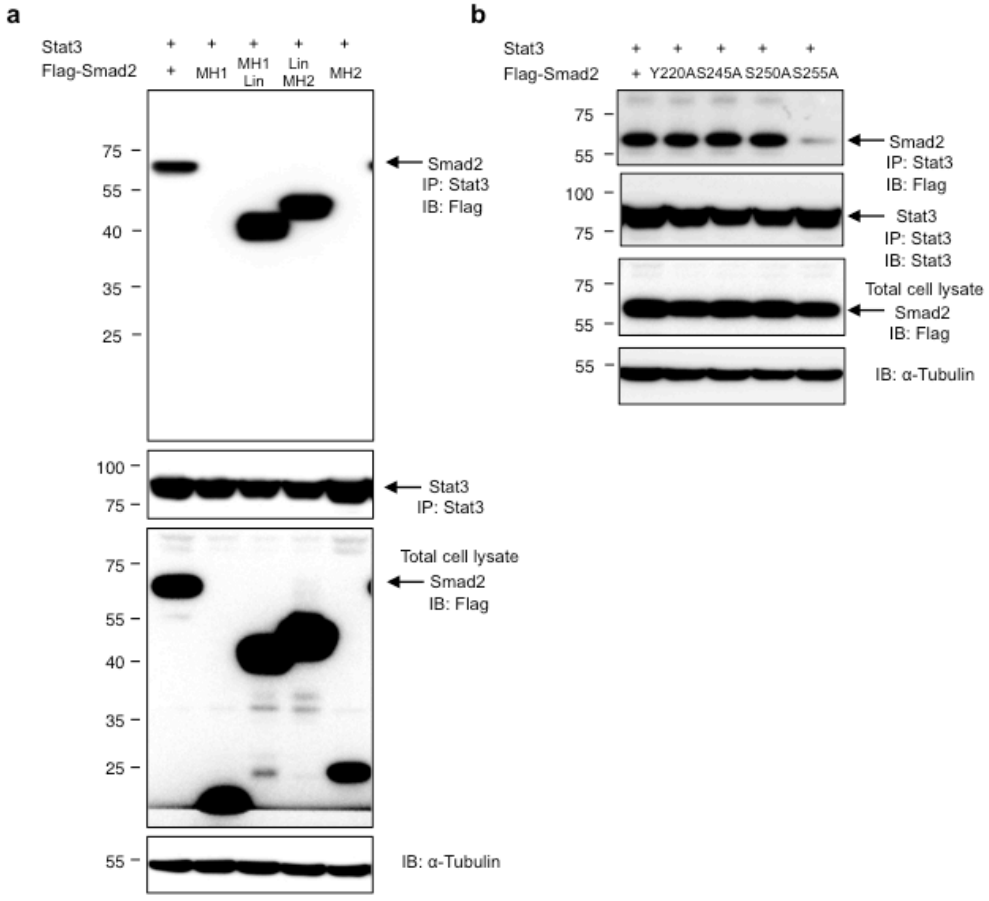

Figure 13 Linker-phosphorylated Smad2 at S255 interacts with STAT3.

Interactions of exogenous Smad2 proteins and STAT3 protein in 293T cells were determined by immunoprecipitation. (**a**) Effects of truncated mutations in Smad2 on the interaction with STAT3 in 293T cells. (**b**) Effects of linker domain variations in Smad2 on the interaction with STAT3 in 293T cells. Data are from one experiment representative of three independent experiments.

Unphosphorylated Smad3 suppresses Th17 differentiation

I investigated the mechanism how Smad3 functions as a transcription corepressor of STAT3. PLA confirmed the endogenous close proximity between Smad3 and STAT3 in Th17 cells (**Fig. 14a**). Unlike R-Smads, Smad4 did not interact with STAT3 (**Fig. 14a**). Although STAT5 and STAT3 oppositely regulate Th17 differentiation by binding the multiple common sites across the locus encoding IL-17 (Yang XP et al, 2011), neither Smad2 nor Smad3 interacted with STAT5 (**Fig. 15**). Furthermore, interactions between Smad2/3 and STAT3 were more significant than the established interaction controls: pSmad2/3C-Smad4 (Massague J et al, 2005; Heldin CH et al, 2012) and Smad2/3-RORγt (Martinez GJ et al, 2009; Martinez GJ et al, 2010) (**Fig. 16**). PLA and immunoprecipitation of 293T cells transfected with the various deletion mutants of Smad3 showed that Smad3 MH2 deletion mutants (MH1 and MH1+L) (Kawabata M et al, 1999; Sekimoto G et al, 2007) failed to bind with STAT3 (**Fig. 14b** and **Fig. 17**). Thus, MH2 domain is required for Smad3 to bind STAT3.

PIAS3 belongs to the mammalian protein inhibitor of activated STAT (PIAS) protein family, which represses STAT3-dependent transcriptional activation by blocking the DNA-binding activity of STAT3, regardless of its small ubiquitin-like modifier-E3 ligase activity (Chung CD et al, 1997). Overexpression of Smad3, the deletion mutant lacking MH2 domain, or the C-terminal mutant in Th17 cells show that Smad3 MH2 domain, but not C-terminal SSXS motif, is functionally responsible for the suppression of Th17 differentiation (**Fig. 14c**). Because PIAS3 interacts with Smad3 at its C-terminal domain (Long J et al, 2004), I examined whether Smad3 recruits PIAS3 to repress STAT3-induced transcription of the *Rorc* and *Il17a* genes. PIAS3 showed the close proximity with both STAT3 and Smad3, but not with C-terminally phosphorylated Smad3 (pSmad3C) or Smad2 in Th17 cells (**Fig. 14d**). STAT3-PIAS3 interaction was completely abolished in *Smad3*$^{-/-}$ Th17 cells (**Fig. 14e**). A mutant of serine residues to alanine in Smad3 SSXS motif, Smad3 (3S-A) was yet capable of binding with STAT3 and PIAS3 in 293T cells (**Fig. 14f**). Consistently, when co-transfected with PIAS3 in Th17 cells, Smad3 (3S-A) was able to suppress STAT3-induced activation of the *Rorc* and *Il17a* reporters (**Fig. 14g**). ChIP revealed that PIAS3 and Smad3, but not pSmad3C, bound to the same sites in the *Rorc* and *Il17a* promoters (**Fig. 14h** and **Fig. 18**). Thus, C-terminal phosphorylation is not required for Smad3 to bind with STAT3 and PIAS3. Overexpression of PIAS3 suppressed Th17 differentiation, whereas knockdown of PIAS3 by siRNA abolished the binding of Smad3 to the *Rorc* and *Il17a* promoter regions, although Th17 differentiation was unaltered by knockdown of PIAS3 presumably because relatively predominant binding of Smad2 over Smad3 in the absence of PIAS3 transactivated the *Rorc* and *Il17a* genes (**Fig. 19**). These data indicate that unphosphorylated Smad3C in cooperation with PIAS3 represses STAT3-induced transcription of the *Rorc* and *Il17a* gene

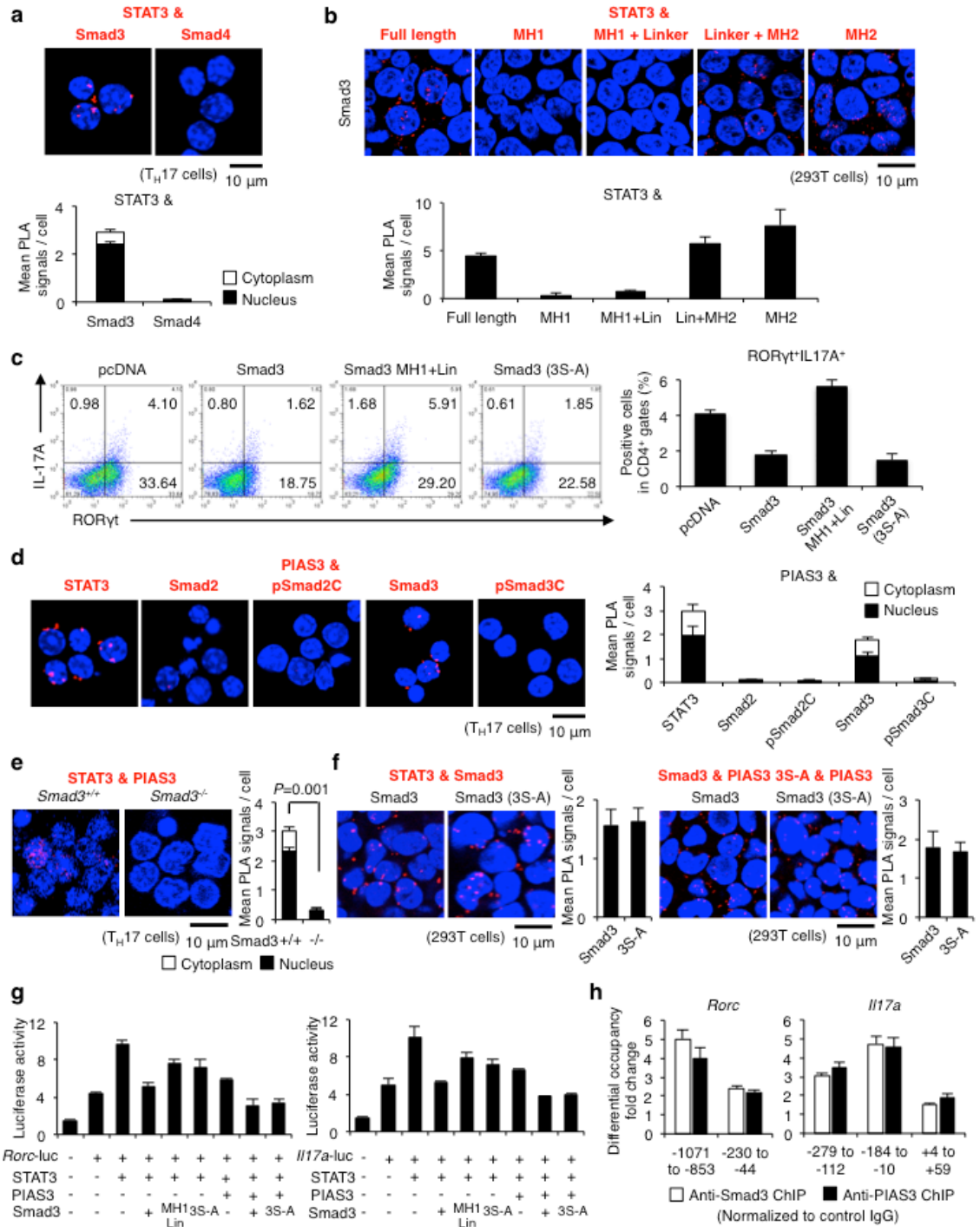

Figure 14 C-terminally unphosphorylated Smad3 recruits PIAS3 to act as a transcription corepressor of STAT3 in Th17 differentiation.

Interactions of endogenous proteins in Th17 cells and exogenous proteins in 293T cells were determined by PLA. PLA signals (**a**, **b**, **d**-**f**) were quantified using BlobFinder software (scale bars: 10 μm, nucleus: black, cytoplasm: white, *n* = 10 fields). (**a**) Endogenous interactions between Smad3/Smad4 and STAT3 in Th17 cells. (**b**) Effects of truncated mutations in Smad3 on the interaction with STAT3 in 293T cells.

(**c**) Flow cytometry analyses of IL-17A^{+}RORγt^{+}CD4^{+} T cells transduced with the indicated DNA constructs using Nucleofector (n = 4). (**d**) Endogenous interactions between PIAS3 and STAT3/Smad2/Smad3 in Th17 cells. (**e**) Endogenous interaction between PIAS3 and STAT3 in *Smad3*$^{+/+, -/-}$ Th17 cells. (**f**) Effects of Smad3 C-terminal mutation on the interaction with STAT3 (left) or the interaction with PIAS3 (right) in 293T cells. (**g**) Effects of PIAS3, Smad3 MH2 deletion, and Smad3C-terminal mutation on STAT3-induced activation of the *Rorc* promoter and the *Il17a* promoter constructs transfected in Th17 cells were determined by luciferase assay. (**h**) Binding of Smad3 (white) and PIAS3 (black) to the *Rorc* and the *Il17a* promoter regions in Th17 cells was determined by ChIP (differential occupancy fold changes). A representative of six (**a**), three (**b**, **f**, **g**), four (**c**, **d**) or two (**e**, **h**) independent experiments is shown. Each experiment (**g**, **h**) was performed in triplicate (n = 3). Data are mean + s.d. or mean + s.d. with P values (**e**, unpaired Student's t-test).

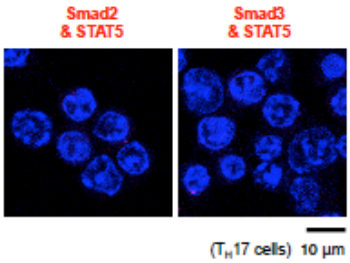

Figure 15 TGF-β R-Smads do not interact with STAT5 in Th17 cells.

PLA shows no close proximity between Smad2/3 and STAT5 in Th17 cells (scale bar: 10 µm). Data are from one experiment representative of three independent experiments.

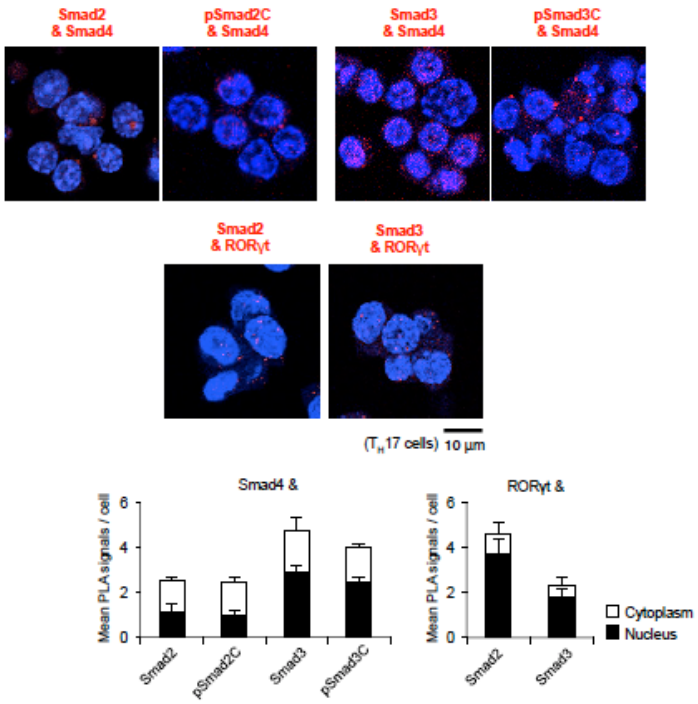

Figure 16 TGF-β R-Smads show close proximity with Smad4 or RORγt in Th17 cells.

PLA shows the endogenous close proximity between Smad2-Smad4, pSmad2C-Smad4, Smad3-Smad4, pSmad3C-Smad4, Smad2-RORγt, and Smad3-RORγt in Th17 cells. PLA signals were quantified using BlobFinder software (scale bars: 10 μm, nucleus: black, cytoplasm: white, *n* = 10 fields). Data are from one experiment representative of three independent experiments. Data are mean + s.d.

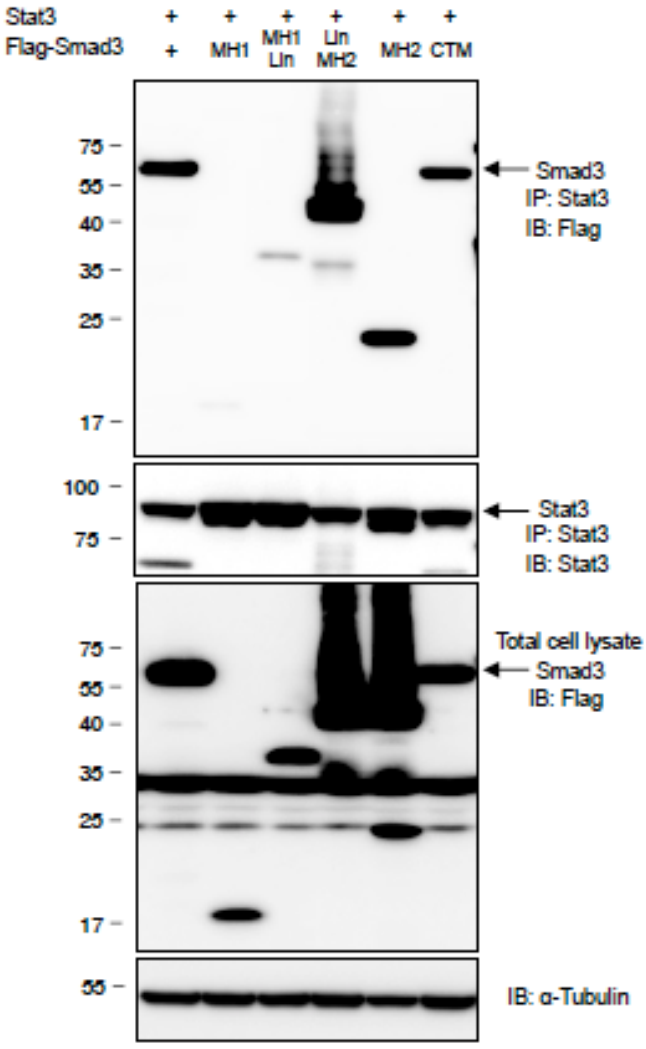

Figure 17 Smad3 MH2 domain interacts with STAT3.

Interactions of Smad3 or various Smad3 mutants and STAT3 in 293T cells were determined by immunoprecipitation. Data are from one experiment representative of three independent experiments.

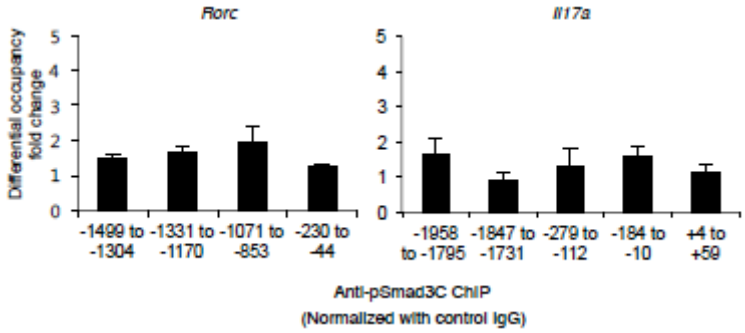

Figure 18 C-terminally phosphorylated Smad3 does not bind to the PIAS3/Smad3-binding sites in the *Rorc* and *Il17a* proximal promoter regions in Th17 cells.

ChIP with the antibody against pSmad3C shows that pSmad3C does not bind to the PIAS3/Smad3-binding sites in the *Rorc* and *Il17a* proximal promoter regions of Th17 cells. Data are from one experiment representative of two independent experiments. Each experiment was performed in triplicate (n = 3). Data are mean + s.d.

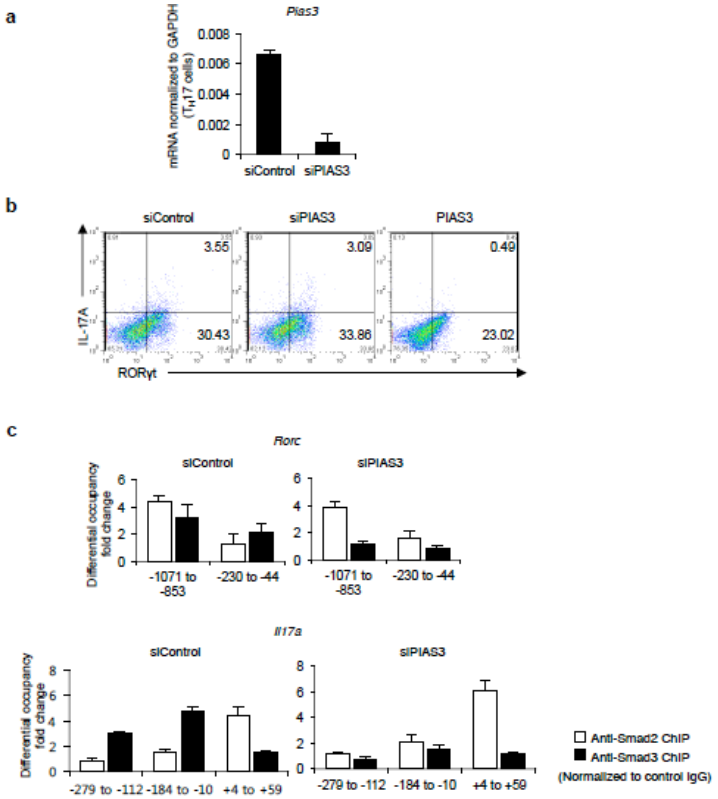

Figure 19 PIAS3 is required for Smad3 to bind to the *Rorc* and the *Il17a* promoter regions.

(a) PIAS3 mRNA levels in Th17 cells transduced with the control siRNA or PIAS3 siRNA were confirmed by quantitative RT-PCR. (b) Flow cytometry analyses of IL-17A$^+$RORγt$^+$CD4$^+$ T cells transduced with control siRNA, PIAS3 siRNA or PIAS3 in Th17-polarizing condition. (c) ChIP analysis of Th17 cells transduced with control siRNA or PIAS3 siRNA with the antibodies against Smad2 and Smad3. One experiment was performed in triplicate (n = 3). Data are mean + s.d.

ERK phosphorylates Smad2 linker in Th17 differentiation

Previous studies have paid attention to C-terminal phosphorylation of R-Smads as TGF-β signaling mediators in Th17 differentiation (Xiao S et al, 2008; Martinez GJ et al, 2009; Lu L et al, 2010; Martinez GJ et al, 2010; Malhotra N et al, 2010; Takimoto T et al, 2010). However, pSmad2L (Ser255) and unphosphorylated Smad3 are not involved in the canonical C-terminally phosphorylated R-Smad/Smad4-mediated TGF-β signaling. Three clustered serine residues in the linker regions of Smad2 (Ser245/250/255) are the phosphorylation sites for MAPKs (ERK, JNK, and p38) (Kretzschmar M et al, 1999; Massague J et al, 2003; Wrighton KH et al, 2009; Heldin CH et al, 2012; Matsuzaki K et al, 2013). Because MAPKs are shared by TGF-β, IL-6, and TCR, I sought to identify the MAPK responsible for Smad2 linker phosphorylation in Th17 differentiation.

Signal intensities of TGF-β, IL-6, and TCR have been reported to correlate with the extent of Th17 differentiation (Veldhoen M et al, 2006; Manel N et al, 2008; Hirahara K et al, 2010). Therefore, I treated $CD4^+$ T cells under Th17-polarizing condition with various concentrations of TGF-β, IL-6, and anti-CD3 antibody. I confirmed that higher doses of TGF-β1, anti-CD3 antibody, and IL-6 induced more Th17 differentiation (**Fig. 20a, 21a** and **22a**). Percentages of $IL\text{-}17A^+ROR\gamma t^+CD4^+$ T cells were directly proportional to phosphorylation of Smad2L (**Fig. 20b, 21b** and **22b**) and ERK, but not to phosphorylation of JNK or p38 (**Fig. 20c**, **23** and **24**).

To confirm whether TβRI-mediated phosphorylation of Smad2L is required for Th17 differentiation, I treated $CD4^+$ T cells under Th17-polarizing condition with specific inhibitors against TβRI (Yoon JH et al, 2013) at the doses that maintain cell viability (**Fig. 25**). A potent selective ATP-competitive inhibitor of TβRI kinase (activin receptor-like kinase5: ALK5), EW-7197 (Yoon JH et al, 2013; Jin CH et al, 2014) completely suppressed Th17 differentiation at the dose of 0.5 mM (**Fig. 20d**). Treatment with EW-7197 suppressed pSmad2L (**Fig. 20e**) and phosphorylation of ERK, but not phosphorylation of JNK and p38 (**Fig. 20f** and **Fig. 26**). One of the prototype ALK5 inhibitors, SB-505124 inhibits TGF-β-induced activation of MAPKs without altering ALK5-independent MAP kinase pathways (DaCosta Byfield S et al, 2004). A more highly selective ALK5 inhibitor, EW-7197 does not directly inhibit MEK1 and ERK1 (Jin CH et al, 2014). Therefore, inhibitory effect of EW-7197 on ERK phosphorylation is ALK5-specific. Culture media containing IL-6, IL-23, and IL-1β is sufficient to induce Th17 in the absence of TGF-β (Ghoreschi K et al, 2010). However, EW-7197 inhibited, whereas TGF-β1 enhanced Th17 differentiation along with ERK phosphorylation even in this culture condition (**Fig. 27**). These results suggest that TGF-β-TβRI signal phosphorylates ERK and pSmad2L in Th17 cells.

To confirm whether ERK-mediated phosphorylation of Smad2L is required for Th17 differentiation, I next treated $CD4^+$ T cells under Th17-polarizing condition with specific inhibitors against MAPKs at the doses that maintain cell viability (**Fig. 28 and 29**). A MEK inhibitor: PD98059 suppressed Th17 differentiation in a dose dependent manner (**Fig. 20g** and **28**), whereas a JNK inhibitor: SP600125 or p38 inhibitor: SB203580 did not affect Th17 differentiation (**Fig. 29**). PD98059 showed the similar effects

with EW-7197 on pSmad2L (**Fig. 20h**). Specific inhibition of MAP kinase by the corresponding inhibitor was confirmed (**Fig. 30**). Taken together, ERK-mediated Smad2 linker phosphorylation is responsible for Th17 differentiation and the concentrations of TGF-β, TCR, and IL-6 determine the intensities of Smad2 linker phosphorylation and the extent of Th17 differentiation.

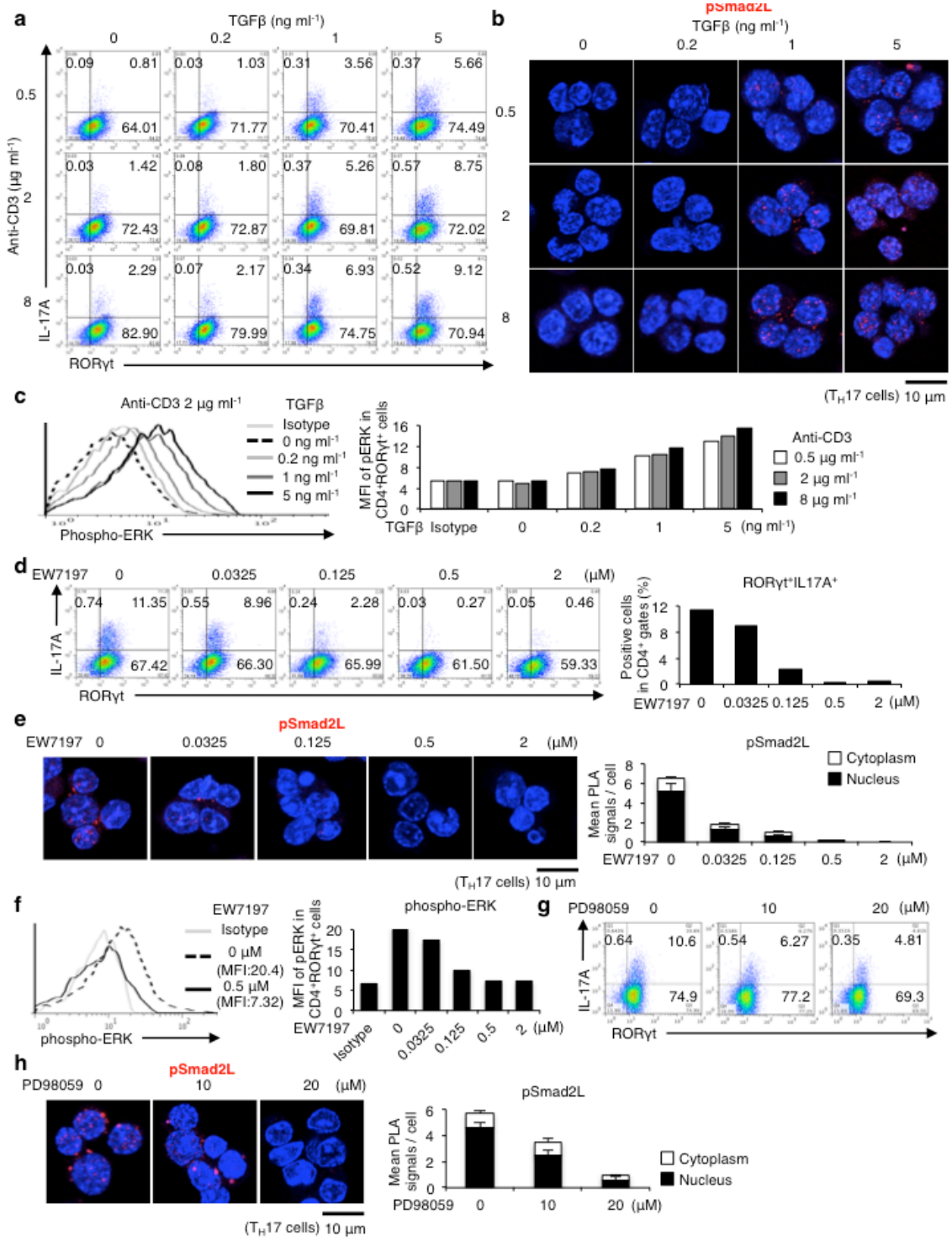

Figure 20 ERK induces Smad2 linker phosphorylation that facilitates Th17 differentiation.

Purified $CD4^+$ T cells were activated under Th17-polarizing condition with the indicated doses of TGF-β1 and plate-coated anti-CD3 antibody, or small molecule inhibitors (EW-7197: ALK5 inhibitor, PD98059: MEK inhibitor) for 3 days. (**a**) Flow cytometry analyses of IL-$17A^+$$ROR\gamma t^+$$CD4^+$ T cells treated with TGF-β1 and plate-coated anti-CD3 antibody. (**b**) Endogenous expression of pSmad2L in Th17 cells treated with TGF-β1 and plate-coated anti-CD3 antibody was determined by PLA. (**c**) Flow cytometry analyses of phospho-ERK in Th17 cells treated with TGF-β1 and plate-coated anti-CD3 antibody. (**d**) Flow cytometry analyses of IL-$17A^+$$ROR\gamma t^+$$CD4^+$ T cells treated with EW-7197. (**e**) Endogenous expression of pSmad2L in Th17 cells treated with EW-7197 was determined by PLA. (**f**) Flow cytometry analyses of phospho-ERK in T_H17 cells treated with EW-7197. (**g**) Flow cytometry analyses of IL-$17A^+$$ROR\gamma t^+$$CD4^+$ T cells treated with PD98059. (**h**) Endogenous expression of pSmad2L in Th17 cells treated with PD98059 was determined by PLA. The values of mean fluorescence intensity (MFI) are shown in histograms. PLA signals (**b**, **e**, **h**) were quantified using BlobFinder software (scale bars: 10 μm, nucleus: black, cytoplasm: white, n = 10 fields). Data are representative of two (**a**-**h**) independent experiments. Data are mean + s.d.

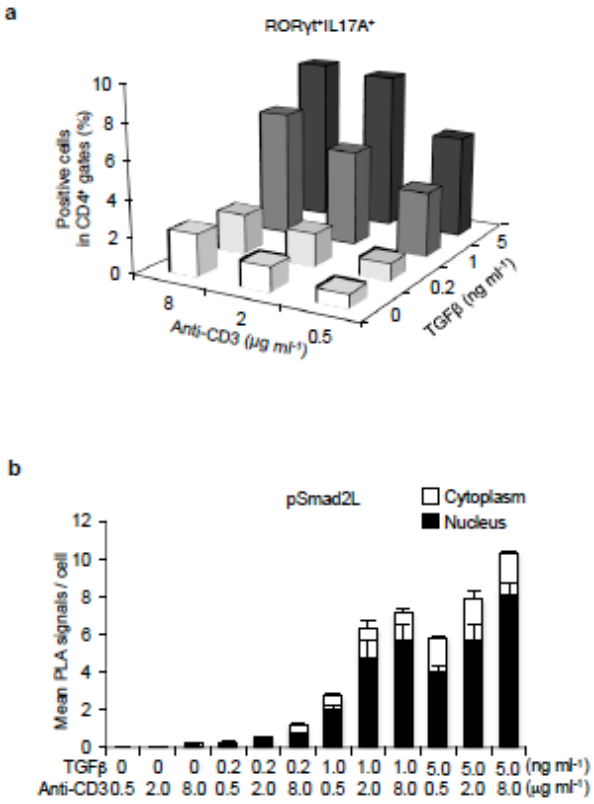

Figure 21 Strength of TGF-β and TCR signals correlate with Th17 differentiation and pSmad2L.
Purified $CD4^+$ T cells were activated under Th17-polarizing condition with the indicated doses of TGF-β and plate-coated anti-CD3 for 3 days. (**a**) Percentages of IL-$17A^+$$ROR\gamma t^+$$CD4^+$ T cells determined by flow cytometry. (**b**) Expression of pSmad2L in $CD4^+$ T cells determined by PLA. PLA signals were

quantified using BlobFinder software (nucleus: black, cytoplasm: white, *n* = 10 fields). Data are from one experiment representative of two independent experiments. Data are mean + s.d.

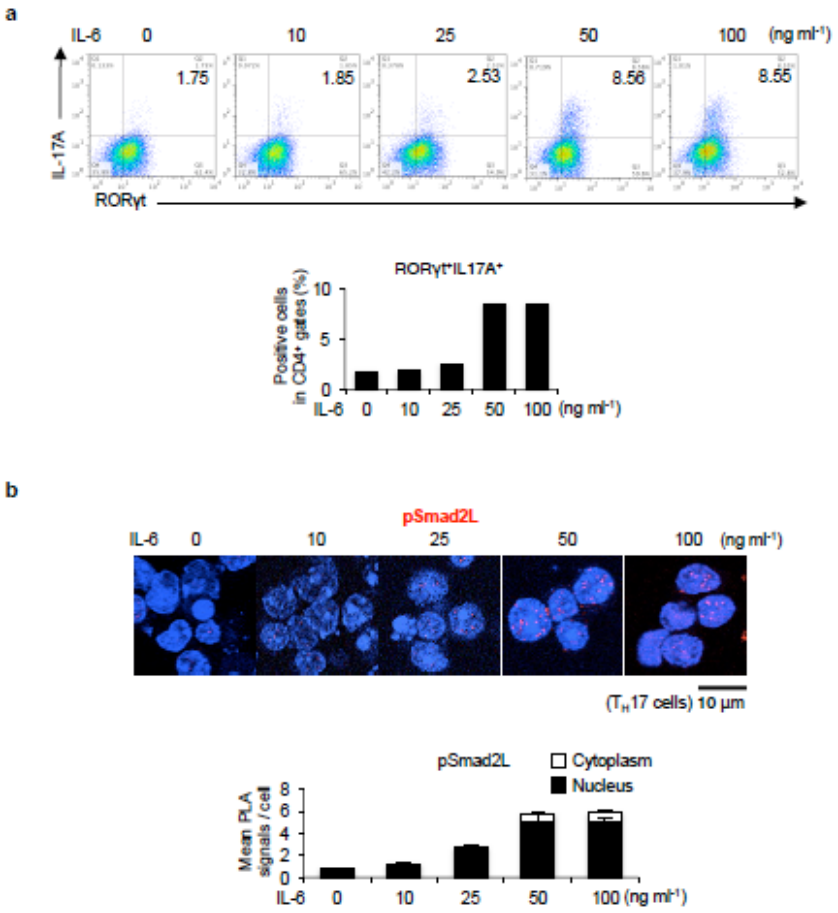

Figure 22 IL-6 doses correlate with Th17 differentiation.

Purified $CD4^+$ T cells were activated under Th17-polarizing condition with the indicated doses of IL-6 for 3 days. (**a**) Flow cytometry analyses of $IL\text{-}17A^+ROR\gamma t^+CD4^+$ T cells. (**b**) Expression of pSmad2L in $CD4^+$ T cells determined by PLA. PLA signals were quantified using BlobFinder software (scale bars: 10 µm, nucleus: black, cytoplasm: white, *n* = 10 fields). Data are from one experiment representative of two independent experiments. Data are mean + s.d.

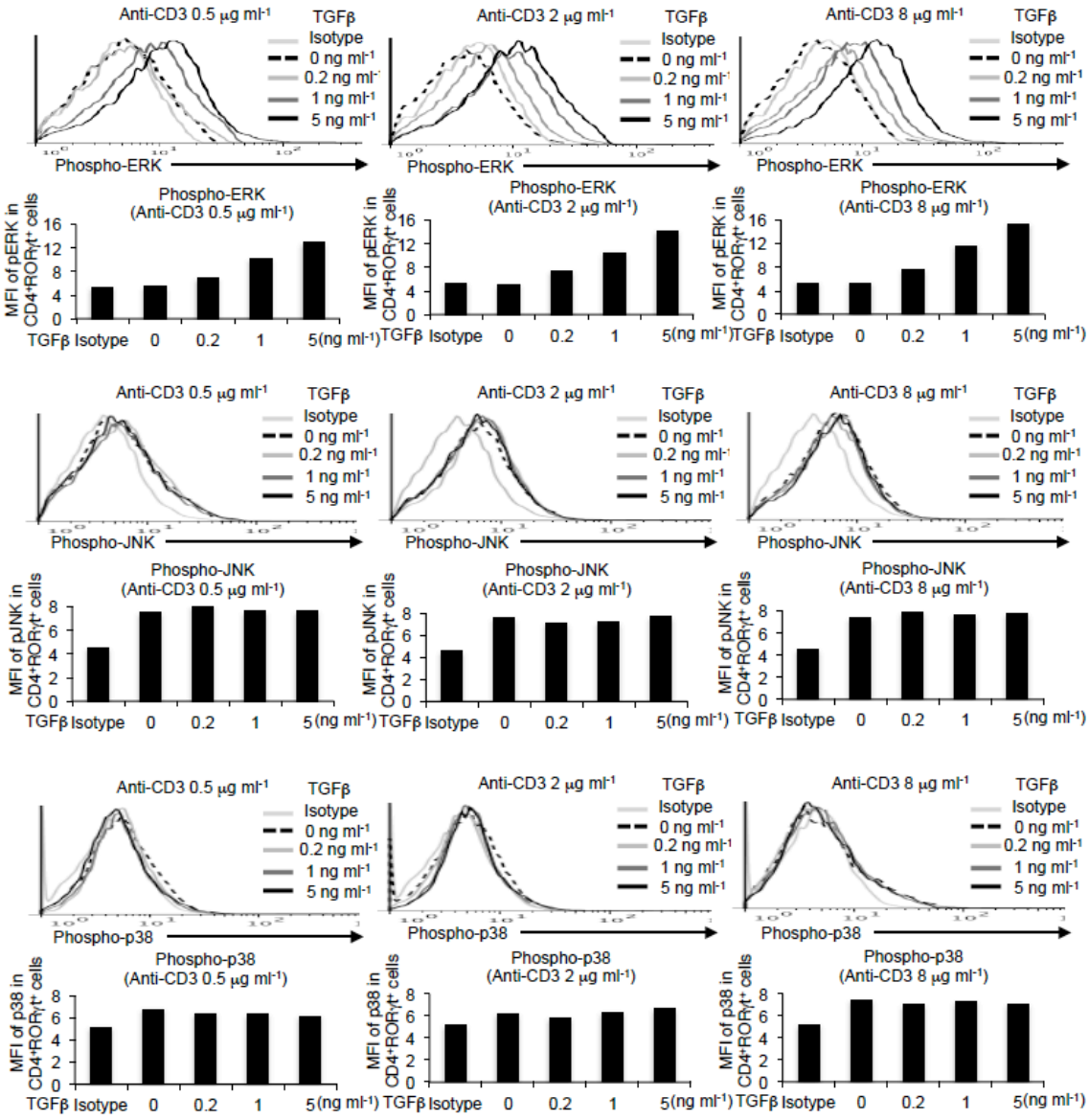

Figure 23 Strength of TGF-β and TCR signals correlate with ERK phosphorylation.

Purified $CD4^+$ T cells were activated under Th17-polarizing condition with the indicated doses of TGF-β, and plate-coated anti-CD3 for 3 days. Flow cytometry analyses of phospho-ERK, phospho-JNK, and phospho-p38 in $ROR\gamma t^+CD4^+$ gate. Graphs show mean fluorescence intensity (MFI). Data are from one experiment representative of two independent experiments.

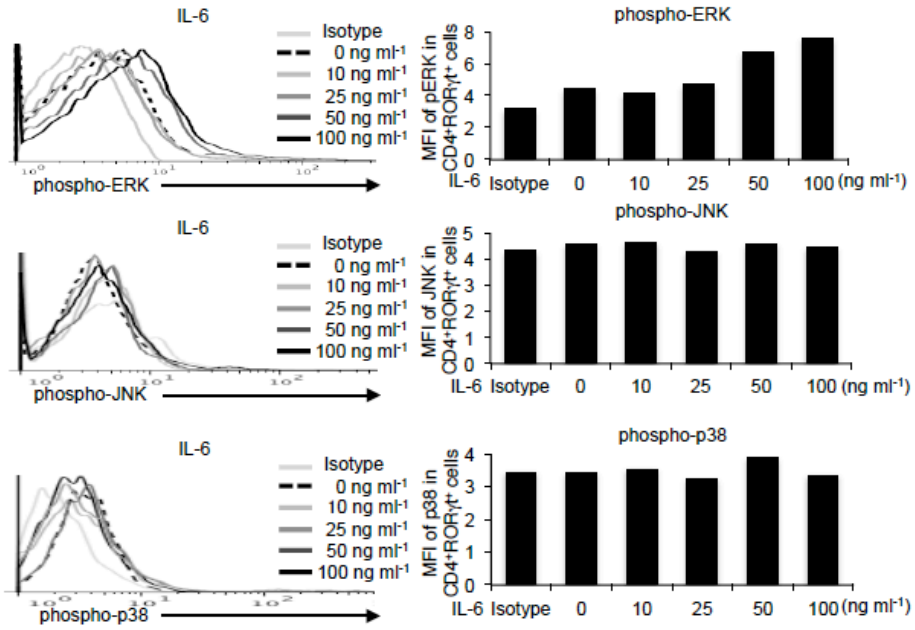

Figure 24 High doses IL-6 enhance ERK phosphorylation.

Purified $CD4^+$ T cells were activated under Th17-polarizing condition with the indicated doses of IL-6 for 3 days. Flow cytometry analyses of phospho-ERK, phospho-JNK, and phospho-p38 in $ROR\gamma t^+CD4^+$ gate. Graphs show mean fluorescence intensity (MFI). Data are from one experiment representative of two independent experiments.

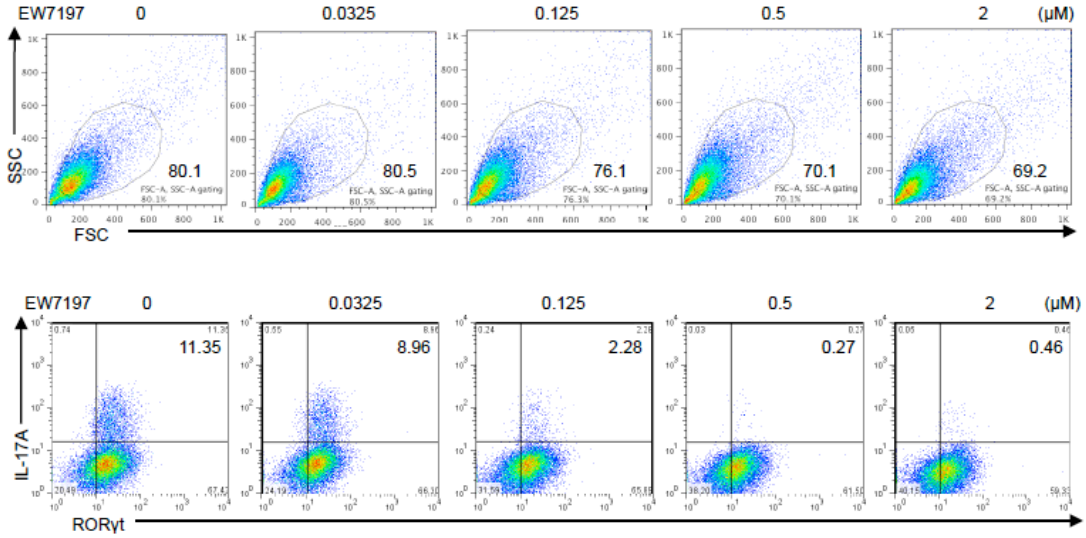

Figure 25 Viability and Th17 differentiation of $CD4^+$ T cells treated with ALK5 inhibitor, EW-7197.

Purified $CD4^+$ T cells were activated under Th17-polarizing condition with the indicated doses of EW-7197 for 3 days. Flow cytometry analyses of FSC/SSC and $IL\text{-}17A^+ROR\gamma t^+CD4^+$ T cells. Data are from one experiment representative of two independent experiments.

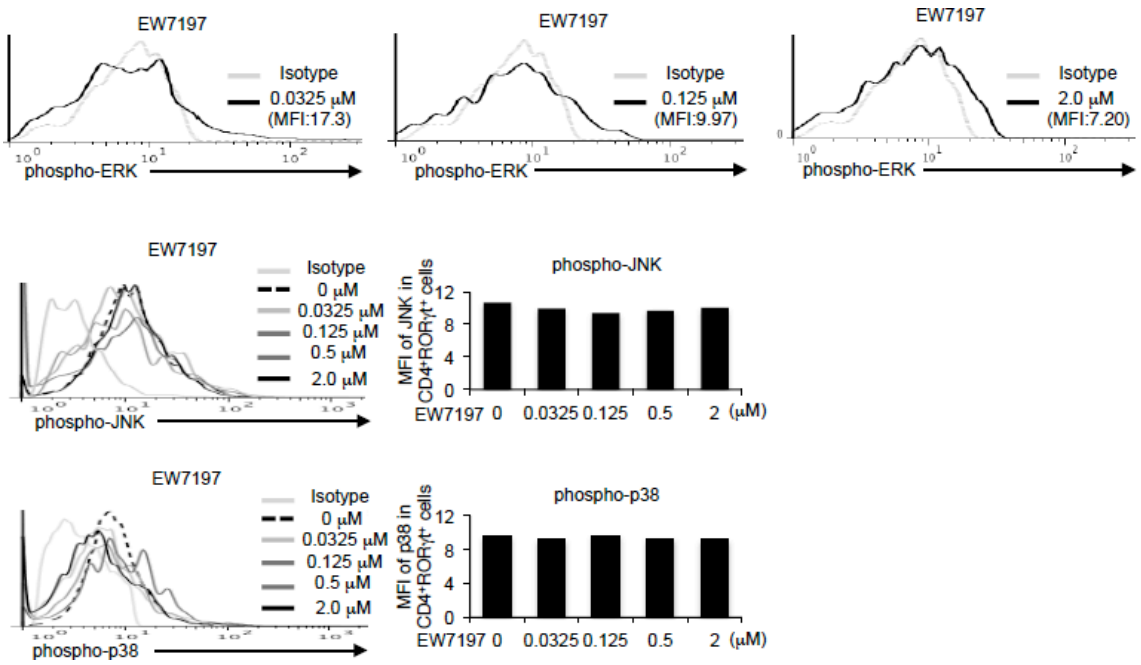

Figure 26 ALK5 inhibitor, EW-7197 suppresses ERK phosphorylation, but not phosphorylation of JNK and p38.

Purified $CD4^+$ T cells were activated under Th17-polarizing condition with the indicated doses of an ALK5 inhibitor: EW-7197 for 3 days. Flow cytometry analyses of phospho-ERK, phospho-JNK, and phospho-p38 in $ROR\gamma t^+CD4^+$ gate. Graphs show mean fluorescence intensity (MFI). Data are from one experiment representative of two independent experiments.

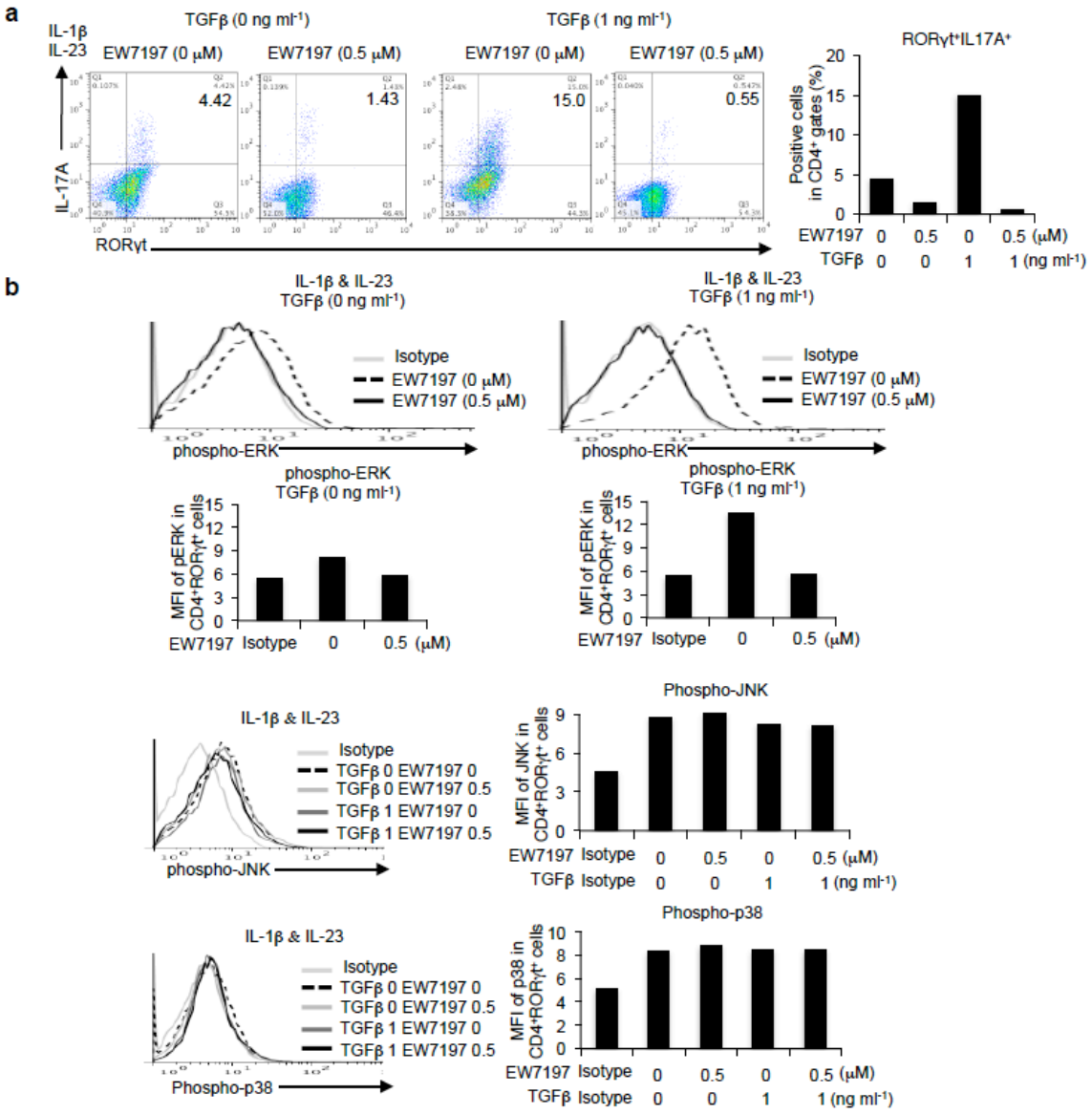

Figure 27 TGF-β enhances, whereas EW-7197 suppresses ERK phosphorylation and Th17 differentiation induced by IL-6, IL-23 and IL-1β.

Purified $CD4^+$ T cells were activated under Th17-polarizing condition with IL-6, IL-23, and IL-1β in the presence or absence of TGF-β1 (1 ng ml^{-1}) or EW-7197 (0.5 mM) for 3 days. (**a**) Flow cytometry analyses of $IL\text{-}17A^+ROR\gamma t^+CD4^+$ T cells. The graph shows the percentages of $IL\text{-}17A^+ROR\gamma t^+$ cells in $CD4^+$ gates are shown. (**b**) Flowcytometry analyses of phospho-ERK, phospho-JNK, and phospho-p38 in $ROR\gamma t^+CD4^+$ gate. Graphs show mean fluorescence intensity (MFI). Data are from one experiment representative of two independent experiments.

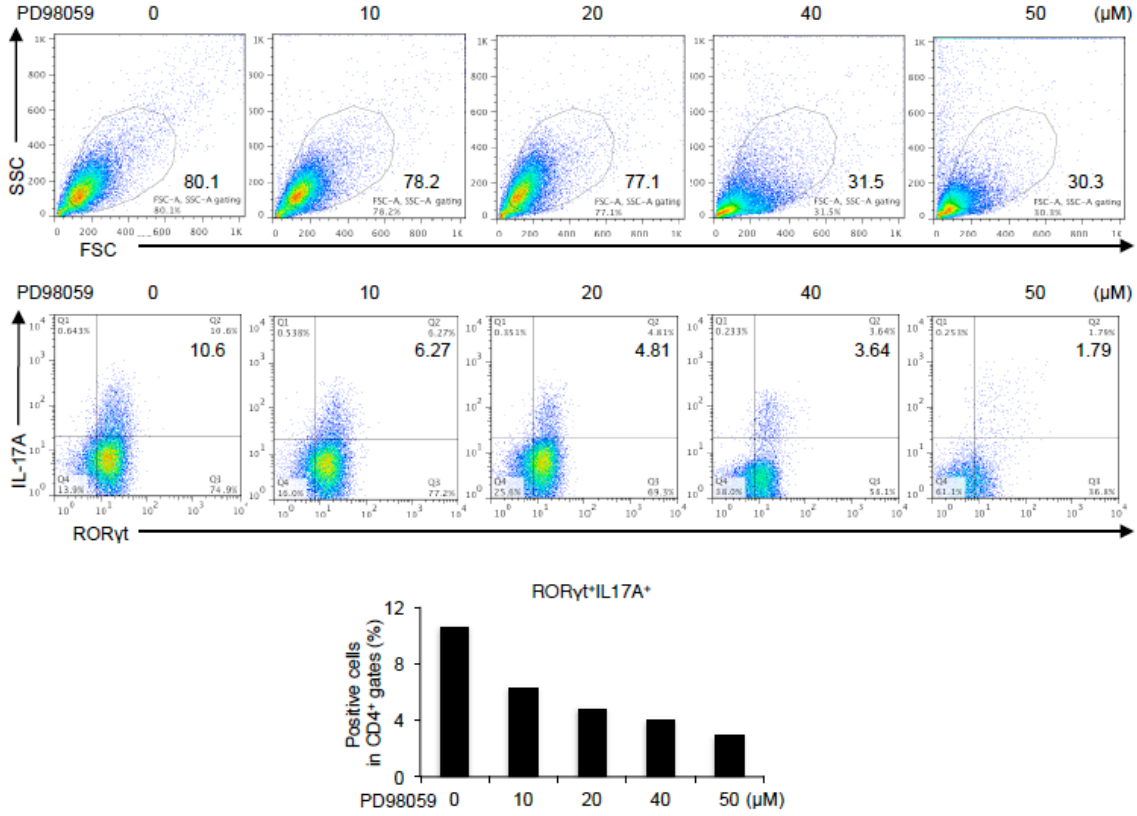

Figure 28 Viability and Th17 differentiation of CD4$^+$ T cells treated with MEK inhibitor, PD98059.

Purified CD4$^+$ T cells were activated under Th17-polarizing condition with the indicated doses of PD98059 for 3 days. Flow cytometry analyses of FSC/SSC and IL-17A$^+$RORγt$^+$CD4$^+$ T cells. Percentages of positive cell populations are shown. Data are from one experiment representative of two independent experiments.

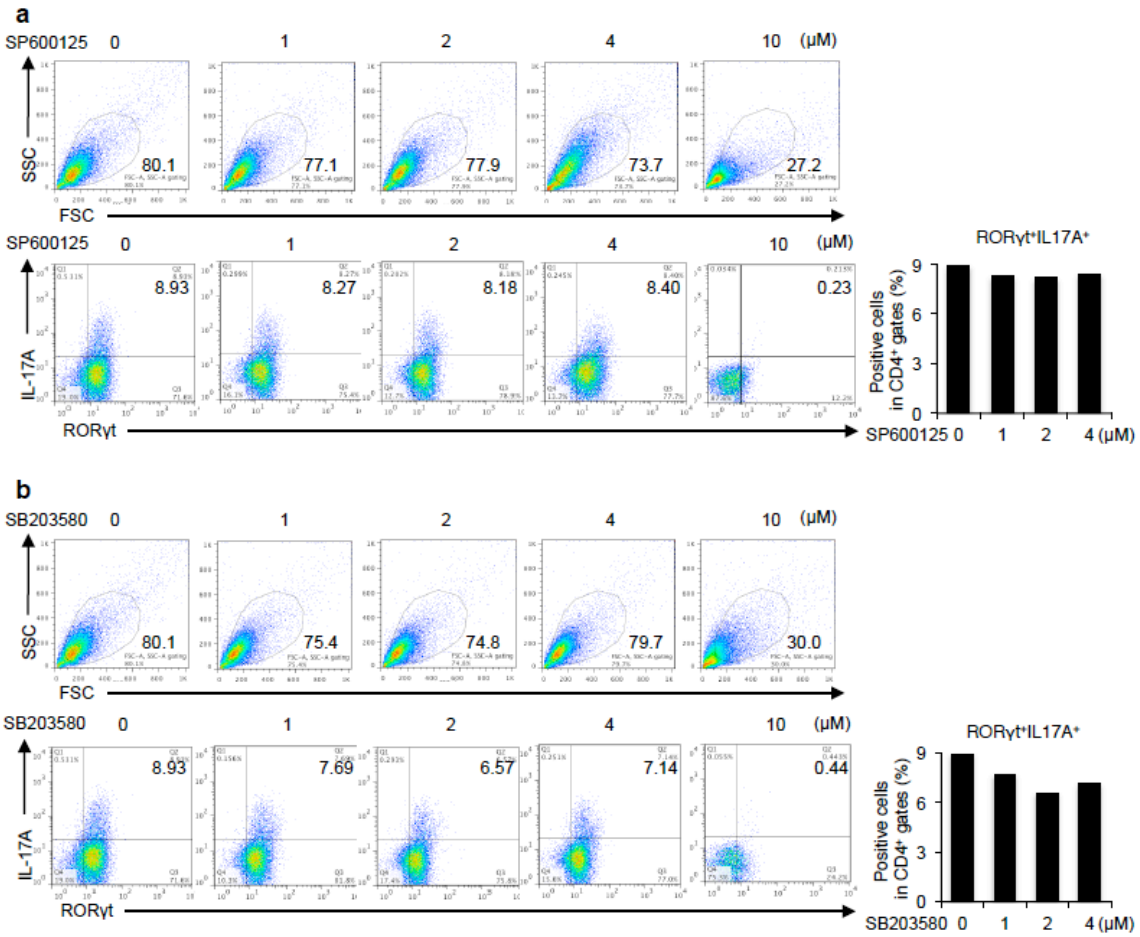

Figure 29 Inhibitors of JNK and p38 do not suppress Th17 differentiation.

Purified $CD4^+$ T cells were activated under Th17-polarizing condition with the indicated doses of (**a**) a JNK inhibitor: SP600125 or (**b**) p38 inhibitor: SB203580 for 3 days. Flow cytometry analyses of FSC/SSCand IL-$17A^+$$ROR\gamma t^+$$CD4^+$ T cells. Data are from one experiment representative of two independent experiments.

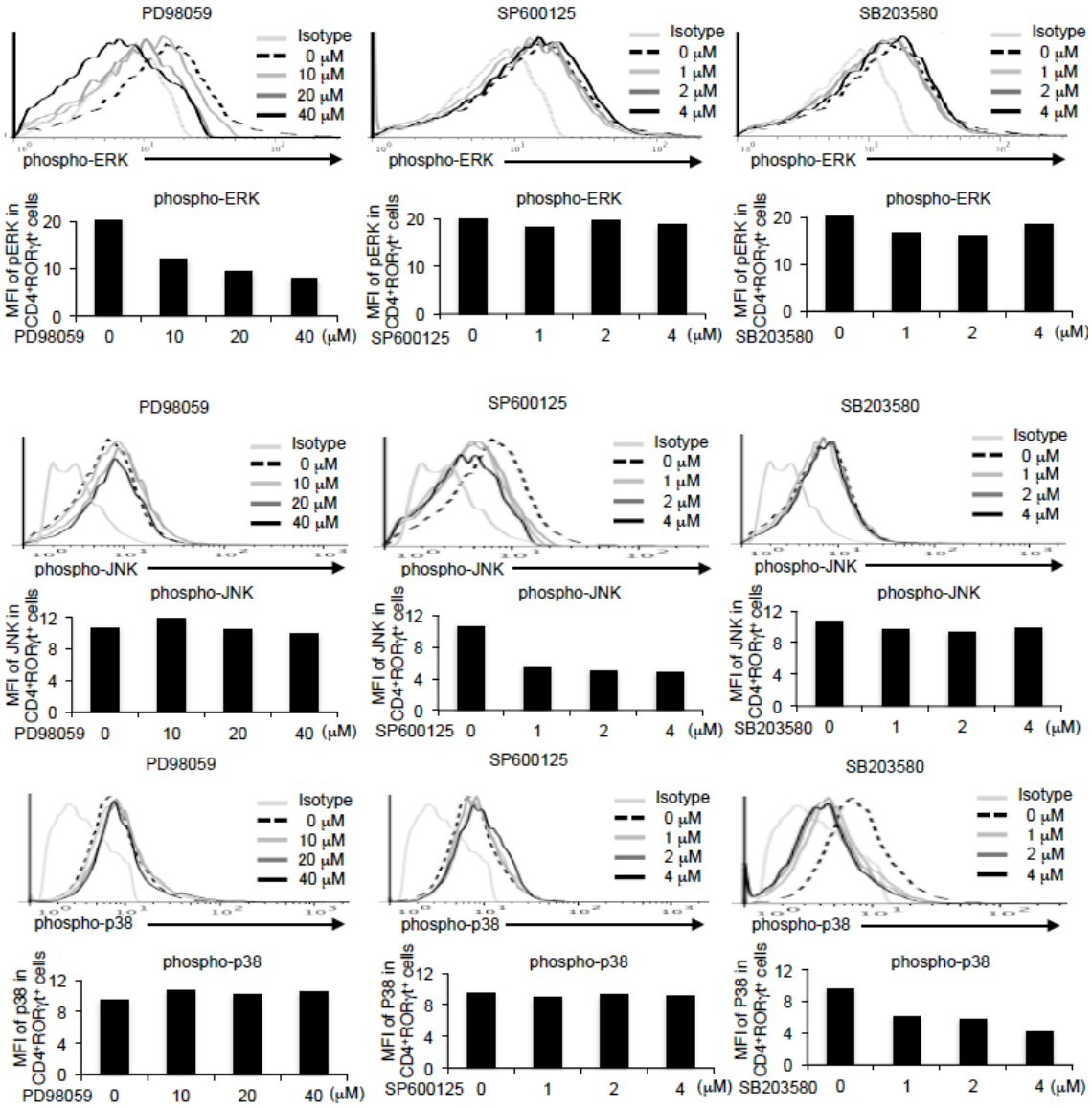

Figure 30 Specificity of MAPK inhibitors.

Purified $CD4^+$ T cells were activated under Th17-polarizing condition with the indicated doses of MAPK inhibitors (PD98059, SP600125, and SB203580) for 3 days. Flow cytometry analyses of phospho-ERK, phospho-JNK, and phospho-p38 in $ROR\gamma t^+CD4^+$ gate. Graphs show mean fluorescence intensity (MFI). Data are from one experiment representative of two independent experiments.

R-Smad-STAT3 interaction balances Th17 differentiation

I next examined the effects of intensities and inhibitions of TGF-β/IL-6/TCR signals on the interactions of STAT3 with pSmad2L or unphosphorylated Smad3C in Th17 cells. Higher doses of TGF-β1, IL-6, and anti-CD3 antibody significantly upregulated pSmad2L-STAT3 interactions with little changes in Smad3-STAT3 interactions (**Fig. 31a,b** and **32**). By contrast, treatments with EW-7197 or PD98059 significantly downregulated pSmad2L-STAT3 interactions (**Fig. 31c,e**), whereas upregulated Smad3-STAT3 interactions (**Fig. 31d**,**f**). Interactions of pSmad2L and STAT3 were directly proportional, whereas interactions of unphosphorylated Smad3C and STAT3 were inversely proportional to Th17 differentiation of EW-7197- or PD98059-treated $CD4^+$ T cells (**Fig. 20d**,**g** and **Fig. 31c-f**). These data suggest that the balances between STAT3-interacting pSmad2L and STAT3-interacting unphosphorylated Smad3C determine the extent of Th17 differentiation.

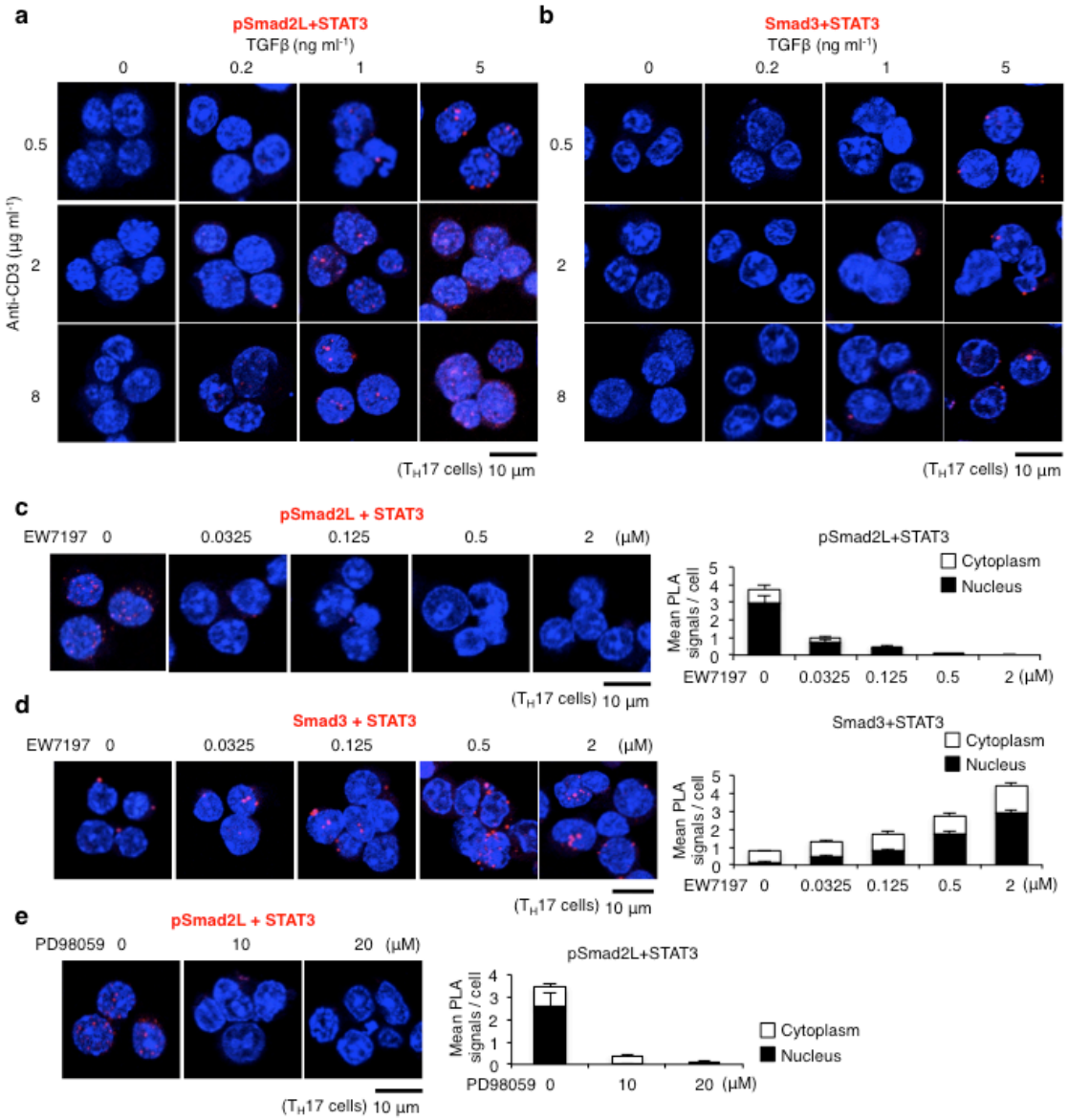

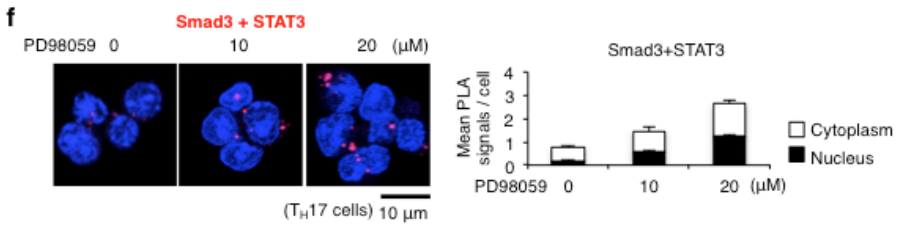

Figure 31 R-Smad-STAT3 interaction balances correlate with Th17 differentiation.

Purified $CD4^+$ T cells were activated under Th17-polarizing condition with the indicated doses of TGF-β1 and plate-coated anti-CD3 antibody, or small molecule inhibitors (EW-7197: ALK5 inhibitor, PD98059: MEK inhibitor) for 3 days. Interactions of endogenous proteins in Th17 cells were determined by PLA. PLA signals (**a**-**f**) were quantified using BlobFinder software (scale bars: 10 μm, nucleus: black, cytoplasm: white, *n* = 10 fields). (**a**) pSmad2L and STAT3, (**b**) Smad3 and STAT3 in Th17 cells treated with the indicated doses of TGF-β1 and plate-coated anti-CD3 antibody. (**c**) pSmad2L and STAT3, (**d**) Smad3 and STAT3 in Th17 cells treated with the indicated doses of EW-7197. (**e**) pSmad2L and STAT3, (**f**) Smad3 and STAT3 in Th17 cells treated with the indicated doses of PD98059. Data are representative of two independent experiments. Data are mean + s.d.

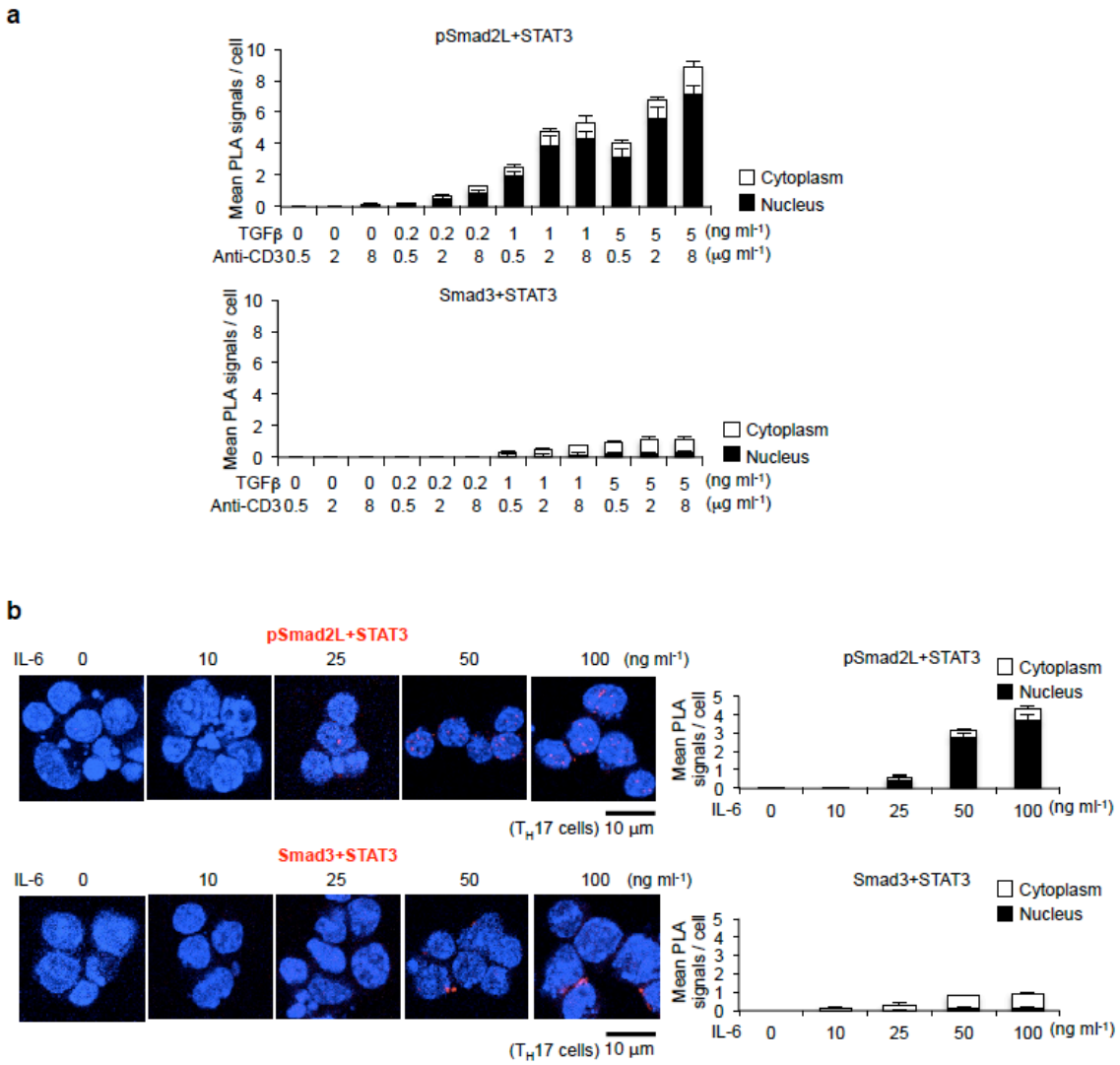

Figure 32. Higher doses of (a) TGF-β1, anti-CD3 antibody, and (b) IL-6 upregulated pSmad2L-STAT3 interaction in the nuclei with miniscule changes in Smad3-STAT3 interaction. Expression of pSmad2L-STAT3 and Smad3-STAT3 was quantified by PLA. PLA signals were quantified using BlobFinder software (scale bars: 10 μm, nucleus: black, cytoplasm: white, *n* = 10 fields). Data are from one experiment representative of two independent experiments. Data are mean + s.d.

Summary

TGF-β/IL-6/TCR-pERK-pSmad2L (Ser255) axis is the positive regulator, whereas unphosphorylated Smad3C-PIAS3 complex is the negative regulator of STAT3-induced transcriptional processes for Th17 differentiation (**Fig. 33**).

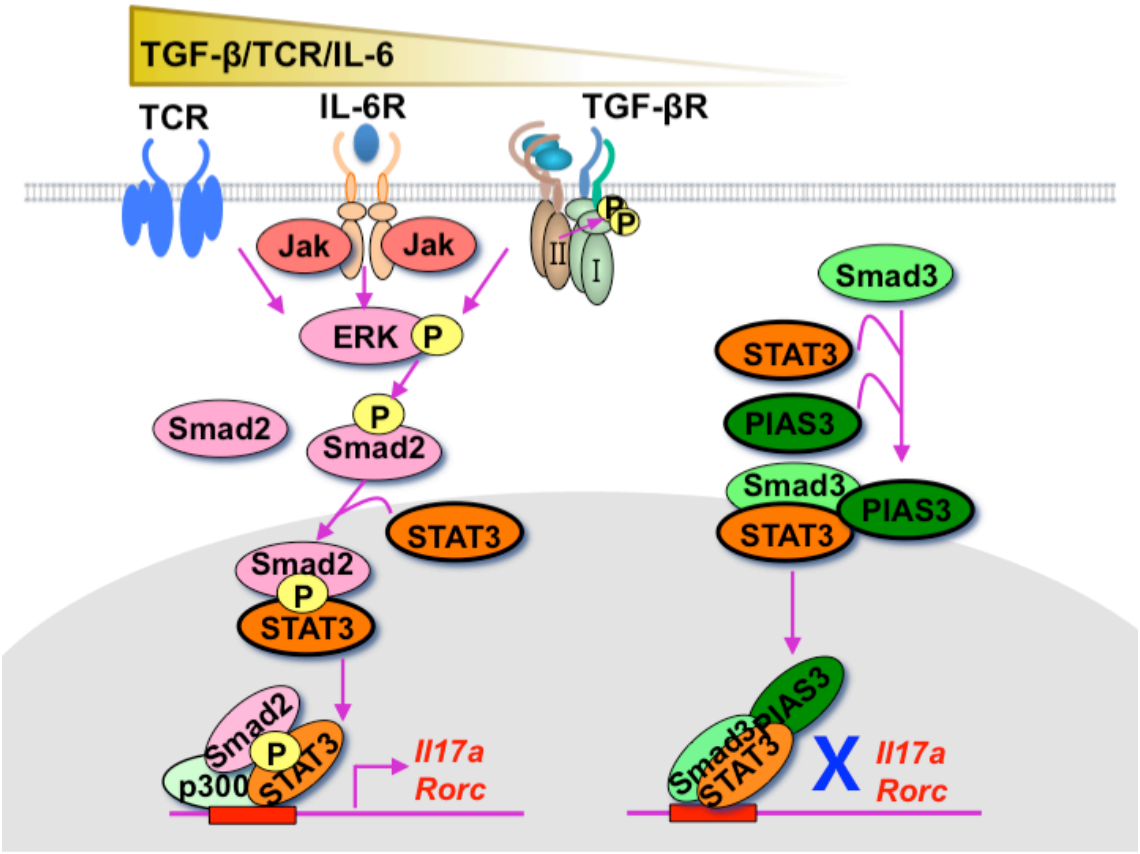

Figure 33 TGF-β R-Smads: Smad2 and Smad3 oppositely regulate Th17 differentiation as transcription cofactors of STAT3.

ERK-phosphorylated Smad2L (S255)/STAT3/p300 activates, whereas unphosphorylated Smad3C/STAT3/PIAS3 represses the transcription of the *Rorc* and *Il17a* genes.

Discussion

I discovered that Smad2 and Smad3 oppositely regulated STAT3-induced Th17 differentiation through the novel direct signaling networks. Transmodulation between the SMAD and STAT signaling pathways balances the interplay between TGF-β and various cytokines. Indirect cross-talk between SMAD and STAT was first reported as the inhibition of Smad3/4-mediated TGF-β signaling by Jak1-STAT1-mediated IFN-γ signaling via induction of the inhibitory Smad, Smad7, which prevents TβRI-induced C-terminal phosphorylation of Smad3 (Ulloa L et al, 1999). Direct cross-talk between SMAD and STAT was discovered as the synergistic signaling of leukemia inhibitory factor and bone morphogenic protein-2, one of the TGF-β superfamily cytokines, via STAT3-Smad1 complex bridged by p300 in fetal neural cells (Nakashima K et al, 1999). Direct cross-talk between Smad3 and STAT3 was reported as the augmentation of IL-6-STAT3-mediated transactivation by TGF-β via interaction of STAT3-pSmad3C complex bridged by p300 in hepatoma cells (Janknecht R et al, 1998; Yang XP et al, 2011). This study clarified the mechanisms whereby R-Smads-STAT3 networks modulate Th17 differentiation; pSmad2L (Ser255) serves as STAT3 coactivator in combination with p300, a coactivator of various transcription factors including both Smads and STAT3, whereas unphosphorylated Smad3C serves as STAT3 corepressor in combination with PIAS3, a negative regulator of STAT3-induced transcription (Chung CD et al, 1997). The preceding reports and my findings indicate that SMAD-STAT signaling networks are highly cell-type-specific and context-dependent. Because of the relatively low DNA binding affinity of Smad3 and lack of DNA-binding ability of Smad2, they interact with a wide variety of DNA-binding proteins to co-regulate the target genes. Recently, genome-wide transcriptome analyses have elucidated the diverse regulatory networks of Smad2/3 with cell-type-specific master transcription factors and/or DNA-binding cofactors in variety of cells (Morikawa M et al, 2013). The thorough iterative approach to delineate the Th17 global transcriptional regulatory network shows that STAT3 works as one of the key activators of the initial transcriptional program, RORγt works as an expression modulator, and Smad3 is the negative regulators (Ciofani M et al, 2012). It is noteworthy that a histone demethylase, JMJD3 (KDM6B) regulates the expression of numerous targets of RORγt and STAT3 (Ciofani M et al, 2012) because JMJD3 causes a loss of the H3K27me3 repressive epigenetic mark by interacting with R-Smads at their target sites (Morikawa M et al, 2013). Therefore, it is possible that Smad2 may interact with JMJD3 to induce active chromatin state for Th17 regulation in the same manner with Nodal-Smad2/3 signaling in embryonic development (Dahle O et al, 2010) (**Fig. 10**). Further studies are required to elucidate the details of divergent context-dependent SMAD-STAT signaling networks implicated by genome-wide transcriptome analyses.

I further uncovered the novel roles of R-Smads with noncanonical phosphorylation status in networking with STAT3: linker phosphorylated Smad2 as a STAT3 coactivator and unphosphorylated Smad3 as a STAT3 corepressor. Serine/threonine-rich R-Smad linker regions contain multiple phosphorylation sites by proline-directed protein kinases such as MAPKs, glycogen synthase kinase 3 (GSK3), and

cyclin-dependent kinase (CDK) family (Massague J et al, 2003; Wrighton KH et al, 2009; Matsuzaki K et al, 2013). Linker residues Ser245/250/255, Thr220 in Smad2, and Ser204/208/213, Thr179 in Smad3 are the sites for phosphorylation (Wrighton KH et al, 2009; Matsuzaki K et al, 2013). Three clustered serine residues are preferred phosphorylation sites for ERK, JNK, and p38 in response to receptor tyrosine kinases and proinflammatory cytokines, whereas threonine residues are preferred phosphorylation sites for CDK family in response to TGF-β. TβRI possesses the intrinsic tyrosine kinase activity to directly induce activation of MAPK pathways and subsequent phosphorylation of R-Smad linker residues in addition to the serine/threonine kinase activity to phosphorylate R-Smads in their conserved C-terminal SSXS motif (Wrighton KH et al, 2009; Matsuzaki K et al, 2013). Mitogens and hyperactive Ras induce ERK-mediated linker phosphorylation of Smad2 at Ser245/250/255/Thr220 and Smad3 at Ser204/208/Thr179 (Massague J et al, 2003; Massague J et al, 2012). Therefore, roles of R-Smad linker phosphorylation in carcinogenesis have been investigated intensively family (Massague J et al, 2003; Wrighton KH et al, 2009; Matsuzaki K et al, 2013). Central role of ERK in TCR signals family (Dong C et al, 2002; Liu H et al, 2013) suggests the important roles of R-Smad linker phosphorylation in T cell signaling network. Thus far, MEKK2/3-ERK1/2 signaling has been reported to induce pSmad3L, which negatively regulates canonical TGF-β signaling for Th17 differentiation (Chang X et al, 2011). Because I found that Smad3 linker region was not involved in STAT3-induced Th17 differentiation (**Fig. 14b**), the mechanisms how pSmad3L regulates Th17 differentiation are independent of STAT3. By contrast to phosphorylated Smads, very little has been known about physiological functions of unphosphorylated R-Smads. It has been reported that PIAS3 enhances TGF-β-induced transcriptional activity of C-terminally phosphorylated Smad3 by recruiting p300 and CBP in COS cells and 293T cells (Long J et al, 2004). By contrast, I discovered that unphosphorylated Smad3C due to less TGF-β signaling was required for PIAS3 to function as a corepressor of STAT3 (Chung CD et al, 1997). Recent genome-wide studies implicate that unphosphorylated Smad3 may bind to some cell-type specific transcription factors in both TGF-β-dependent and TGF-β-independent manners (Morikawa M et al, 2013; Mullen AC et al, 2011; Isogaya K et al, 2014). My finding shed light on as-yet-unrecognized functions of unphosphorylated Smad3 as a transcription cofactor.

The discovery of a new proinflammatory effetor T cell subset, Th17 revised the functions of TGF-β, which had been long considered as the most potent immunosuppressive cytokine. TGF-β has been identified as the requisite factor for Th17 differentiation in combination with IL-6 and other proinflammatory cytokines such as IL-21, IL-23, IL-1β, and TNF-α. However, as functions of TGF-β have been frequently described as dual, bidirectional, pleiotropic, complex, or contextual, the roles of TGF-β in Th17 differentiation have become controversial. Requirement of TGF-β for Th17 differentiation remains contradictory, indispensable or dispensable (Manel N et al, 2008; DaCosta Byfield S et al, 2004). My results provide explanation for these conflicting reports. TGF-β ligand-independent Th17 differentiation is possible because Smad2 linker phosphorylation could be induced by ERK signals

downstream of IL-6 receptor and TCR. However, significantly more effective inhibitory effect of the ALK5 inhibitor than that of a MEK inhibitor suggests that TβRI-pERK-pSmad2L axis is more efficient than non-TGF-β growth stimulatory signal-pERK-pSmad2L axis for Th17 differentiation. Nonetheless, the report showing the dispensability of TGF-β demonstrates that TGF-β induces significantly more Th17 differentiation (DaCosta Byfield S et al, 2004). Likewise, my results provide explanations for the discrepancies in the reported roles of Smads in Th17 differentiation. My data are consistent with the previous reports showing that Smad2 is a positive regulator and Smad3 is a negative regulator of Th17 differentiation although the mechanisms of actions are distinct. It has been reported that TGF-β signaling via Smad2 indirectly induced STAT3 phosphorylation by inducing the expression of mRNA and protein of IL-6Rα (Malhotra N et al, 2010), however, I could not confirm the differences in IL-6Rα mRNA expression in my systems (**Fig. 9**). It has been reported that Smad3 interacted with RORγt and decreased its transcriptional activity (Martinez GJ et al, 2009). I confirmed that not only Smad3 but also Smad2 interacted with RORγt (**Fig. 16**). Whether RORγt forms the complex with STAT3 and R-Smads remains to be determined. My data also suggest that the signaling intensity balances of TCR, co-stimulation, IL-6, TGF-β, and other cytokines could yield the seeming dispensability of R-Smads (Lu L et al, 2010; Takimoto T et al, 2010) because of their opposing effects. The signaling balances between TβRI-PKCα-mediated C-terminal phosphorylation of R-Smads (Meisel M et al, 2013) and pERK-pSmad2L may be also crucial for Th17 differentiation.

An ALK5 inhibitor is efficacious against a mouse type II collagen antibody-induced arthritis model (Sakuma M et al, 2007). My results of a CIA model showed the promoting role of pSmad2L at Ser255 and the suppressive role of unphosphorylated Smad3 in the arthritogenic Th17 differentiation.

Activin receptor-like kinase5 inhibition suppresses mouse melanoma by ubiquitin degradation of Smad4, thereby derepressing eomesodermin in cytotoxic T lymphocytes

（**TGF-β I** 型受容体阻害は、細胞障害性 **T** リンパ球に発現する **Smad4** ユビキチン分解による **eomesodermin** 抑制解除を誘導しマウス悪性黒色腫を抑制する）

Materials and Methods

Mice

Mice homozygous for a conditional *Smad4* allele (*Smad4*$^{loxp/loxp}$) (Kim et al, 2006) and *Smad2* allele (*Smad2* $^{loxp/loxp}$) (Liu et al, 2004) were bred with *Cd4Cre* recombinase transgenic mice (Lee et al, 2001) for the selective deletion of the genes flanked by loxP targeting sequences in thymocytes at the double positive stage. They were backcrossed to C57BL/6 (The Jackson Laboratory) for eight generations. *Smad3*$^{+/-}$ mice (Yang et al, 1999) were backcrossed to C57BL/6 for two generations because the probability of *Smad3*$^{-/-}$ dropped to less than 1% in my facility due to the increased embryonic lethality. All experiments used age-matched mice. All animals were maintained in a SPF environment and used in experiments according to the ethical guidelines for animal experiments and the safety guidelines for gene manipulation experiments at University of Tsukuba, Japan, Tokyo Medical University, Japan, Gachon University, Korea, and Konkuk University, Korea under approved animal study protocols.

B16 melanoma model and treatment with ALK5 inhibitors

Parental B16F1 (B16) cells and B16 cells transfected with the FG12 lentiviral vector expressing green fluorescent protein (GFP) were cultured in DMEM media (Gibco) containing 10% heat-inactivated FBS (Gibco) supplemented with 1% penicillin and streptomycin. Mice (8-12 wk) were subcutaneously injected with GFP-expressing B16 cells (4×10^4/20 μl) into the left footpads or with GFP-expressing B16 cells (2×10^5/100 μl) into the left lower abdomen. Tumor size was measured by a caliper everyday. Volume was calculated by ([short diameter]^2 × long diameter)/2 (Pedroza-Gonzalez et al, 2011). Resected tumor was weighed. Tumors, dLNs (left axillary, brachial, and inguinal), non-dLNs, and spleens were harvested for evaluation. EW-7197 (2.5 mg/kg daily) or LY-2157299 (75 mg/kg bid) dissolved in artificial gastric fluid formulation (vehicle; ddH_2O 900 ml, conc. HCl 7 ml, NaCl 2.0g, pepsin 3.2g) was given orally by feeding needle to mice from 4 days after inoculation. To delete $CD8^+$, $CD4^+$ T cells, or NK cells, mice were intraperitoneally injected with LEAF purified anti-CD4 (GK1.5), anti-CD8 (53-6.7) (150 μg/mouse; BioLegend) or anti-asialo GM1 (20 μl/mouse ; Wako) antibody on day -4, 0, 7, and 14 of melanoma inoculation (day 0). Rat IgG2a κ (150 μg/mouse; BioLegend) was used as a representative control.

Isolation of TILs

Melanoma infiltrating T cells were isolated following the reported protocol (Watkins et al, 2012). Briefly, B16 melanoma tumors measuring up to 250 mm^2 were cut into small pieces and incubated in RPMI medium supplemented with 5% FBS, Collagenase type I (200U/ml; Sigma-Aldrich) and DNase I (100 μg/ml; Sigma-Aldrich) for 30 min at 37°C. Cells were enriched by density gradient centrifugation using Ficoll-Paque 1.084 (GE Healthcare). Enriched cells were isolated by filtering through Cell Strainers (pore size: 40-μm diameter) (BD Falcon). Erythrocytes were lysed using RBC Lysis Buffer (Rhoche) and cells

were washed in PBS containing 2% FBS (Hyclone Laboratories). Viable cells were counted by hemacytometer using trypan blue exclusion.

Flowcytometry

Single cell suspensions were prepared from spleens and LNs. After blocking Fc receptors by anti-mouse CD16/CD32, cells were stained with APC-Cy7-anti-CD4, Pacific blue-anti-CD8, PE-anti-CD19, APC-anti-CD11b, PE-anti-Gr-1, APC-anti-CD11c, APC-anti-DX5, and APC-anti-CD45. To measure cytokine production, dLN cells were stimulated with PMA (2.5 ng/ml; Sigma-Aldrich) and ionomycin (2.5 ng/ml; Sigma-Aldrich) with GolgiPlug (BD Pharmingen) for 1-4 h. Cells were fixed, permeabilized with a Cytoperm/Cytofix Kit (eBiosciences). For intracellular staining, PE-anti-T-bet, APC-anti-Eomes, PE-anti-GATA3, PE-anti-RORγt, PE-Cy7-anti-FoxP3, PE-anti-perforin, APC-anti-granzyme B, and PE-Cy7-anti-IFN-γ were used. Antibodies were obtained from BD Pharmingen and eBiosciences. The samples were acquired by LSRII (BD Bioscience) and analyzed using the FlowJo software (Tree Star).

Cytotoxicity assay

$CD8^+$ cells enriched from the spleens of melanoma-bearing mice by mouse T cell enrichment column (R&D Systems) and magnetic activated cell separation (MACS) using CD8a microbeads (Miltenyi Biotec) as effector cells (0, 5×10^4, 1×10^5, 2×10^5) were co-cultured with GFP tagged B16 cells (2×10^3) as target cells in U-bottom 96-well plates (NUNC) for 72 h. Annexin V/propidium iodide (PI) (BD Pharmingen) staining in the large FSC/SSC GFP^+ gate was determined by LSRII.

Histology

The detail procedures of immunohistochemistry were described in chapter 1 report material and methods part. Briefly, tumors were harvested and fixed in 10% neutral-buffered formalin. Fixed samples were then dehydrated with 70% ethanol, embedded in paraffin, and sectioned at 3 μm. For immunohistochemistry, sections were stained with anti-CD8, anti-Eomes, anti-phospho-Smad3 (Abcam), anti-phospho-Smad2 (Cell Signaling Technology), and anti-Smad4 (Santa Cruz) antibodies. Slides were observed using an optical microscope, Imager Z1 (Carl Zeiss).

Immunocytochemistry: Proximity Ligation Assay (PLA)

The detail procedures of immunocytochemistry were described in chapter 1 report material and methods part. Freshly isolated spleen, dLN cells from melanoma-bearing mice were fixed on the slides by 3.7% formaldehyde. PLA was performed using the Duolink II Fluorescence kit (OLINK) according to the manufacturer's protocol using the rabbit antibodies against: Smad2, Smad3, phospho-Smad2, phospho-Smad3, Smad4, and mouse antibodies against: Smad2/3 and ubiquitin (Cell Signaling Technology, BD Bioscience). One respective primary antibody and the secondary antibodies conjugated

with oligonucleotides (PLA probe anti-rabbit PLUS and PLA probe anti-rabbit MINUS) were used to detect endogenous Smad protein expression for single recognition. Two primary antibodies raised in different species and the secondary antibodies conjugated with oligonucleotides (PLA probe anti-rabbit PLUS and PLA probe anti-mouse MINUS) were used to detect protein interactions (rabbit anti-Smad2 and mouse anti-ubiquitin, rabbit anti-Smad3 and mouse anti-ubiquitin, rabbit anti-Smad4 and mouse anti-ubiquitin, mouse anti-Smad2/3 and rabbit anti-Smad4). After incubation of the slides with Blocking Solution for 30 min at 37°C, they were incubated with primary antibodies diluted in the Antibody Diluent overnight at 4°C, in PLA probe solution for 1 h at 37°C and in Ligation-Ligase solution for 30 min at 37°C with washing with Wash Buffer A in the interim of each step. The slides were incubated in Amplification-Polymerase solution for 100 min at 37°C and then washed in Wash Buffer B. To co-stain CD8, rat anti-CD8 antibody was added in the Antibody Diluent with primary antibodies for PLA and the slide were incubated with Alexa Fluor 488 conjugated anti-rat IgG (Abcam) after washing in Wash Buffer B. Nucleus was stained with DAPI. Then, the slides were dried at room temperature in the dark. Slides were observed using a confocal microscope, LSM700 (Carl Zeiss). PLA signals were quantified using BlobFinder software (Centre for Image Analysis, Uppsala University).

T cell stimulation in vitro

The detail procedures of T cell isolation were described in chapter 1 report material and methods part. Briefly, suspended whole dLN cells (1×10^6/ml) of melanoma-bearing mice were labeled with CFSE (Invitrogen) for stimulation with H-2D^b human gp100 peptide (5 μg/ml, Medical and Biological Laboratories). After 5 days, CFSE dilution of CD8$^+$ gate was analyzed by flowcytometry. CD8$^+$ or CD4$^+$ cells (1×10^6 cells/ml) enriched from spleens and LNs by MACS using CD4 or CD8a microbeads were stimulated with plate-coated anti-CD3 (1 μg/ml) and soluble anti-CD28 (3 μg/ml) antibodies (BD Pharmingen) with or without TGF-β1 (5 ng/ml; R&D Systems), EW-7197 (0, 0.5, 1.0, 2.0, 5.0 μM), MG-132 (0.5 μM; Sigma-Aldrich) for 3 days in 50 μM 2-mercaptoethanol containing RPMI 1640 media in 24-well plates (NUNC).

Western blotting and in vivo ubiquitination assay

Cells lysed with lysis buffer (PBS containing 0.5% Triton X-100, 20 mM HEPES (pH 7.4), 150 mM NaCl, 12.5 mM β-glycerol phosphate, 1.5 mM MgCl2, 10 mM NaF, 2 mM DTT, 1 mM NaOV, 2 mM EGTA, 1 mM PMSF, and protease inhibitor cocktail) were electrophoresed on 10% SDS-polyacrylamide gel and transferred to PVDF membrane, and probed with antibodies against phospho-Smad2, phospho-Smad3 (Abcam), Smad2, Smad3, Smad4 and β-actin (Santa Cruz). Blots were visualized using an electrochemiluminescence kit (GE Healthcare). Ubiquitinated Smad4 in CD8$^+$ dLN cells was detected using an UbiQapture-Q kit (Enzo Life Sciences) according to the manufacturer's protocol. Isolated CD8$^+$ dLN cells by MACS were pooled (5×10^6 cells from 5-7 mice/sample) for lysis. Equal amounts of protein

of $CD8^+$ LN cells were incubated overnight at 4°C with the UbiQapture-Q matrix beads, which capture mono/poly-ubiquitinated proteins. The matrix was then washed and the ubiquitin-protein conjugates were eluted by addition of PBS and denaturating buffer. Samples were quenched by incubation for 15 min at 4°C and then denaturated by heating at 95°C for 10 min. Proteins were eluted in Laemli's sample buffer, and subsequently processed for Western blotting with anti-Smad4 antibody (Cell Signaling) and the ubiquitin-conjugate antibody supplied by the kit. Ubiquitinated Smad4 in cultured $CD8^+$ T cells was detected as previously described (Lee YS et al, 2011). Briefly, $CD8^+$ cells stimulated with anti-CD3/CD28 antibodies (2×10^7 $CD8^+$ cells/sample) were harvested and non-covalent protein interactions were dissociated with 1% SDS and boiling for 10 min. Samples were diluted ten times with lysis buffer and subsequently suspended using a 1 ml syringe. The samples were cleared by centrifugation at 16,000 *g* for 10 min. Lysates were incubated with protein A/G agarose beads and with anti-Smad4 antibody (Santa Cruz) at 4 °C for 12-16 h. The beads were washed three times with lysis buffer and immunoprecipitates were separated from the beads by adding 2× sample buffer and boiled. SDS–PAGE-separated immunoprecipitates were transferred onto PVDF membranes. The membranes were denatured with denaturation buffer containing 6 M guanidine chloride, 20 mM Tris (pH 7.5), 100 mM PMSF, and 5 mM β-mercaptoethanol at 4 °C for 30 min and washed three times with TBST. The membranes were blocked with 5 % BSA and incubated with anti-ubiquitin-HRP antibody (Biomol).

Quantitative RT-PCR

Total RNA extracted using Trizol (Invitrogen) was reverse transcribed with a cDNA Reverse Transcription Kit (Invitrogen). Real-time quantitative PCR (triplicate/sample) was performed using an ABI 7900 Analyzer with SYBR Green Master Mix (Applied Biosystems) with the primers listed in Table 4.

Table 4 Primer sequences for quantitative RT-PCR

Gene	Sense primer	Antisense primer
Gapdh	TGGTGAAGGTCGGTGTGAAC	CCATGTAGTTGAGGTCAATGAAGG
T-bet	GCCAGGGAACCG CTTATATG	GACGATCATCTGGGTCACATTGT
Eomes	TGAATGAACCTTCCAAGACTCAGA	GGCTTGAGGCAAAGTGTTGACA
Ifng	ACTGGCAAAAGGATGGTGAC	GACCTGTGGGTTGTTGACCT
Gzmb	GGACTGCAAAGACTGGCTTC	ATAACATTCTCGGGGCACTG
Prf1	TTTCGCCTGGTACAAAAACC	AGGGCTGTAAGGACCGAGAT
Fasl	CATCACAACCACTCCCACTG	GTTCTGCCAGTTCCTTCTGC

Luciferase assay

The proximal promoter regions of Eomes were generated by PCR from C57BL/6 genomic DNA using the

primers listed in Table 5. Products were verified by sequencing and subcloned into the pGL4 luciferase vector (Promega) using KpnI and XhoI sites, XhoI and HindIII sites respectively. The resulting constructs were transfected into in vitro-stimulated $CD8^+$ cells along with control thymidine kinase-pRL *Renilla* plasmid (Promega) using Amaxa Nucleofector II (Lonza). Flag-tagged Smad4, with or without Flag-tagged Smad2 or Smad3, or an empty pcDNA3 plasmid were co-transfected. At 6 h after transfection, cells were restimulated with anti-CD3 and anti-CD28 antibodies as described above for 4 h and lysed for luminometer measurements.

Table 5 Primer sequences for the proximal promoter regions of Eomes

Eomes promoter	Sense primer	Antisense primer
-2.0 kb	TTTGGTACCCTGTGCCACGCCAGCG TTTCC	AAACTCGAGGCTTTAGCGAATCGCAG ACGG
-0.7 kb	TTTGGTACCATGTTCGCAGACTTCA AACCC	AAACTCGAGGCTTTAGCGAATCGCAG ACGG
-0.37 kb	TTTGGTACCTGTGAGTGTAGGGGTC CTGA	AAACTCGAGGCTTTAGCGAATCGCAG ACGG
-0.23 kb	TTTGGTACCTTTCTTGCGGAAGGAA AGG	AAACTCGAGGCTTTAGCGAATCGCAG ACGG

Chromatin immunoprecipitation (ChIP)

Chromatin was prepared from 1×10^7 $CD8^+$ cells isolated from C57BL/6, *Cd4Cre;Smad4*$^{+/+}$, and *Cd4Cre;Smad4*$^{fl/fl}$ mice stimulated for 3 days as described above. Immunoprecipitation was performed with anti-Smad4 antibody and rabbit IgG using a ChIP Kit (Cell Signaling). Immunoprecipitated DNA released from the cross-linked proteins was quantified by real-time quantitative PCR with the primers listed in Table 6 and normalized to input DNA.

Table 6 Primer sequences for ChIP

Eomes promoter	Sense primer	Antisense primer
-912 to -720	AGTCTCAACAATGGGGTCGT	CGTGTGAGTGTGCATGTCTG
-680 to -449	GGGTCGTAGAAACCCTAGAAATCA	GAGACAGGGTCTCCCATGGA
-538 to -321	ATCCTCCACAGACATGCACA	GTTCTTAGCCCCAGGGAGAC
-239 to -86	AGAGCACTGGGTGCTACTGGTT	CCCTTCGCTCCCAGCAT
-172 to +72	CTGCCCTCTCCACGCCAGGT	AAACAGCAGGGCAGGAGCCG

Detection of cell cycle and apoptosis of B16 cells

B16 cells were cultured in the absence or presence of TGF-β (0, 0.5, 1.0, 5.0 ng/ml) and/or EW-7197 (0,

0.25, 0.5, 1.0 μM). For cell cycle analysis, DNA content was determined by Propidium iodide (PI) (BD Pharmingen). Briefly, B16 cells were fixed by cold 80% ethanol overnight at -20°C. Fixed cells were washed twice in phosphate-buffered saline (PBS), 1% bovine serum albumin (BSA), and then resuspended in PI solution in PBS containing RNase A (0.1 mg/ml; Sigma-Aldrich). Phosphatidylserine exposure was measured using Annexin V Apoptosis Detection Kit APC (eBioscience). B16 cells were resuspended in 1× binding buffer (10^5 cells/100 μl) and incubated with Annexin V-APC for 15 minutes at room temperature in the dark. Cells were washed, resuspended in 1× binding buffer (200 μl). Propidium iodide (PI) staining solution was added into each sample and analyzed by flowcytometry immediately.

Knockdown of Smurf1 and Smurf2 by shRNA

The short hairpin RNA (shRNA) sequences specific for endogenous *Smurf1* and *Smurf2* are described previously (Lee YS et al, 2011). To generate shRNAs specific for endogenous *Smurf1* and *Smurf2*, double-stranded oligomers containing restriction enzyme sites, a sense sequence, and a loop sequence with its antisense sequence were designed and cloned into *Age*I and *Eco*RI sites of the pLKO-puro vector (Clontech). Lentiviruses expressing each shRNA were produced by a lentiviral packaging system from Invitrogen. Lentivirus expressing mutant *Gfp* shRNA was used as a negative control for lentivirus infection. Expression levels of *Smurf1* and *Smurf2* mRNA were measured by real-time quantitative PCR with the primers: Smurf1 5'-TGCCATCAGCAGATTGAAAG-3', 5'-GTTCCTTCGTTCTCCAGCAG-3', Smurf2 5'-GTGAAGAGCTCGGTCCTTTG-3', 5'-TCGCTTGTATCTTGGCACTG-3'

Statistics

Statistical analyses were performed using analysis tools provided on the VassarStats statistical computation site (http://vassarstats.net/). Data were analyzed using the two-tailed unpaired Student's *t* test and two-way ANOVA test. A *P*-value <0.05 was considered to indicate statistical significance.

Results

Selective inhibition of ALK5 suppresses the progression of melanoma with enhanced CTL activity

To examine the therapeutic efficacy of EW-7197 for melanoma in comparison with LY-2157299 for eventual use in a Phase 2 clinical trial (Akhurst & Hata, 2012; Calvo-Aller et al, 2008; Hawinkels et al, 2011), C57BL/6 mice were orally administered with vehicle or vehicle containing EW-7197 (2.5 mg/kg daily) or LY-2157299 (75 mg/kg bid) starting from four days after inoculation of GFP-expressing B16 cells (4×10^4) into the left footpads. Low-dose EW-7197 was more efficient than high-dose LY-2157299 in suppressing the growth of transplanted tumors (**Fig. 34a**). Treatment with EW-7197 and LY-2157299 efficiently suppressed the lymph node (LN) metastases, which were detected by $CD11c^-CD11b^-B220^-GFP^+$ cells in the draining lymph nodes (dLNs) (**Fig. 34b and Fig. 35**).

Because TGF-β and EW-7197 showed no direct effects on apoptosis and cell cycle of B16 cells in vitro (**Fig. 36**) and TGF-β antagonism mainly targets the immune system rather than the cancer cells (Donkor et al, 2011; Nam et al, 2008), I we evaluated the effect of EW-7197 on immunophenotypes of melanoma-bearing mice. Treatment with EW-7197 increased the proportions and numbers of $CD8^+$ T cells significantly in the dLNs (**Fig. 34c and 37a**), non-dLNs and spleens (**Fig. 37b**). Other effector T cell subsets were unaltered (**Fig. 37c**). Splenic $CD8^+$ T cells as effector cells were prepared from vehicle- or EW-7197-treated mice for co-culture with target B16 cells to examine CTL function. $CD8^+$ T cells from EW-7197-treated mice induced significantly more apoptosis of target B16 cells (**Fig. 34d**). The mRNA expression of the cytolytic molecules, perforin, granzyme B, and FasL in whole dLNs and $CD8^+$ dLN cells and protein expression of perforin and granzyme B in dLN $CD8^+$ T cells of EW-7197-treated mice increased significantly (**Fig. 34e, 34f, 37d and 37e**).

To confirm whether enhanced $CD8^+$ T cell responses by EW-7197 are antigen-specific, I stimulated the carboxyfluorescein diacetate succinmidyl ester (CFSE)-labeled dLN cells with gp100 peptide, a melanosomal differentiation Ag expressed by melanomas and melanocytes (Thomson et al, 1988) and determined CFSE dilution of $CD8^+$ gate by flowcytometry. $CD8^+$ cells from EW-7197-treated mice showed significantly enhanced proliferation compared with $CD8^+$ cells from vehicle-treated mice (**Fig. 34g**). Tumor-infiltrating lymphocytes (TILs) increased significantly in the melanomas of EW-7197-treated mice, which were rarely observed in those of vehicle-treated mice (**Fig. 34h and Fig. 37f**). Especially, $CD8^+$ cell infiltration was remarkable in the melanomas of EW-7197-treated mice, which was absent in those of vehicle-treated mice (**Fig. 34h and i**). These data show that oral administration of a novel ALK5 inhibitor, EW-7197 has a potent therapeutic effect on B16 melanoma by upregulating CTL activities.

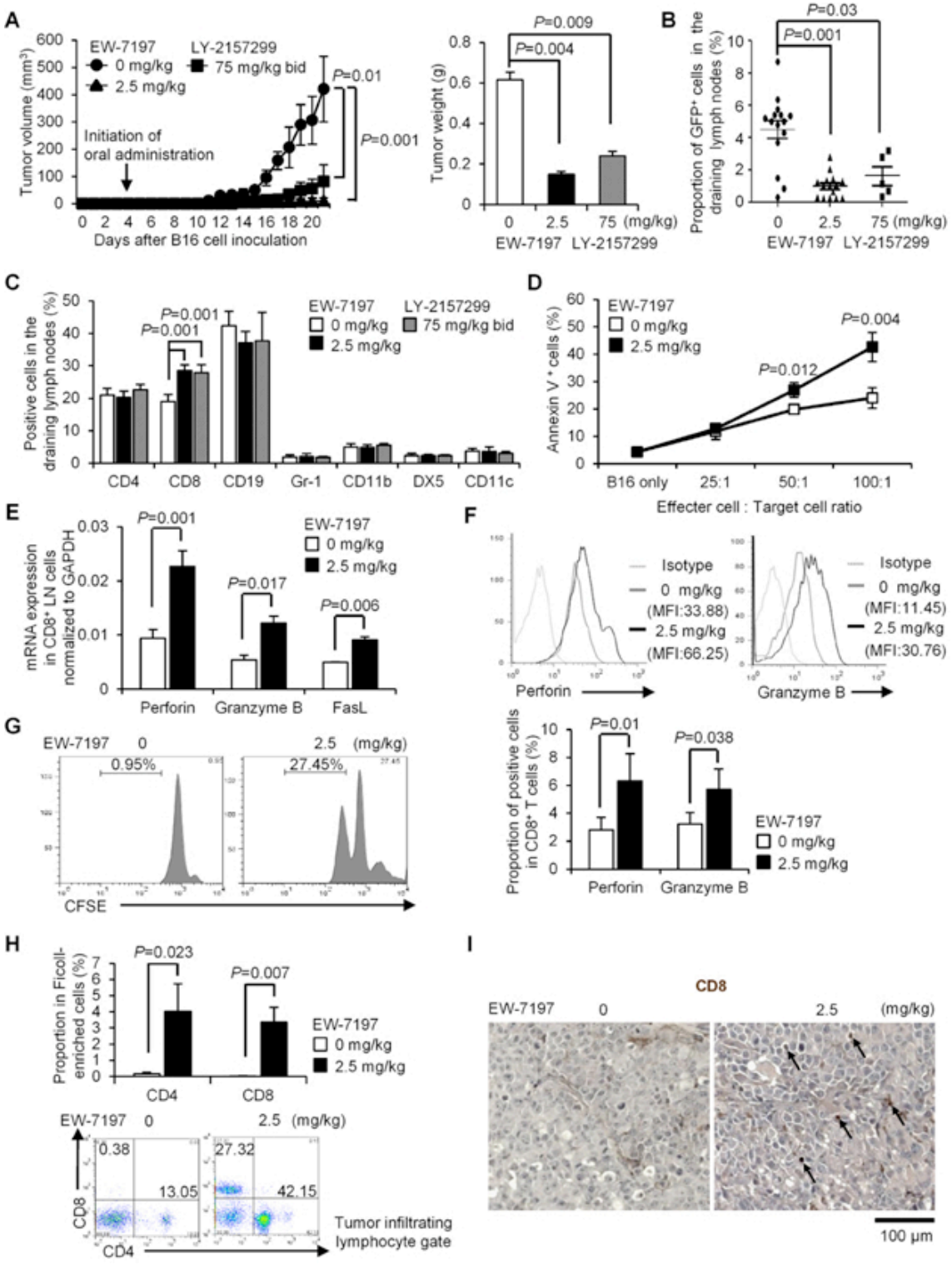

Figure 34 Oral administration of ALK5 inhibitors suppresses melanoma and LN metastases with enhanced CTL activity.

C57BL/6 mice were treated with vehicle or EW-7197 (2.5 mg/kg daily) (n = 15/group) /LY-2157299 (75 mg/kg bid) (n = 5) from 4 days after inoculation of GFP-expressing B16 cells (4×10^4) into the left footpads.

Data are shown as mean ± or + SEM. *P* values were calculated by 2-tailed unpaired Student's *t* test or by two-way ANOVA test for A.

(a) Chronological tumor volumes (left), tumor weights on day 21 (right). **(b,c)** The % of GFP^+ B16 cells (medians ± interquartile) and immune cell subsets in dLNs were determined by flowcytometry. **(d)** Target cytolysis at the indicated ratios of effector $CD8^+$ T cells: target B16 cells was evaluated by Annexin V/PI. **(e)** qPCR analyses for mRNA levels of the cytolytic molecules in $CD8^+$ dLN cells (*n* = 5/group). **(f)** Histograms show $CD8^+$ gate with MFI. Graphs show the % of positive cells in $CD8^+$ gate (*n* = 10/group). **(g)** Proliferation of $CD8^+$ dLN cells stimulated with gp100 peptide was assessed by CFSE dilution. **(h)** Representative CD4/8 dot plots of TILs. Graphs show the % of $CD4^+$ or $CD8^+$ cells in the Ficoll-enriched cells (*n* = 8/group). **(i)** Representative immunohistochemistry sections of inoculated melanomas (scale bar: 100 μm). Arrows indicate $CD8^+$ cells.

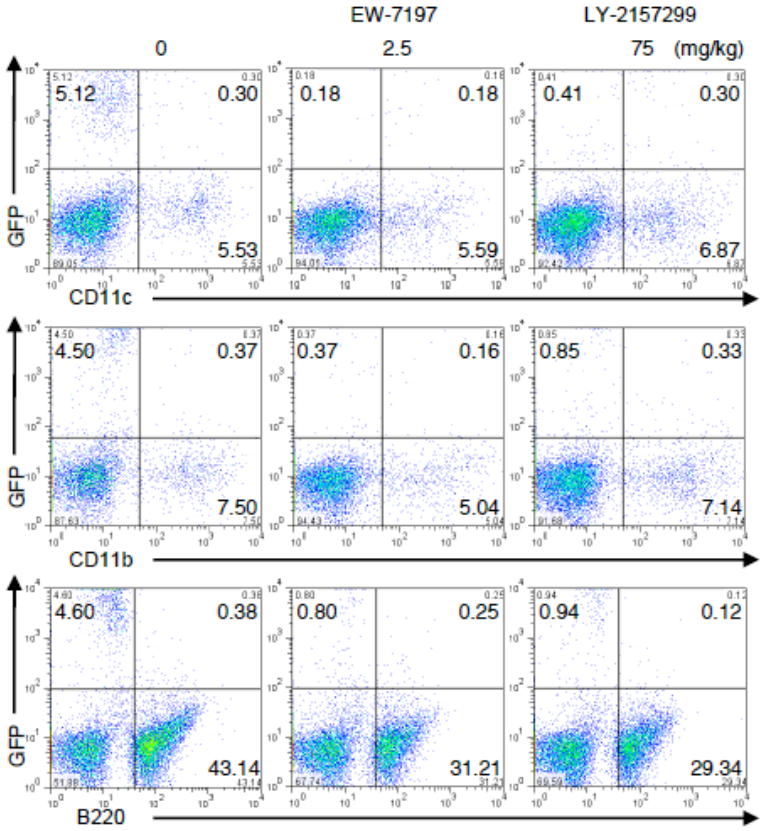

Figure 35 Dot plots by FACS analyses show GFP^+CD11c^-, GFP^+CD11b^-, GFP^+B220^- cells in the dLNs of melanoma-bearing mice three weeks after inoculation.

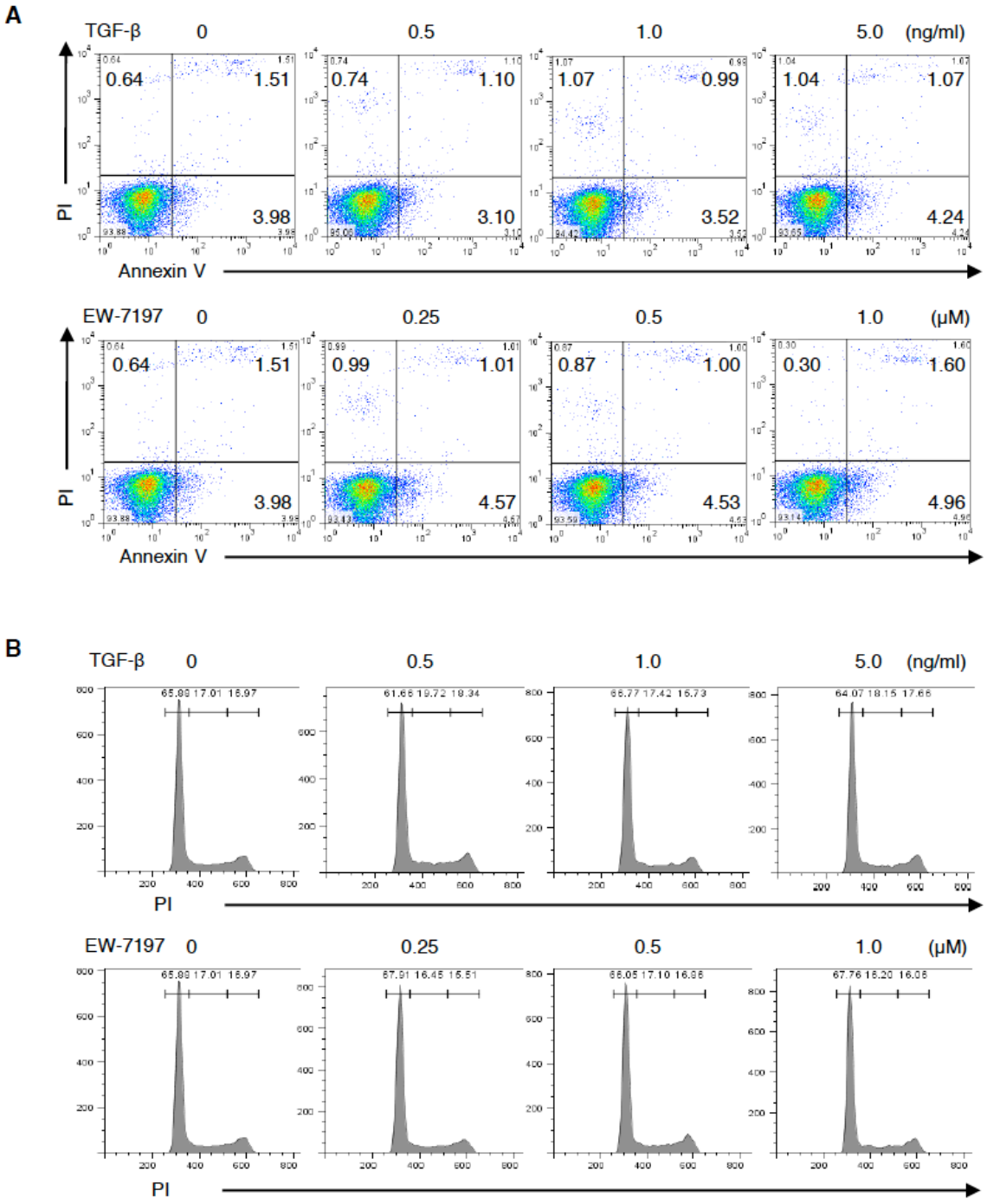

Figure 36 TGF-β does not affect apoptosis and cell cycle of B16 cells.

B16 cells were treated with TGF-β (0, 0.5, 1.0, 5.0 ng/ml) or EW-7197 (0, 0.25, 0.5, 1.0 μM) for 72 h. **(a)** Apoptosis was determined by Annexin V and PI staining. **(b)** Cell cycle was determined by PI staining using flow cytometry.

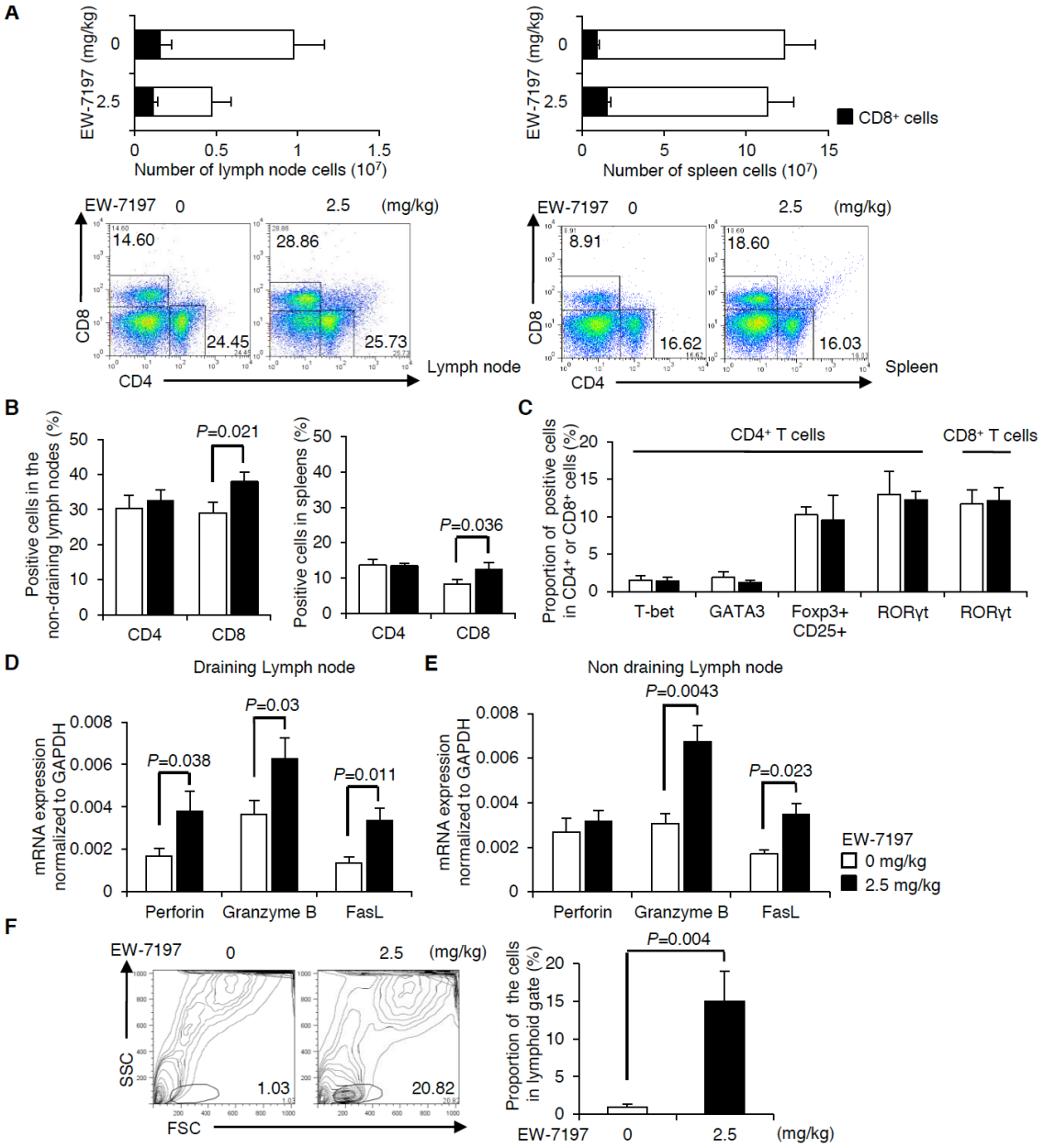

Figure 37 Oral administration of EW-7197 suppresses melanoma and LN metastases with enhanced CTL activity.

Data are shown as mean + SEM (n = 5-10/group). P values were calculated by 2-tailed unpaired Student's t test. **(a)** Total and $CD8^+$ cell numbers of LNs and spleens in the melanoma-bearing mice. Representative dot plots of CD4/8 are shown. **(b)** Percentages of CD4/8 subsets in the non-dLNs and spleens. **(c)** Percentages of effector T cell subsets in the dLNs. **(d,e)** qPCR analyses for mRNA levels of the cytolytic molecules in the dLNs and the non-dLNs. **(f)** Representative FSC/SSC contour plots of enriched tumor-infiltrated cells by density gradient centrifugation.

ALK5 inhibition downregulates Smad4 in melanoma-bearing mice

I next confirmed the blockade of TGF-β signaling by EW-7197 in vivo. Cells of dLNs and spleens from melanoma-bearing mice were immediately fixed for proximity ligation assay (PLA) to quantify endogenous Smad protein levels in vivo by single recognition protocol or to quantify protein interactions. EW-7197 blocked phosphorylation of Smad2 and Smad3 in dLN cells, while the expression levels of Smad2 and Smad3 were intact (**Fig. 38a-d**). Although phosphorylation of R-Smads is often monitored to confirm the efficacy of TGF-β antagonists (Donkor et al, 2011), their effect on Smad4 has not been evaluated. Treatment with EW-7197 blocked the interaction between Smad2/3 and Smad4 (**Fig. 38e**). Moreover, I found that EW-7197 significantly reduced Smad4 protein in both nucleus and cytoplasm of dLN cells (**Fig. 38f**). The same pattern was confirmed in spleens of EW-7197-treated mice and dLNs of LY-2157299-treated mice (**Fig. 39 and 40a-d**). Western blot analysis confirmed the reduction in Smad4 protein and R-Smad phosphorylation with intact R-Smad expression in dLNs and $CD8^+$ dLN cells by ALK5 inhibitors (**Fig. 38g and 40e**). However, EW-7197 did not affect Smad4 mRNA (**Fig. 38h**), indicating that EW-7197 did not downregulate Smad4 at the transcriptional level. Reduction in Smad4 protein was most remarkable in $CD8^+$ T cells (**Fig. 38g and i**).

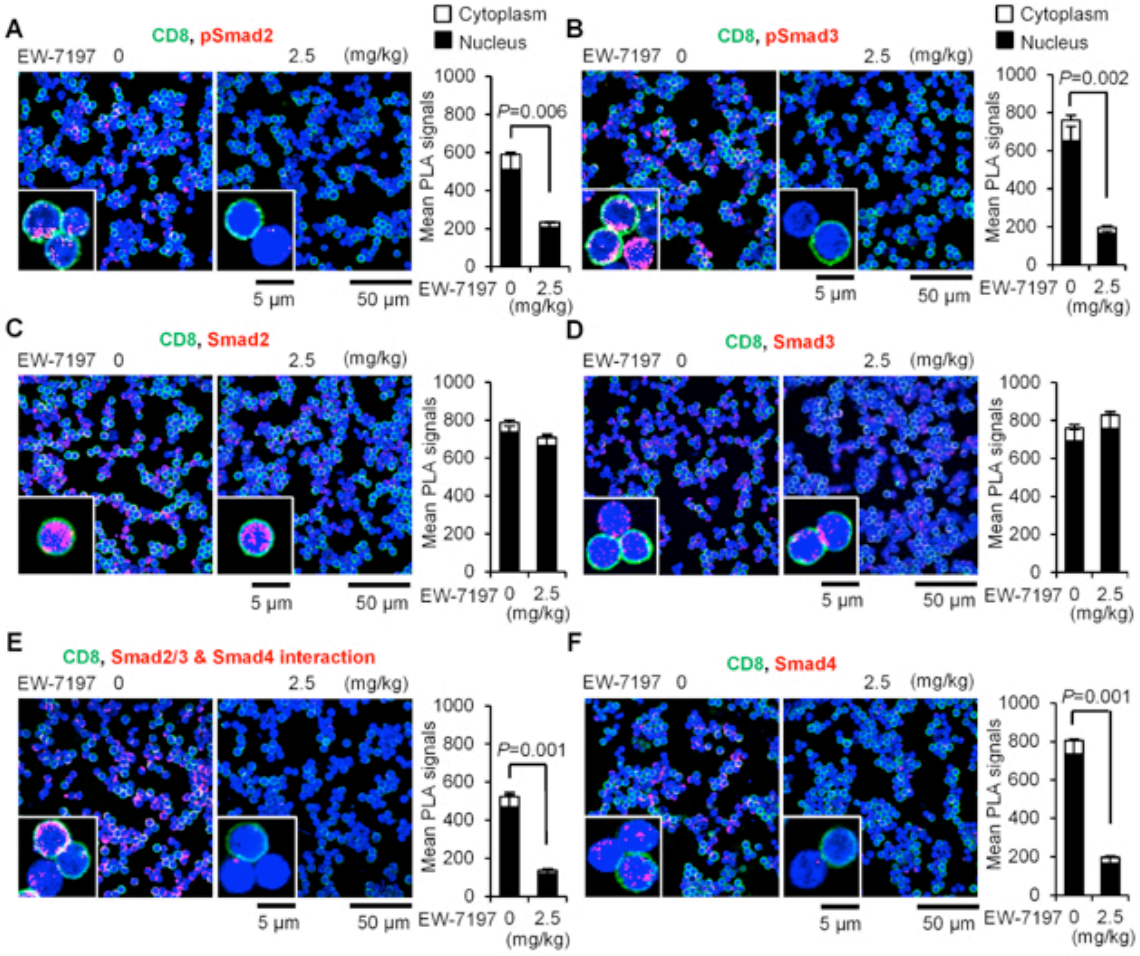

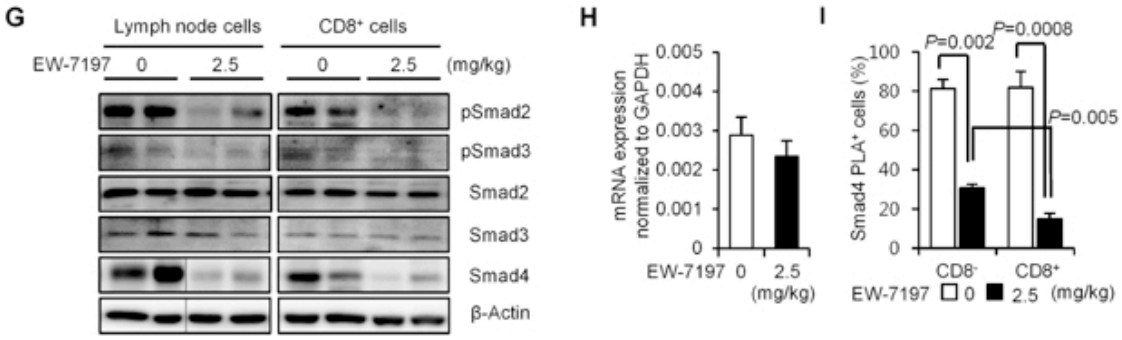

Figure 38 EW-7197 downregulates Smad4 and blocks R-Smad phosphorylation in melanoma -bearing mice.

Data are shown as mean + SEM (n = 5/group). P values were calculated by 2-tailed unpaired Student's t test. **(a-f)** PLA (red) show the expression of phosho-Smad2, phosho-Smad3, Smad2, Smad3, Smad4, and the interaction between Smad2/3 and Smad4 in dLN cells co-stained with anti-CD8 (green) (scale bars: 5 μm, 50 μm). Graphs show mean PLA signals quantified using BlobFinder software. **(g)** Western blots show Smads in whole or $CD8^+$ dLN cells from EW-7197-treated or vehicle-treated melanoma-bearing mice (2-3 mice/group). **(h)** qPCR analyses for Smad4 mRNA levels of dLN cells. **(i)** Graph shows the % of the Smad4 PLA^+ cells in $CD8^-$ and $CD8^+$ dLN cells.

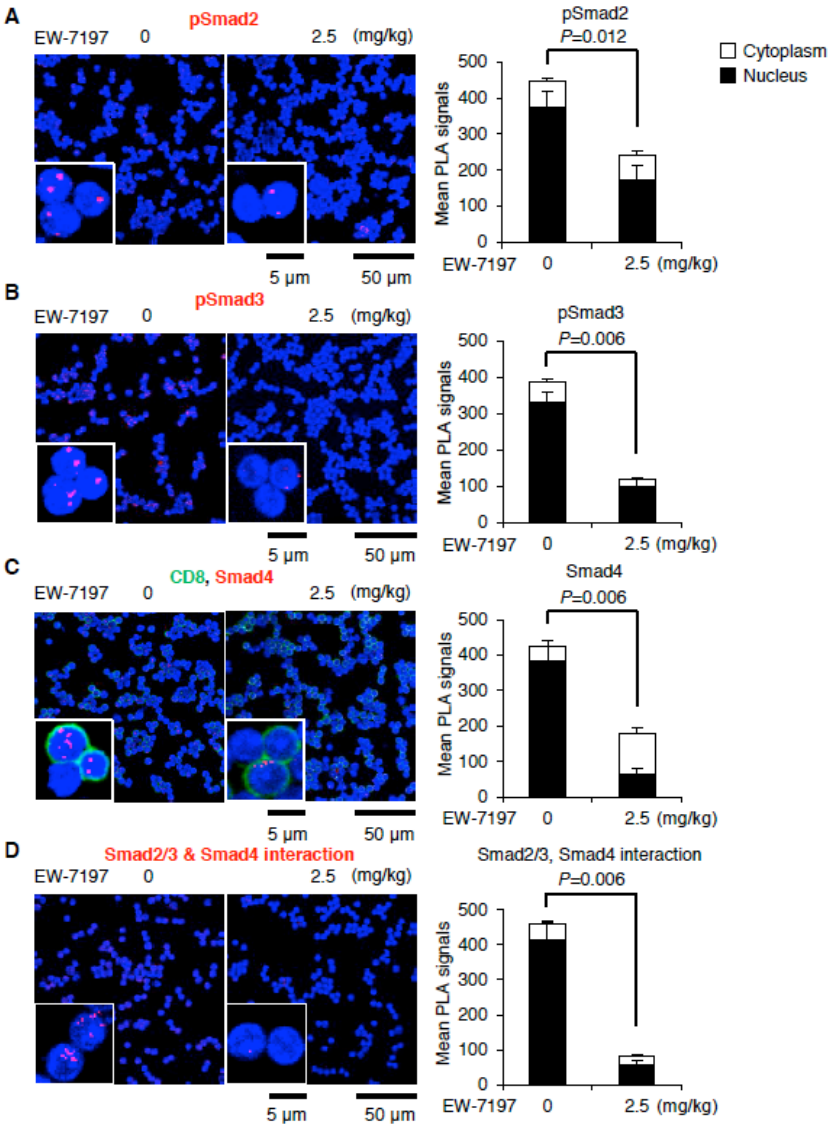

Figure 39 Oral administration of EW-7197 inhibits TGF-β signaling and downregulates Smad4 in spleen cells of melanoma-bearing mice.

(a-d) Expression of phospho-Smad2, phospho-Smad3, Smad4, and the interaction between Smad2/3 and Smad4 from EW-7197-treated mice was determined by PLA. Images were acquired by confocal microscope, LSM700 (scale bars: 5 μm, 50 μm). Graphs show the quantification of the red dots expressed in nucleus and cytoplasm. Data are shown as mean + SEM (n = 5/group). P values were calculated by 2-tailed unpaired Student's t test.

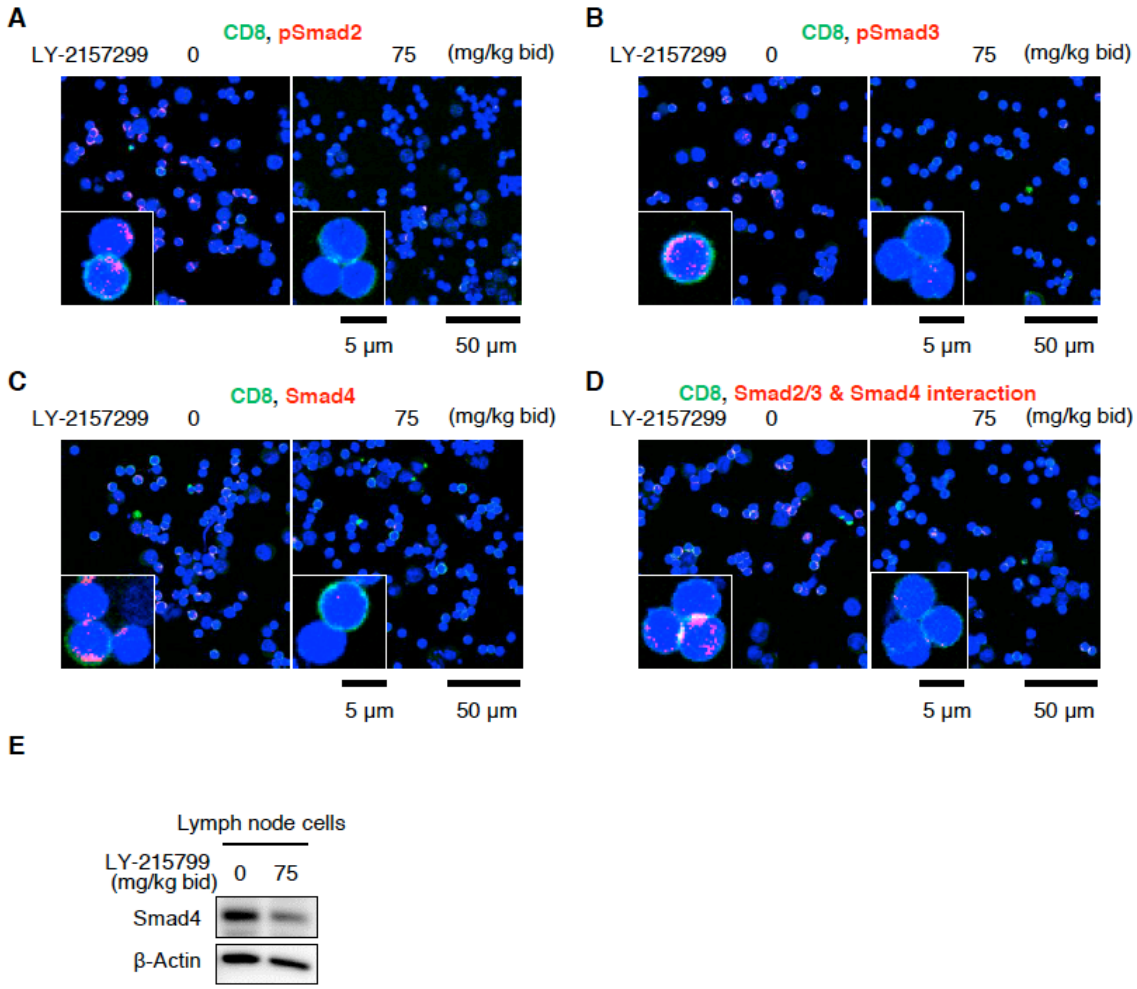

Figure 40 Oral administration of LY-2157299 inhibits TGF-β signaling and downregulates Smad4 in dLN cells of melanoma-bearing mice.

(a-d) Expression of phospho-Smad2, phospho-Smad3, Smad4, and the interaction between Smad2/3 and Smad4 in dLN cells from vehicle- or LY-2157299-treated mice was determined by PLA. Images were acquired by confocal microscope, LSM700 (scale bars: 5 μm, 50 μm). **(e)** Smad4 and β-Actin in dLN cells from vehicle- or LY-2157299-treated mice were detected by Western blotting.

ALK5 inhibition induces ubiquitin-mediated degradation of Smad4 in melanoma-bearing mice

Ubiquitination is a post-translational modification of proteins, which plays a key role in TGF-β signal transduction by regulating Smad protein levels (De Boeck et al, 2012; Izzi et al, 2004). PLA detected the significantly increased interaction of ubiquitin with Smad4 in dLN cells, especially in $CD8^+$ T cells of the melanoma-bearing mice treated with EW-7197 or LY-2157299 (**Fig. 41a and 42**). By contrast, neither Smad2 nor Smad3 interacted with ubiquitin in dLN cells of both vehicle- and EW-7197-treated mice (**Fig. 43**). Endogenous ubiquitinated Smad4 captured by UbiQapture-Q matrices was increased in $CD8^+$ dLN cells from EW-7197-treated mice (**Fig. 41b**). Consistently, EW-7197 also induced downregulation of Smad4 protein in $CD8^+$ T cells stimulated with anti-CD3/CD28 antibodies in vitro, but not in $CD4^+$ T cells, although it inhibited R-Smad phosphorylation in both $CD4^+$ and $CD8^+$ T cells (**Fig. 41c**). A proteasome inhibitor, MG-132 abolished EW-7197-induced downregulation of Smad4 in $CD8^+$ T cells (**Fig. 41c**), indicating that the ubiquitin-proteasomal system is responsible for Smad4 protein degradation. EW-7197 induced ubiquitination of Smad4 in activated $CD8^+$ T cells in a dose dependent manner (**Fig. 41d**). Unlike $CD8^+$ T cells, treatment with EW-7197 did not affect Smad4 protein expression in both transplanted B16 melanoma in vivo and B16 melanoma cells in vitro, despite the inhibition of R-Smad phosphorylation (**Fig. 41e and f**).

Among the E3 ubiquitin ligases, which modulate TGF-β signaling, Smurf2 is upregulated by IL-7 in $CD8^+$ T cells (Pellegrini et al, 2009). However, knockdown of Smurf1 and/or Smurf2 by shRNA did not affect Smad4 downregulation by EW-7197 in $CD8^+$ T cells (**Fig. 44**).

Taken together, systemic ALK5 inhibition in melanoma-bearing mice blocks TGF-β signaling by not only inhibiting R-Smad phosphorylation, but also inducing ubiquitin-mediated degradation of Smad4 protein in immune cells, especially in $CD8^+$ T cells, but not in melanoma cells.

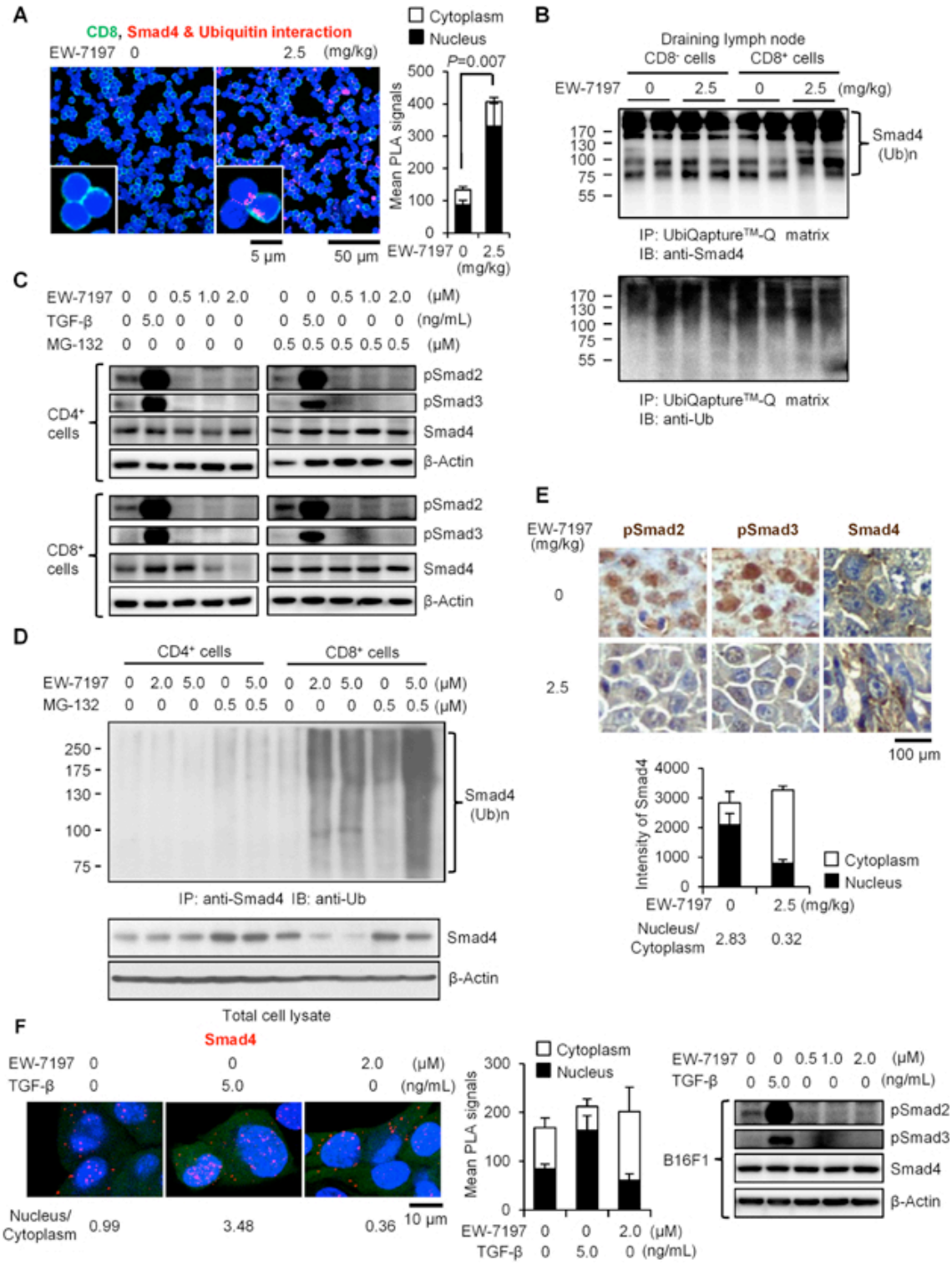

Figure 41 ALK5 inhibition induces ubiquitin-mediated degradation of Smad4 in CD8$^+$ T cells in melanoma-bearing mice.

(a) PLA (red) show ubiquitinated Smad4 in the dLN cells co-stained with anti-CD8 (green) (scale bars: 5 μm, 50 μm).

(b) Western blot shows endogenous ubiquitinated Smad4 in $CD8^+$ dLN cells captured using an UbiQapture^{TM}-Q kit. **(c)** Western blots show Smads in $CD4^+$ and $CD8^+$ cells stimulated with anti-CD3/CD28 with/without EW-7197 and/or MG-132 for 3 days. **(d)** IP-Western blot shows endogenous ubiquitinated Smad4 in $CD8^+$ cells stimulated with anti-CD3/CD28 with/without EW-7197 and/or MG-132 for 3 days. **(e)** Representative immunohistochemistry sections of inoculated melanomas (scale bar: 100 μm). **(f)** Smad4 protein in B16 cells was detected by PLA (red) (scale bars: 10 μm) (left). Western blots show Smads in B16 cells cultured with EW-7197 with or without TGF-β1 (right).

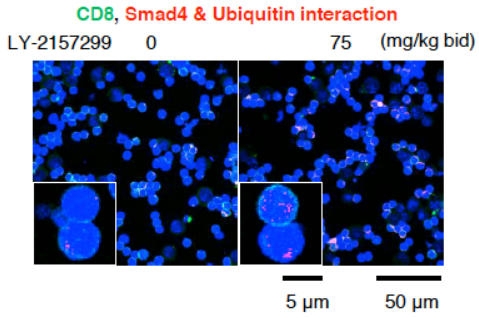

Figure 42 LY-2157299 induces Smad4 ubiquitination in dLN cells of melanoma-bearing mice.
Interaction between Smad4 and ubiquitin in dLN cells of vehicle- or LY-2157299-treated melanoma-bearing mice was determined by PLA. Images were acquired by confocal microscope, LSM700 (scale bars: 5 μm, 50 μm).

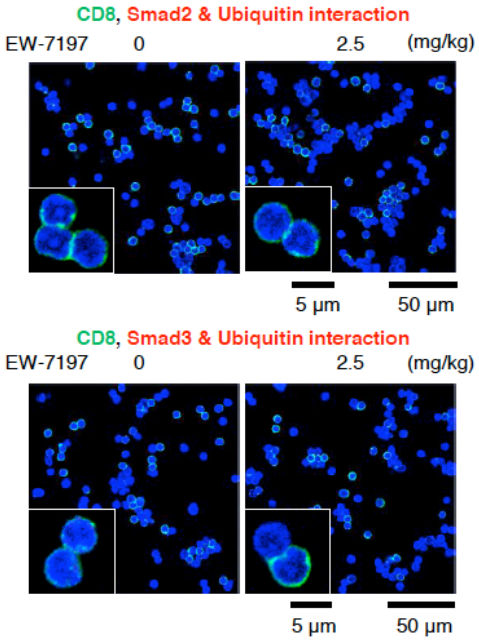

Figure 43 R-Smads are not ubiquitinated in dLN cells of EW-7197-treated melanoma-bearing mice.
Interaction between Smad2 and ubiquitin or Smad3 and ubiquitin in dLN cells of vehicle- or

EW-7197-treated melanoma-bearing mice was determined by PLA. Images were acquired by confocal microscope, LSM700 (scale bars: 5 μm, 50 μm).

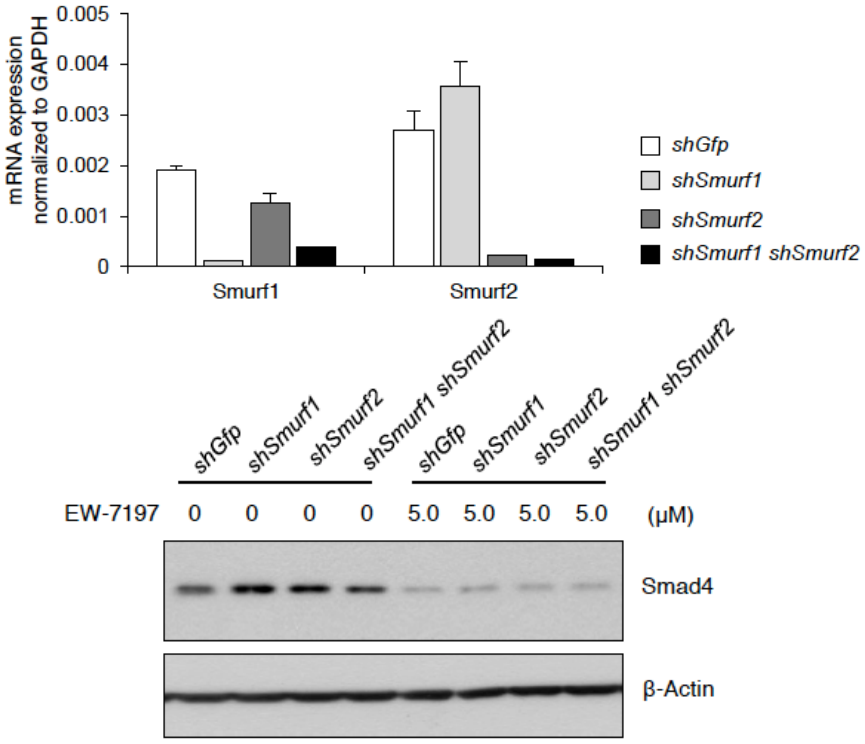

Figure 44 Smurf1 and Smurf2 are not involved in degradation of Smad4 by ALK5 inhibition.
Knockdown of Smurf1 and/or Smurf2 by shRNA was confirmed by qPCR. Western blots show Smad4 and β-Actin in $CD8^+$ T cells stimulated with anti-CD3/28 antibodies with or without EW-7197 in vitro.

T cell-specific Smad4 deletion suppresses the progression of melanoma with enhanced CTL activity

Similarly with Smad4 downregulation by EW-7197 treatment, the orthotopic B16 melanoma model using T cell-specific Smad4 knockout mice (Kim et al, 2006) showed significant suppression of melanoma growth and LN metastases (**Fig. 45a and b**). $CD8^+$ T cells increased significantly in the dLNs (**Fig 45c**), non-dLNs, and spleens (**Fig. 46a**) of *Cd4Cre;Smad4*$^{fl/fl}$ (*Smad4*$^{-/-}$) mice. Other effector T cell subsets were unaltered by the *Smad4* genotypes (**Fig. 46b**). The cytotoxicity assay showed significantly more B16 lysis by *Smad4*$^{-/-}$ $CD8^+$ T cells (**Fig. 45d**). The mRNA and protein expression of cytolytic molecules increased significantly in whole dLNs and $CD8^+$ dLN cells of *Smad4*$^{-/-}$ mice, as in EW-7197-treated mice (**Fig. 45e, f and 46c**).

Stimulation with gp100 peptide induced significantly more proliferation of $CD8^+$ dLN cells from *Smad4*$^{-/-}$ mice compared with *Cd4Cre;Smad4*$^{+/+}$ (*Smad4*$^{+/+}$) mice (**Fig. 45g**). TILs increased significantly in the melanomas of *Smad4*$^{-/-}$ mice, which were rarely observed in those of *Smad4*$^{+/+}$ mice (**Fig. 45h and 46d**). Especially, $CD8^+$ cell infiltration was remarkable in the melanomas of *Smad4*$^{-/-}$ mice, which was absent in those of *Smad4*$^{+/+}$ mice (**Fig. 45h and i**). These data are essentially identical to those obtained from EW-7197-treated mice, suggesting that TGF-β suppresses antigen-specific CTL functions via Smad4 without affecting other effector T cell subsets, and that treatment with EW-7197 phenocopies the effect of T-cell specific Smad4 knockout.

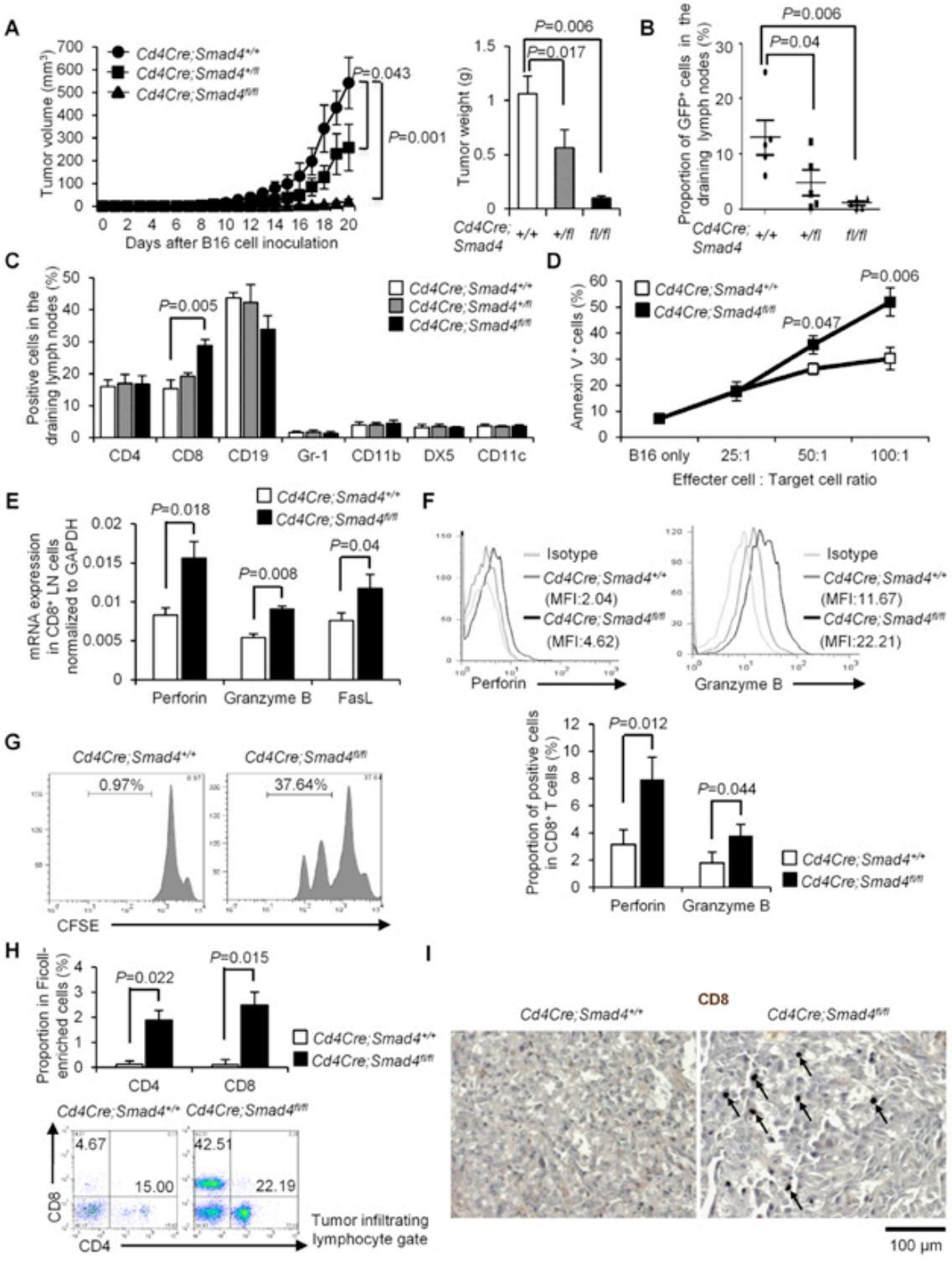

Figure 45 T cell-specific Smad4 deletion suppresses melanoma and LN metastases with enhanced CTL activity. GFP-expressing B16 cells were inoculated into the left footpads of *Cd4Cre;Smad4*$^{+/+}$, *Cd4Cre;Smad4*$^{+/fl}$, and *Cd4Cre;Smad4*$^{fl/fl}$ mice. Data are shown as mean ± or + SEM (n = 5-8/genotype). P values were calculated by 2-tailed unpaired Student's t test or by two-way ANOVA test for (a). **(a)**

Chronological tumor volumes (left), tumor weights on day 21 (right). **(b,c)** The % of GFP^+ B16 cells (medians ± interquartile) and immune cell subsets in dLNs were determined by flowcytometry. (*n* = 25/genotype). **(d)** Cytolysis at the indicated ratios of effector $CD8^+$ T cells: target B16 cells. (**e)** qPCR analyses for mRNA levels of the cytolytic molecules in $CD8^+$ dLN cells (*n* = 5/genotype). **(f)** Histograms show $CD8^+$ gate with MFI. Graphs show the % of positive cells in $CD8^+$ gate (*n* = 25/genotype). **(g)** Proliferation of $CD8^+$ dLN cells stimulated with gp100 peptide was assessed by CFSE dilution. **(h)** Representative CD4/8 dot plots of TILs. Graphs show the % of $CD4^+$ or $CD8^+$ cells in the Ficoll-enriched cells (*n* = 5/genotype). **(i)** Representative immunohistochemistry sections of inoculated melanomas (scale bar: 100 μm). Arrows indicate $CD8^+$ cells.

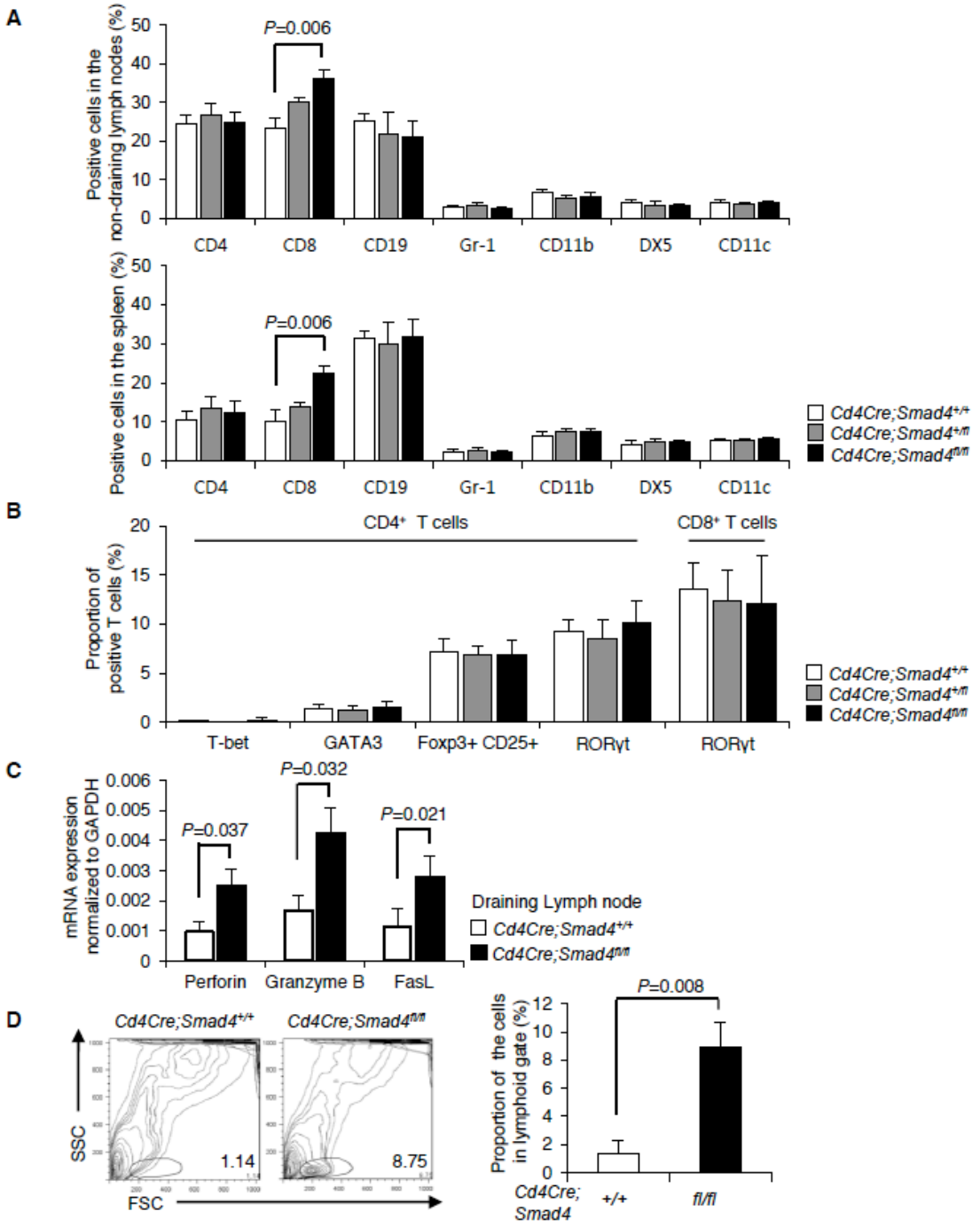

Figure 46 T cell-specific Smad4 deletion suppresses melanoma and LN metastases with enhanced CTL activity.

Data are shown as mean + SEM (n = 25/group). P values were calculated by 2-tailed unpaired Student's t test. **(a)** Percentages of immune cell subsets in the non-dLNs and spleens (n = 25/genotype). **(b)** Percentages of effector T cell subsets in the dLNs. **(c)** qPCR analyses for mRNA levels of the cytolytic molecules in the dLNs. **(d)** Representative FSC/SSC contour plots of enriched tumor-infiltrated cells by density gradient centrifugation.

ALK5 inhibition and T cell-specific Smad4 deletion upregulate Eomes in $CD8^+$ T cells of melanoma-bearing mice

To address underlying mechanisms of enhanced CTL activity by Smad4 downregulation, I examined the master transcription factors for CTLs, T-bet and Eomes. T-bet suppresses metastases (Peng et al, 2004), and TGF-β1 suppresses T-bet and IFN-γ in $CD4^+$ T cells (Park et al, 2007). However, expression of neither T-bet nor IFN-γ in $CD8^+$ T cells was affected (**Fig. 47a and b**). Instead, I found that $Eomes^+$ $CD8^+$ T cells increased significantly in dLNs of melanoma-bearing mice by the treatment with EW-7197, LY-2157299, or T cell-specific Smad4 deletion (**Fig. 47a, b and 48a-c**). Eomes mRNA expression in dLNs and $CD8^+$dLN cells also increased significantly by EW-7197 or T cell-specific Smad4 deletion (**Fig. 47c and 48d**). Expression of Eomes in $CD4^+$ T cells was very low in any melanoma-bearing mice (**Fig. 49**). $CD8^+$ TILs in EW-7197-treated or *Smad4*$^{-/-}$ mice expressed high levels of Eomes (**Fig. 47d**). Significantly more $Eomes^+$ cells infiltrated into the melanomas by EW-7197 or T cell-specific Smad4 deletion (**Fig. 47e**). Proportions of TIL subsets except T cells in EW-7197-treated or *Smad4*$^{-/-}$ mice were unaltered compared with the controls (**Fig. 50**). These data suggest that Smad4-mediated TGF-β signaling suppresses CTLs by specific downregulation of Eomes.

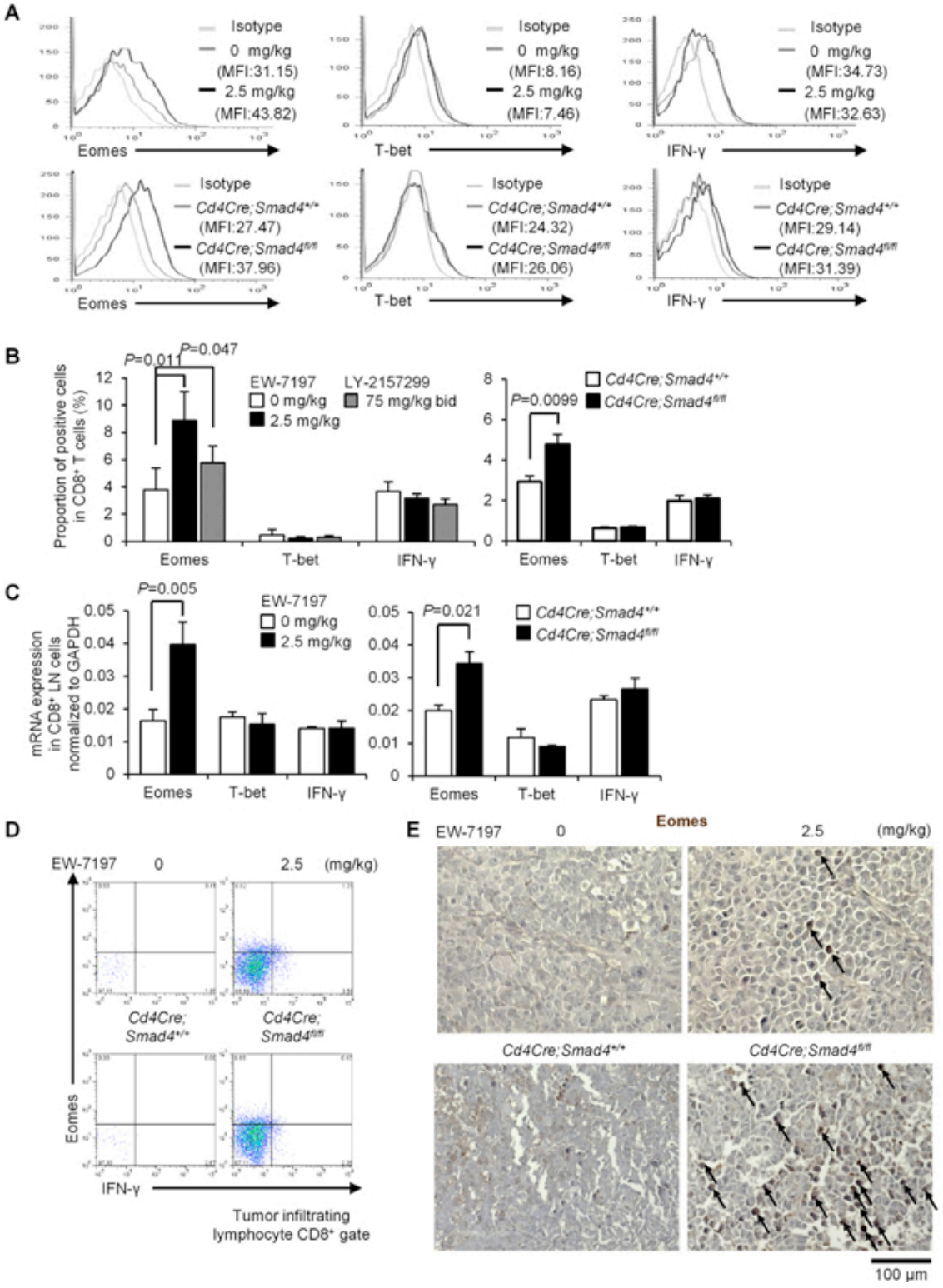

Figure 47 Upregulation of Eomes in CD8$^+$ T cells of melanoma-bearing mice by the treatment with ALK5 inhibitors and T cell-specific Smad4 deletion.

Data are shown as mean + SEM. *P* values were calculated by 2-tailed unpaired Student's *t* test. **(a)**

Representative histograms show Eomes, T-bet, and IFN-γ expression in $CD8^+$ dLN cells with MFI. **(b)** Graphs show the % of positive cells in $CD8^+$ dLN cells of EW-7197 (n = 10) or LY-2157299 (n = 5) treated or *Cd4Cre;Smad4*$^{+/+}$ and *Cd4Cre;Smad4*$^{fl/fl}$ (n = 10/genotype) melanoma-bearing mice. **(c)** qPCR analyses for mRNA levels in $CD8^+$ dLN cells (n = 5/group, n = 5/genotype). **(d)** Representative Eomes/IFN-γ dot plots of $CD8^+$ gated TILs. Graphs show the % of positive cells in the Ficoll-enriched cells (n = 8/group, n = 5/genotype). **(e)** Representative immunohisochemistry sections of inoculated melanomas (scale bar: 100 μm). Arrows indicate $Eomes^+$ cells.

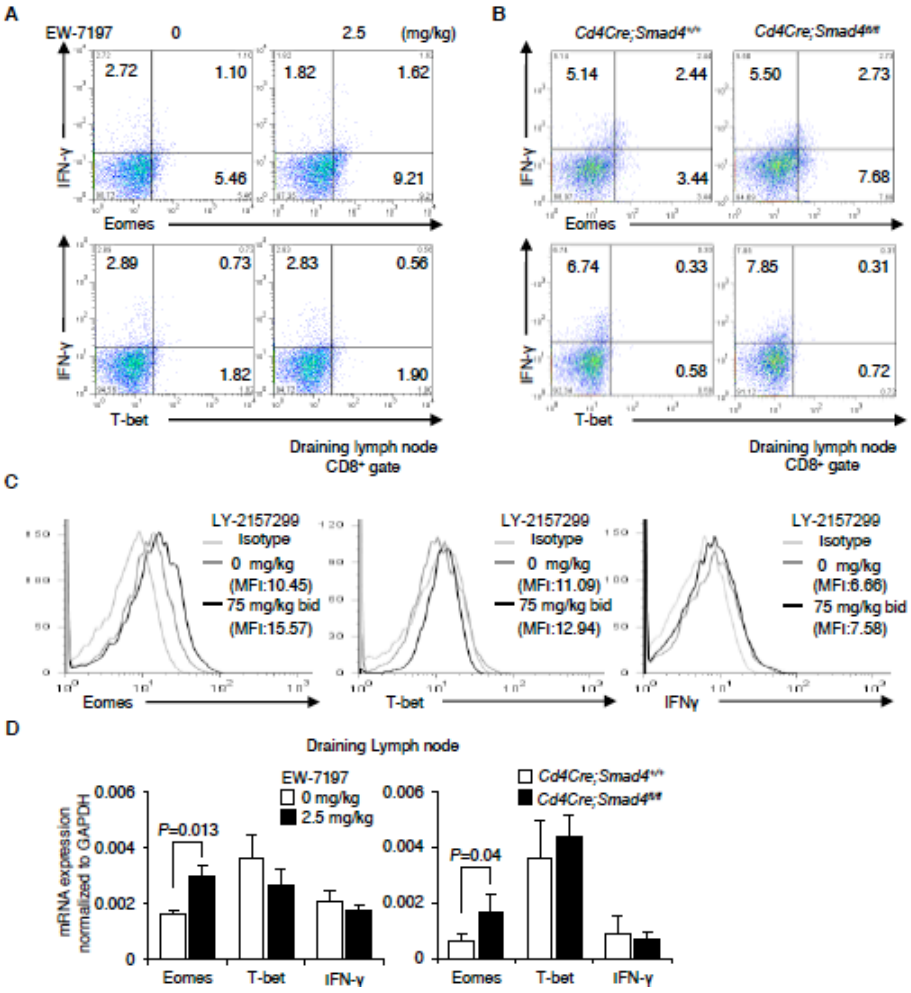

Figure 48 Upregulation of Eomes in CD8+ T cells by ALK5 inhibition or T cell-specific Smad4 deletion.

(a) Representative dot plots show the expression of Eomes, T-bet, and IFN-γ _in dLN $CD8^+$ cells of vehicle- or EW-7197-treated melanoma-bearing mice. **(b)** Representative dot plots show the expression of Eomes, T-bet, and IFN-γ _in dLN $CD8^+$ cells of *Cd4Cre;Smad4*$^{+/+}$ or *Cd4Cre;Smad4*$^{fl/fl}$ mice. **(c)** Representative histograms show the expression of Eomes, T-bet, and IFN-γ _in dLN $CD8^+$ cells of vehicle- or LY-2157299-treated melanoma-bearing mice. **(d)** qPCR analyses for mRNA levels in dLN cells of vehicle- or EW-7197-treated melanoma-bearing and *Cd4Cre;Smad4*$^{+/+}$ or *Cd4Cre;Smad4*$^{fl/fl}$ mice

(n = 10/group, n = 10/genotype).

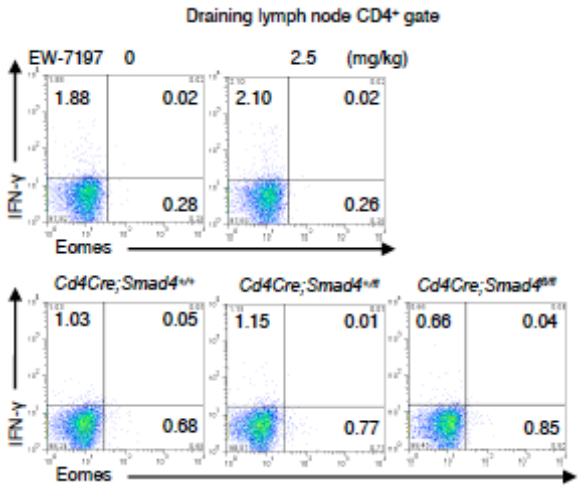

Figure 49 Eomes is not expressed in CD4$^+$ cells in the dLNs of melanoma-bearing mice. Representative dot plots show the expression of IFN-γ _and Eomes in CD4$^+$ cells from vehicle-treated, EW-7197-treated, *Cd4Cre;Smad4*$^{+/+}$, *Cd4Cre;Smad4*$^{+/fl}$, and *Cd4Cre;Smad4*$^{fl/fl}$ mice.

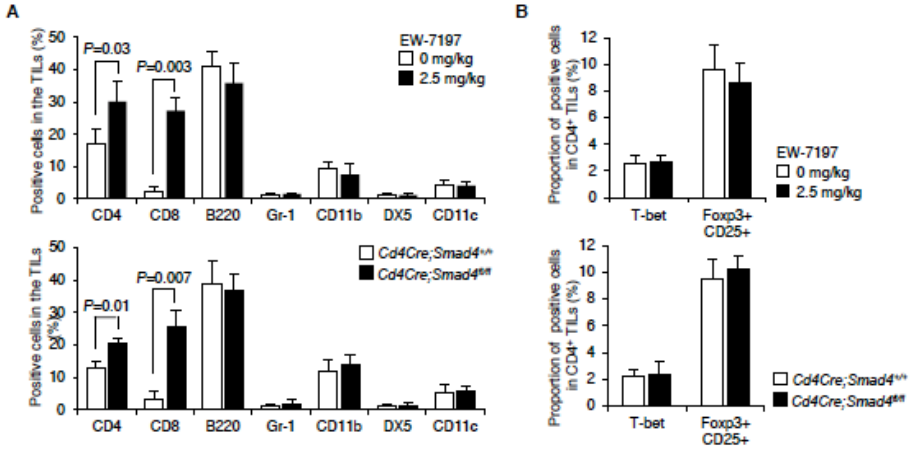

Figure 50 Characterization of TILs.

TILs subsets in melanomas of control, EW-7197-treated or *Smad4*$^{-/-}$ mice were determined by flowcytometry. Graphs show the percentages of positive cells. **(a)** Percentages of immune cell subsets in TIL gates were determined by flowcytometry. **(b)** Percentages of T-bet$^+$ or Foxp3$^+$CD25$^+$ in CD4$^+$ TIL gates were determined by flowcytometry.

Anti-melanoma effect of EW-7197 depends on $CD8^+$ T cells

To confirm whether $CD8^+$ T cells are necessary for anti-melanoma effect of EW-7197, I deleted $CD8^+$, $CD4^+$ or NK cells in C57BL/6 mice inoculated with GFP-expressing B16 cells (2×10^5). Intraperitoneal injection of anti-CD8, anti-CD4, or anti-asialo GM1 antibody efficiently deleted the specific cell compartment, respectively (**Fig. 51b-d and 52a**). EW-7197 significantly suppressed tumor growth even with this aggressive protocol (**Fig. 51a**). Deletion of $CD8^+$, $CD4^+$ or NK cells did not affect tumor growth in the absence of EW-7197 treatment (**Fig. 51a-d**). Anti-tumor effect of EW-7197 was completely abolished on deletion of $CD8^+$ cells, rather, EW-7197 slightly exacerbated tumor growth in $CD8^+$-deleted mice (**Fig. 51b and e**). In contrast, EW-7197 showed significant anti-tumor efficacy on deletion of $CD4^+$ cells or NK cells (**Fig 51c-e**). In NK-deleted mice, I observed approximately 40% reduction in the efficacy of EW-7197 on tumor growth and $CD8^+$ T cell expansion (**Fig. 51d-f**), suggesting that EW-7197 exerts the efficacy partially via NK cells, similarly to the previous report on the efficacy of the neutralizing anti-TGF-β antibody 1D11 on a mouse 4T1 model of metastatic breast cancer (Nam et al, 2008). Treatment with EW-7197 resulted in a significant increase in $CD8^+$ T cells with upregulated Eomes expression in $CD4^+$-deleted and NK-deleted mice as well as control (**Fig. 51f, g and 52b**). These data verify the previous reports that anti-tumor effect of the TGF-β antagonism mainly depends on $CD8^+$ T cells (Donkor et al, 2011; Gorelik et al, 2001; Nam et al, 2008; Zhang et al, 2005).

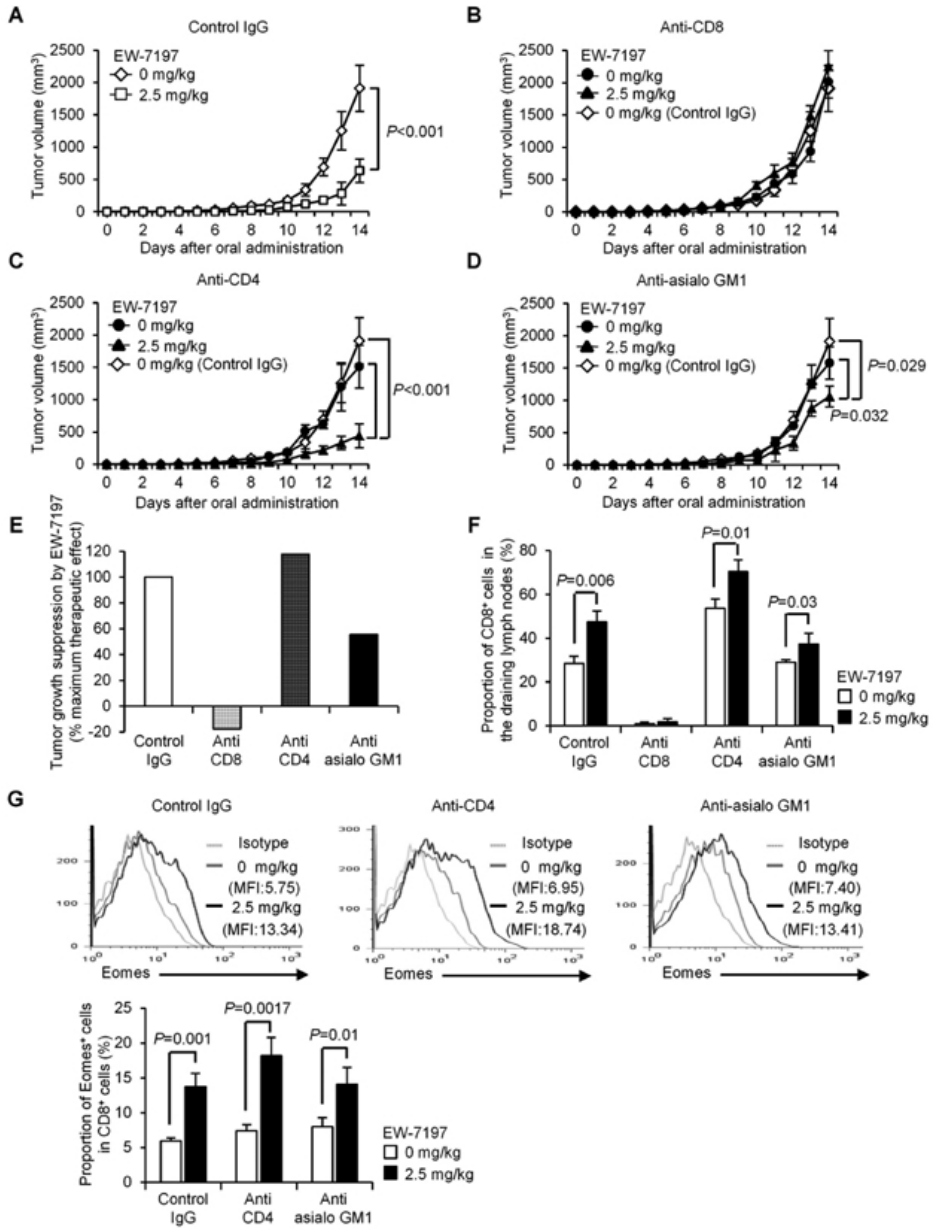

Figure 51 CD8$^+$ T cells are necessary for anti-melanoma effect of EW-7197.

C57BL/6 mice were i.p. injected with control, anti-CD8, anti-CD4, or anti-asialo GM1 antibody at day -4, 0, 7, and 14 of melanoma inoculation (day 0), with vehicle or EW-7197 from 4 days after inoculation of GFP-expressing B16 cells (2×10^5) into the left lower abdomen (n = 5-8/group). Data are shown as mean ± or + SEM. P values were calculated by 2-tailed unpaired Student's t test or by two-way ANOVA test. **(a-d)** Chronological tumor volumes of the mice treated with the indicated antibodies. **(e)** The efficacy of EW-7197 following each antibody treatment was expressed as a % of the maximum therapeutic effect seen in the intact system (control IgG). **(f)** The % of CD8$^+$ cells in dLNs were determined by flowcytometry. **(g)** Histograms show the expression of Eomes in CD8$^+$dLN cells. The graph shows the % of Eomes$^+$ in CD8$^+$dLN cells were determined by flowcytometry.

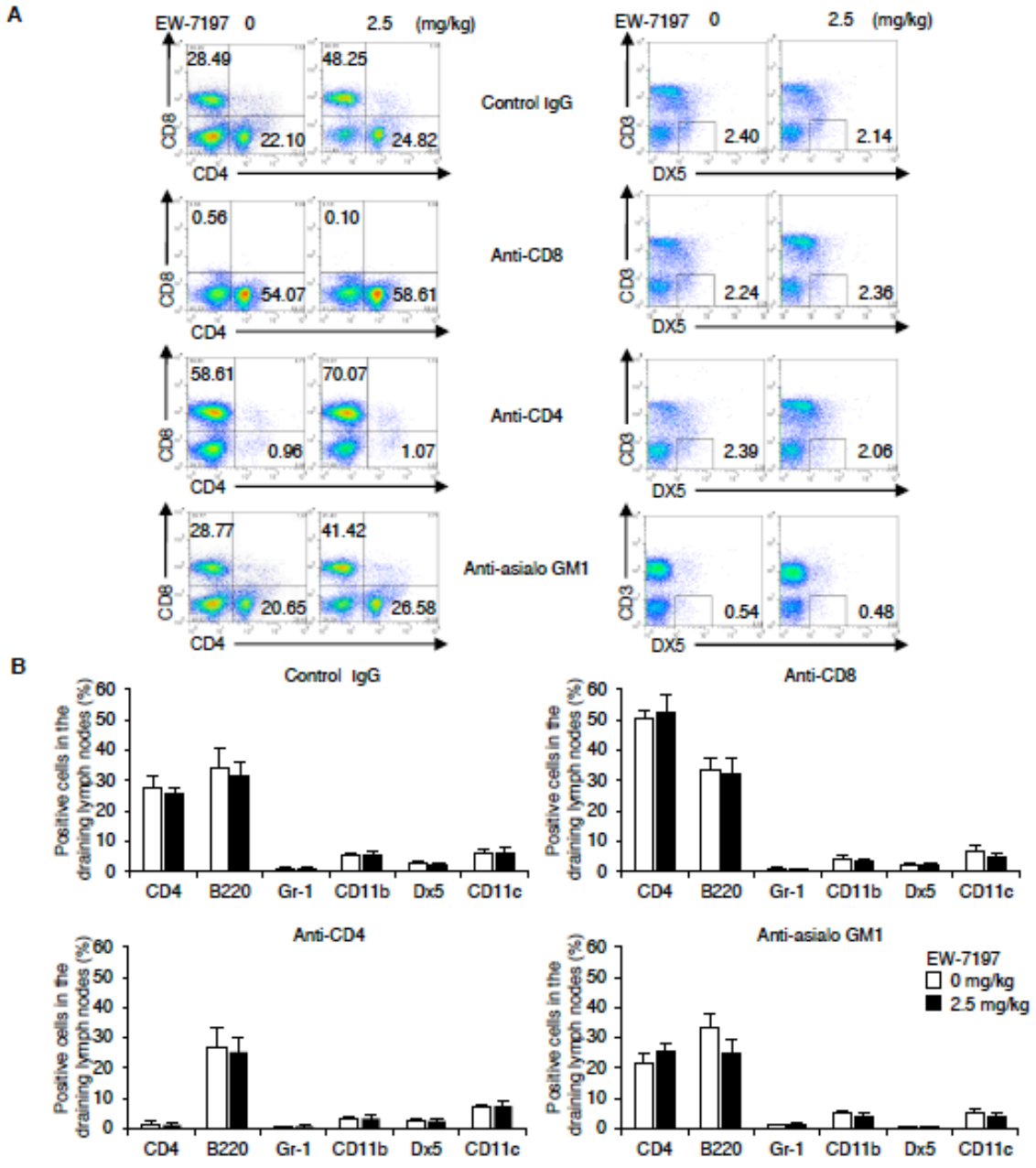

Figure 52 Deletion of CD8$^+$ T cells, CD4$^+$ T cells, NK cells in vivo.

C57BL/6 mice were i.p. injected with control, anti-CD8, anti-CD4, or anti-asialo GM1 antibody at day -4, 0, 7, and 14 of melanoma inoculation (day 0), with vehicle or EW-7197 from 4 days after inoculation of GFP-expressing B16 cells (2´105) into the left lower abdomen (*n* = 5-8/group). Data are shown as mean + SEM. **(a)** Representative dot plots are shown for each antibody treatment. **(b)** Graphs show the percentages of immune cell subsets.

Long-term systemic administration of EW-7197 and T cell-specific Smad4 deletion maintain normal immune homeostasis

I determined whether Smad4 downregulation by ALK5 inhibition or gene deletion causes pro-inflammatory untoward effects because T cell-specific Smad4 deficient mice with mixed backgrounds (C57BL/6, Sv129, and FVB) develop inflammation and carcinogenesis in gastrointestinal tract (Hahn et al, 2011; Kim et al, 2006). *Cd4Cre;Smad4*$^{+/fl}$ mice were backcrossed to C57BL/6 strain for eight generations and confirmed the deletion of the *Smad4* gene in both $CD4^+$ and $CD8^+$ T cells (**Fig. 54**). C57BL/6 mice were treated with vehicle or vehicle containing EW-7197 (2.5 mg/kg daily) for 8 weeks. The proportions and numbers of immune cells, naïve/memory $CD4^+$/$CD8^+$ T cells, and Treg in the spleens and superficial LNs of vehicle-treated or Smad4$^{+/+}$ mice were comparable to those of EW-7197-treated mice or *Smad4*$^{-/-}$ mice at 16 week-old (**Fig. 53a-c**). Low expression levels of Eomes and T-bet in steady-state $CD8^+$ T cells were not altered by EW-7197 or T cell-specific Smad4 deletion (**Fig. 53d**). Consistent with normal immune homeostasis by lifetime exposure to a soluble TGF-β antagonist (Yang et al, 2002), treatment with EW-7197 for 8 weeks maintained normal immune homeostasis (**Fig. 53a-d**).

Thus, long-term systemic administration of EW-7197 or T cell-specific Smad4 deletion did not affect systemic immune homeostasis in C57BL/6 mice without melanoma challenge in a specific pathogen-free (SPF) environment.

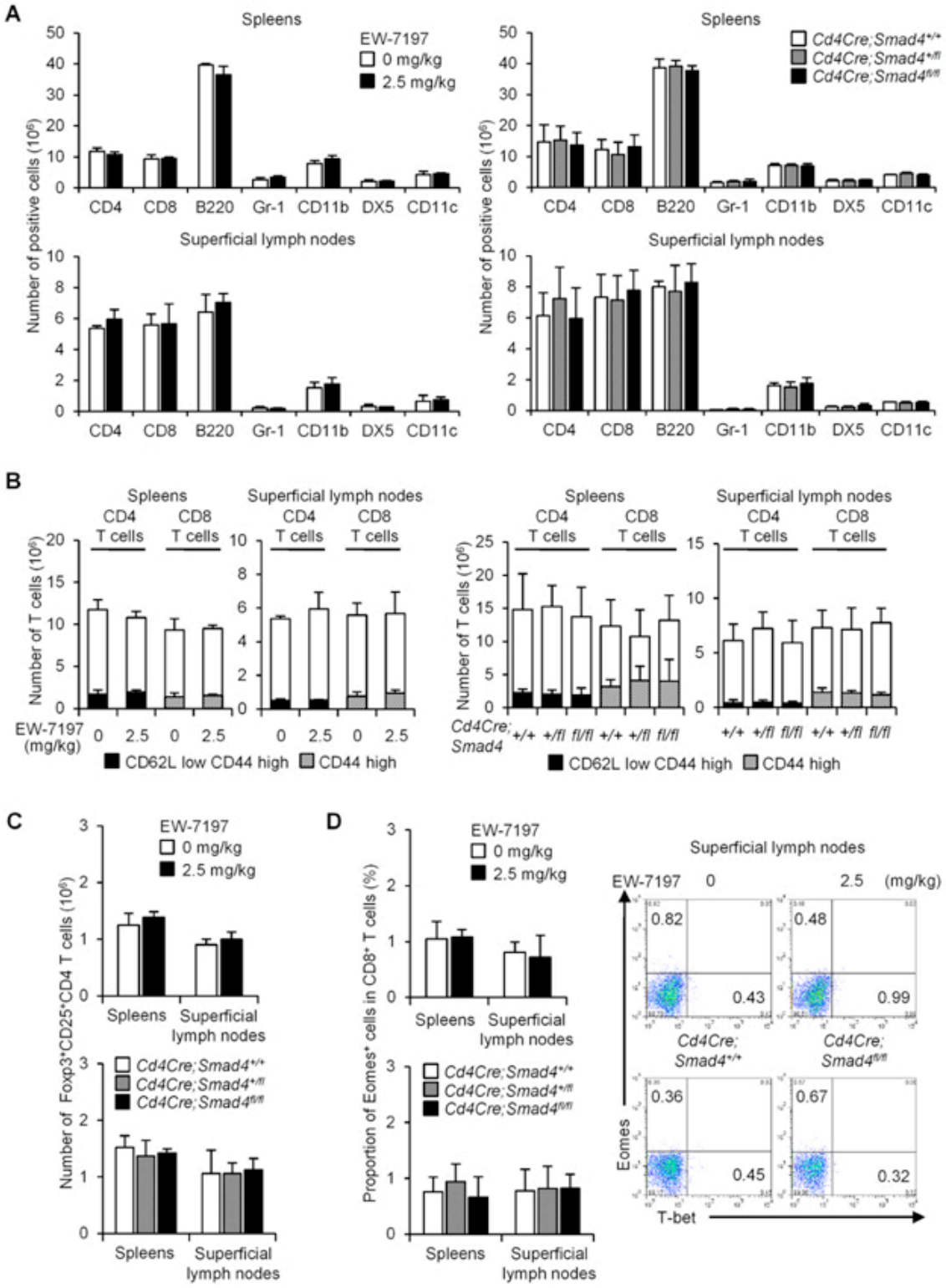

Figure 53 Normal immune homeostasis by long-term systemic administration of EW-7197 or T cell-specific Smad4 deletion.

Immune cell populations in the spleens and superficial LNs of C57BL/6 mice treated with vehicle or

vehicle containing EW-7197 (2.5 mg/kg daily) for 8 weeks (n = 5/group), *Cd4Cre;Smad4*$^{+/+}$, *Cd4Cre;Smad4*$^{+/fl}$ and *Cd4Cre;Smad4*$^{fl/fl}$ mice (n = 15/genotype) at 16 weeks of age were analyzed by flowcytometry. Graphs show mean + SEM. No statistical significance was observed by 2-tailed unpaired Student's *t* test. **(a-c)** Graphs show the cell numbers of immune cell subsets, naïve/memory CD4$^+$/CD8$^+$ T cells, and Foxp3$^+$CD25$^+$CD4$^+$ cells in the spleens and superficial LNs determined by flowcytometry. **(d)** Graph shows the % of Eomes$^+$ in CD8$^+$ gate. Representative dot plots show the expression of Eomes and T-bet in CD8$^+$ gate.

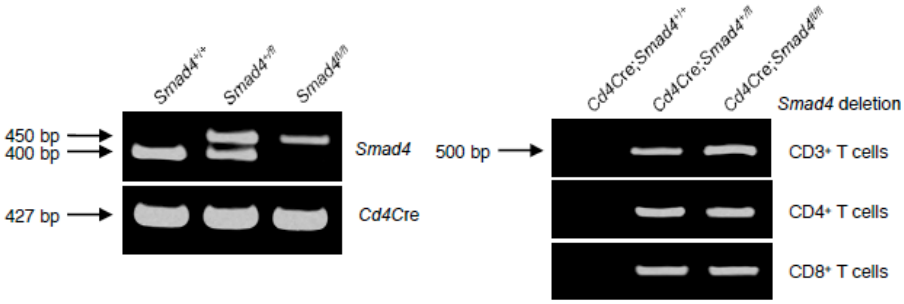

Figure 54 T cell-specific Smad4 deletion.

Genomic DNA was obtained from CD3$^+$ T cells, CD4$^+$ T cells, and CD8$^+$ T cells sorted by MACS from the spleens and superficial LNs of *Cd4Cre;Smad4*$^{+/+}$, *Cd4Cre;Smad4*$^{+/fl}$, and *Cd4Cre;Smad4*$^{fl/fl}$ mice. Deletion of the *Smad4* gene was confirmed by PCR by the primers reported in the references (Kim et al, 2006; Lee et al, 2001; Yang et al, 1999).

TGF-β suppresses Eomes via Smad4 and Smad3 in $CD8^+$ T cells

I examined the effect of Smad4 deficiency on the expression of IFN-γ, T-bet, and Eomes in $CD8^+$ T cells stimulated with anti-CD3 and anti-CD28 antibodies in vitro. Consistent with the in vivo data, *Smad4*$^{-/-}$ $CD8^+$ T cells expressed significantly higher levels of Eomes than those in *Smad4*$^{+/+}$ $CD8^+$ T cells (**Fig. 55a**). TGF-β1 (5 ng/ml) completely suppressed Eomes in *Smad4*$^{+/+}$ $CD8^+$ T cells, whereas the suppressive effect of TGF-β1 on Eomes was partially impaired in *Smad4*$^{-/-}$ $CD8^+$ T cells (**Fig. 55a**). However, TGF-β1 and Smad4 deficiency had only a slight effect on T-bet in $CD8^+$ T cells (**Fig. 55b**). Stimulation with phorbol-12-myristate-13-acetate (PMA) and ionomycin showed the same trend (**Fig. 56**).

I activated $CD8^+$ T cells from *Cd4Cre;Smad2*$^{+/+}$/*Cd4Cre;Smad2*$^{fl/fl}$ or *Smad3*$^{+/+}$/*Smad3*$^{-/-}$ mice in vitro to examine which R-Smad was responsible for Smad4-mediated suppression of Eomes. Eomes$^+$ cells increased significantly in the absence of Smad3, but not Smad2 (**Fig. 55c**). Deficiency of Smad3 showed the intermediate effect between deficiency of Smad2 and Smad4 on the increase of Eomes$^+$ cells.

I examined the effects of Smad deficiency on mRNA expression of granzyme B and FasL in $CD8^+$ T cells because Eomes upregulates these cytolytic molecules (Pearce et al, 2003). Consistent with the in vivo expression patterns, Eomes, granzyme B, and FasL mRNA levels in *Smad4*$^{-/-}$ $CD8^+$ T cells were significantly higher than those in *Smad4*$^{+/+}$ $CD8^+$ T cells, whereas T-bet and IFN-γ mRNA levels in *Smad4*$^{-/-}$ $CD8^+$ T cells were similar to those in *Smad4*$^{+/+}$ $CD8^+$ T cells (**Fig. 55d**). Eomes, granzyme B, and FasL mRNA levels were unaltered in *Smad2*$^{-/-}$ $CD8^+$ T cells, whereas those in *Smad3*$^{-/-}$ $CD8^+$ T cells were intermediate between *Smad4*$^{-/-}$ and *Smad2*$^{-/-}$ $CD8^+$ T cells (**Fig. 55d**).

Effector CTL differentiation occurs in two sequential phases, early induction of T-bet and late induction of Eomes (Cruz-Guilloty et al, 2009). Smad4 deficiency did not affect T-bet mRNA, which peaked at 12 h (**Fig 55e**). By contrast, late induction of Eomes (48, 72 h), granzyme B and FasL mRNA (72 h) was further upregulated in *Smad4*$^{-/-}$ $CD8^+$ T cells (**Fig. 55e**). Thus, TGF-β signaling through Smad4 does not affect T-bet even at the early phase. Taken together, TGF-β signaling through Smad4 and Smad3, but not Smad2, suppresses Eomes and the cytolytic molecules.

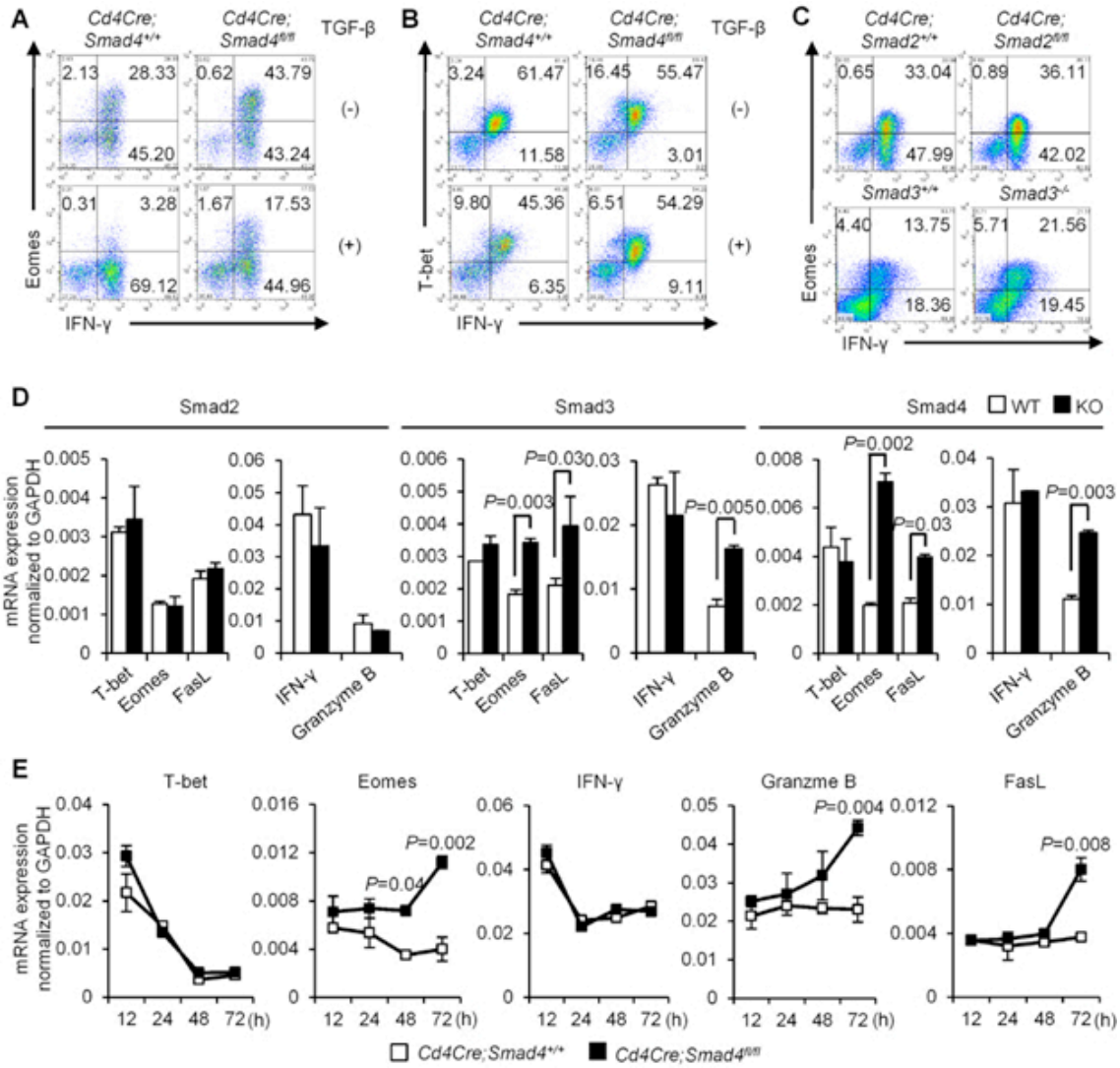

Figure 55 TGF-β signaling through Smad4 and Smad3 suppresses Eomes and the cytolytic molecules in CD8$^+$ T cells.

CD8$^+$ cells from the indicated mice were stimulated with anti-CD3/CD28 with or without TGF-β1 for 3 days. Data are shown as mean ± or + SEM. *P* values were calculated by 2-tailed unpaired Student's *t* test. **(a-c)** Representative dot plots show Eomes/IFN-γ, T-bet/IFN-γ in CD8$^+$ cells from *Cd4Cre;Smad4*$^{+/+}$/*Cd4Cre;Smad4*$^{fl/fl}$ mice and Eomes/IFN-γ in CD8$^+$ cells from *Cd4Cre;Smad2*$^{+/+}$/*Cd4Cre;Smad2*$^{fl/fl}$, and *Smad3*$^{+/+}$/*Smad3*$^{-/-}$ mice (*n* = 5-7/genotype). **(d,e)** qPCR analyses (*n* = 5/genotype) for T-bet, Eomes, IFN-γ, granzyme B, and FasL mRNA levels in CD8$^+$ cells from *Cd4Cre;Smad4*$^{fl/fl}$/*Cd4Cre;Smad2*$^{fl/fl}$/*Smad3*$^{-/-}$/control mice at 72 h and *Cd4Cre;Smad4*$^{+/+}$/*Cd4Cre;Smad4*$^{fl/fl}$ mice at the indicated time points.

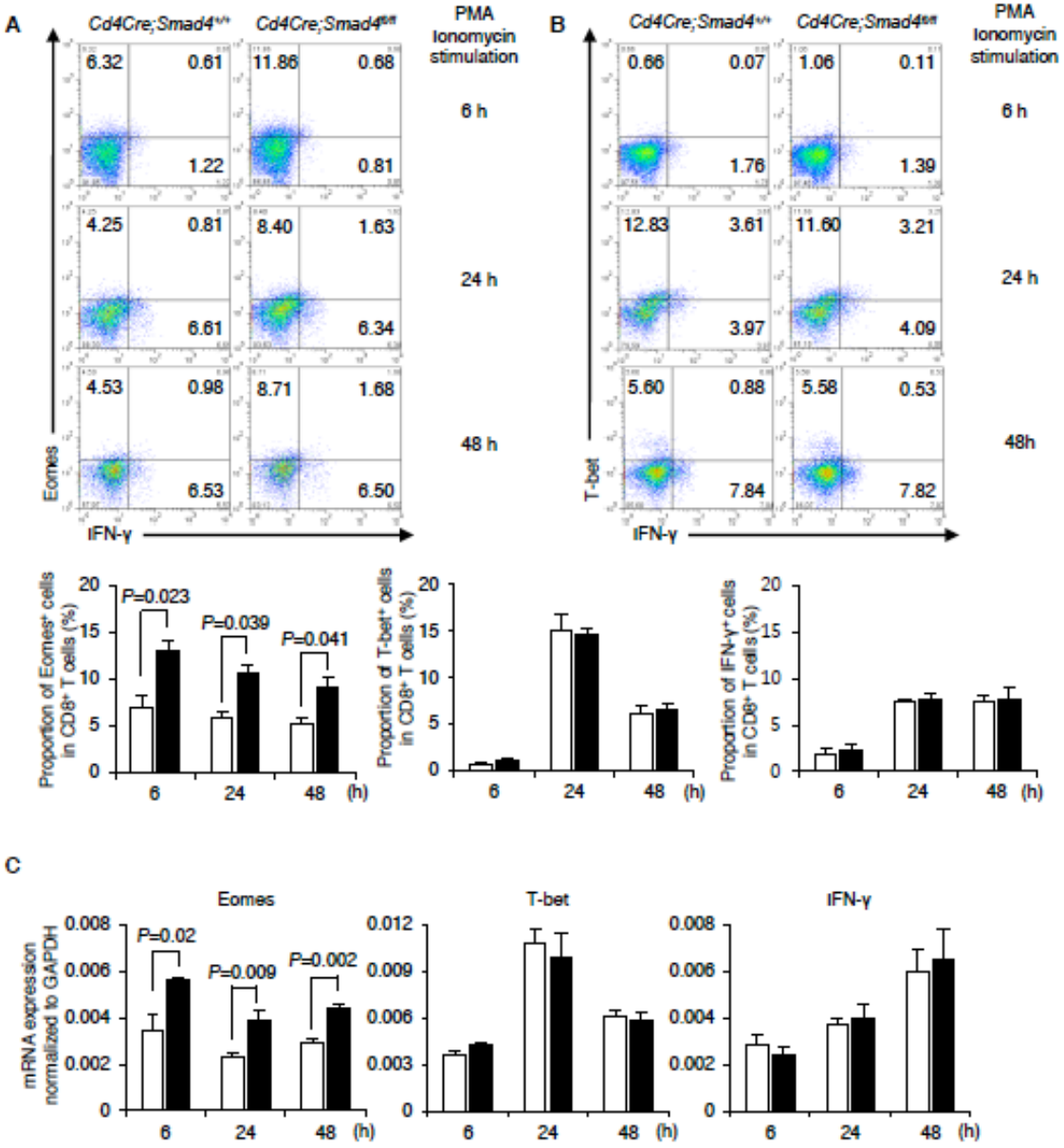

Figure 56 Effect of Smad4 on PMA/ionomycin-stimulated CD8$^+$ T cells.

CD8$^+$ cells from the indicated mice were stimulated with PMA and ionomycin for 3 days. **(a,b)** Representative dot plots show Eomes/IFN-γ, T-bet/IFN-γ _in CD8$^+$ cells from *Cd4Cre;Smad4*$^{+/+}$ /*Cd4Cre;Smad4*$^{fl/fl}$ mice (n = 2/genotype). **(c)** qPCR analyses for Eomes, T-bet, and IFN-γ mRNA levels in CD8$^+$ cells from *Cd4Cre;Smad4*$^{+/+}$/*Cd4Cre;Smad4*$^{fl/fl}$ mice (n = 2/genotype).

Smad4 represses the *Eomes* gene in CD8$^+$ T cells

I next assessed the direct transcriptional regulation of the *Eomes* gene by Smads in CD8$^+$ T cells using luciferase assays. Smad4 inhibited Eomes-luc activity (-2.0 kb) in a dose dependent manner (**Fig. 57a**). Smad4 inhibited Eomes-luc activity to the same level as TGF-β1 (5 ng/ml), whereas Smad3 inhibited it to a lesser degree, and Smad2 was inactive (**Fig. 57b**). Smad2 reversed, whereas Smad3 further enhanced, the inhibitory effect of Smad4 on Eomes-luc activity (**Fig. 57b**). Thus, Smad4 is the main repressor and Smad3 is the corepressor of the *Eomes* gene.

To screen the Smad4 binding regions in the *Eomes* promoter, I generated serial truncated luciferase reporter constructs (**Fig. 57c**). Inhibition of luciferase activity by Smad4 was abolished in a -0.37 kb reporter construct, whereas a -0.7 kb construct remained susceptible to Smad4 inhibition (**Fig. 57c**), indicating that the Smad4 binding sites are located between -0.37 kb and -0.7 kb. Screening Smad-binding sequence, CAGAC (Massague et al, 2005) by ChIP showed that Smad4 bound to (-680 to -499) and (-538 to -321) in the *Eomes* proximal promoter (**Fig. 57d**). Specificity of Smad4 pull-down was confirmed by completely abolished enrichment at these sites in *Smad4*$^{-/-}$ CD8$^+$ T cells (**Fig. 57d**). Thus, Smad4 binds to the proximal promoter of the *Eomes* gene, thereby repressing its transcription in CD8$^+$ T cells.

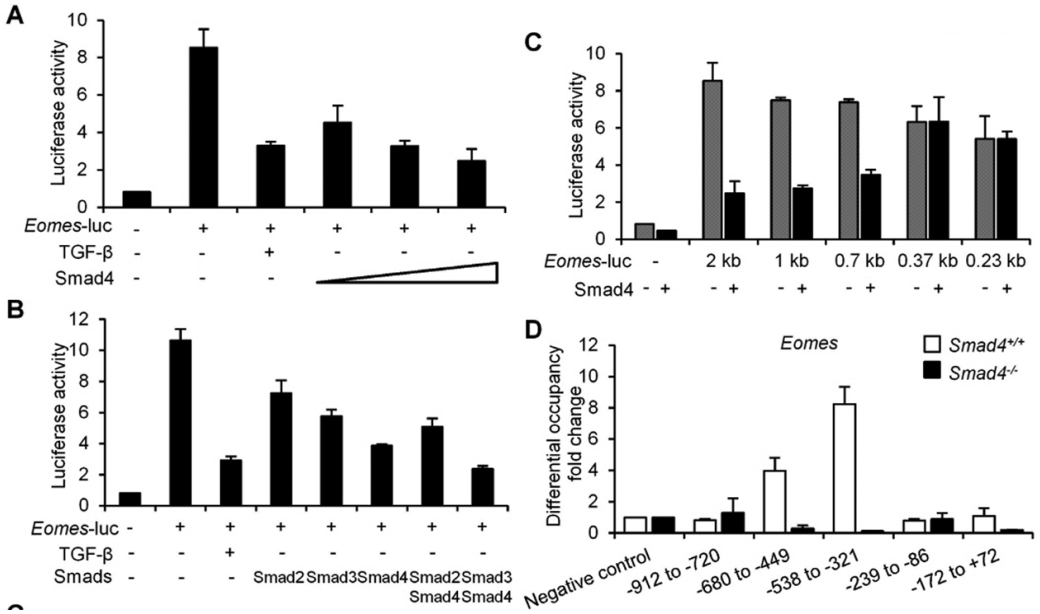

Figure 57 Smad4 binds to the *Eomes* promoter to repress transcription.

(a-c) C57BL/6 CD8$^+$ cells stimulated with anti-CD3/CD28 for 3 days were transfected with the *Eomes* luciferase reporter construct with various dosages of Smad4, Smad2, Smad3, and Smad4, or the various truncated *Eomes* luciferase reporter constructs with or without Smad4. TGF-β1 was treated as a control.

(d) CD8$^+$ cells from *Cd4Cre;Smad4*$^{+/+}$ and *Cd4Cre;Smad4*$^{fl/fl}$ mice were stimulated with anti-CD3/CD28 for 3 days, lysed, and immunoprecipitated with either anti-Smad4 or rabbit IgG. Bound DNA was measured by qPCR using primers specific to the *Eomes* promoter. Graphs show mean + SEM (n = 3). Differential occupancy fold changes from four independent experiments are shown.

Summary

Among TGF-β antagonisms, ALK5 inhibition induced ubiquitin-mediated degradation of Smad4 in $CD8^+$ T cells in addition to the direct inhibition of R-Smad phosphorylation to enhance anti-melanoma CTL responses through derepressing Eomes (**Fig. 58**).

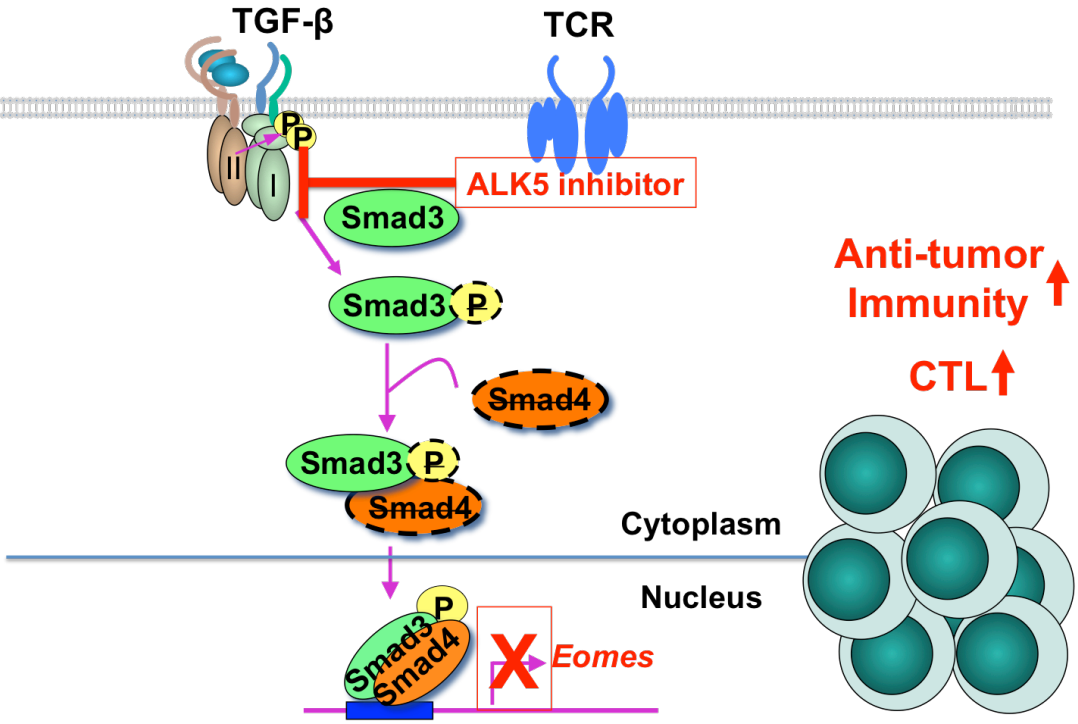

Figure 58 ALK5 Inhibition suppresses melanoma by inducing ubiquitin degradation of Smad4, thereby derepressing anti-tumor CTL activity.

Discussion

It has been well documented that systemic TGF-β antagonism mainly targets $CD8^+$ T cells in cancer (Nam et al, 2008) and selective blockade of TGF-β signaling in pan T cells or $CD8^+$ T cells is sufficient to eradicate tumors (Donkor et al, 2011; Gorelik et al, 2001; Zhang et al, 2005). Meanwhile, the precise molecular mechanisms whereby TGF-β antagonists enhance T cell-mediated anti-tumor immunity remain unknown. Here, I show that ALK5 inhibition by LY-2157299 and a novel ALK5 inhibitor, EW-7197 induced ubiquitin-mediated degradation of Smad4 protein in immune cells, most profoundly in $CD8^+$ T cells. However, pharmacologic ALK5 inhibition did not affect Smad4 protein in melanoma cells, although cell-autonomous TGF-β antagonism affects melanoma progression (Javelaud et al, 2005). TGF-β signaling pathway is controlled by ubiquitin protein modification (De Boeck et al, 2012; Izzi et al, 2004). Various E3 Ub ligases, such as Smurfs, WWP1, NEDD4-2, CHIP, and SCF target Smad4 for degradation to negatively regulate TGF-β signaling (Li et al, 2004; Moren et al, 2005; Wan et al, 2004). Jab1 antagonizes TGF-β function by inducing uniquitin-mediated degradation of Smad4 (Wan M et al, 2002). Although R-Smads are also controlled by ubiquitin-mediated degradation (De Boeck et al, 2012; Izzi et al, 2004), ALK5 inhibitors did not reduce R-Smads. Ubiquitnation of proteins by E3 ligases has emerged as an indispensable signaling pathway that regulates T-cell tolerance (Paolino et al, 2009). I investigated the possible involvement of Smurf, because IL-7 modulates TGF-β signaling via Smurf 2 activity in $CD8^+$ T cells (Pellegrini et al, 2009). However, Smurf1/2 were found to be irrelevant to Smad4 degradation by ALK5 inhibition in $CD8^+$ T cells (**Fig. 44**). Future studies are required for elucidating precise mechanisms whereby ALK5 inhibition induces ubiquitin-mediated degradation of Smad4 specifically in $CD8^+$ T cells.

EW-7197 and T cell-specific Smad4 gene targeting enhanced anti-tumor CTL responses with specific upregulation of Eomes in melanoma-bearing mice. $CD8^+$ T cells lacking the *Smad2/3/4* genes and the promoter analyses showed that Smad4 was the main repressor of the *Eomes* gene. As reported that Smad2 and Smad3 had distinct regulatory effects in epithelial cells and Th17 cells despite of their high homology (Brown et al, 2007; Martinez et al, 2009; Martinez et al, 2010), Smad3, but not Smad2 had an additive effect on transcriptional repression of Eomes by Smad4. By contrast, it has been reported that TGF-β suppresses Eomes via Smad2/3-independent, JNK-dependent signaling in Th17 induction (Ichiyama et al, 2011; Takimoto et al, 2010). Discrepancy between their reports and my study might be due to several reasons: TGF-β signaling pathways to suppress Eomes might be different between $CD4^+$ and $CD8^+$ T cell effector subsets, Smad4 was not investigated in their reports, they used T cells from *LckCreSmad2*$^{fl/fl}$*Smad3*$^{-/-}$ (Smad2/3-DKO) or *LckCreSmad2*$^{fl/fl}$*Smad3*$^{+/-}$ (Smad2cKO/Smad3hetero) mice, so that Smad4 alone or Smad4 and haploid expression of Smad3 could still transduce TGF-β signaling to repress the *Eome*s gene according to my findings (**Fig. 57a and b**). They speculated JNK-dependent, Smad2/3-independent pathway from the similar attenuating effect of ALK5 inhibitor, SB431542 and JNK inhibitor, SP600125 on Eomes repression in T cells stimulated with TCR and TGF-β. However,

specificity of ALK5 inhibitors for Smad-mediated TGF-β signaling pathway (Akhurst & Hata, 2012; Flavell et al, 2010; Hawinkels et al, 2011; Jin et al, 2011) and cooperation of Smad3 and Smad4 with c-Jun/c-Fos to mediate TGF-β-induced transcription (Zhang et al, 1998) suggest that both Smad3/4 and JNK pathways are involved in TGF-β-induced Eomes suppression.

Although TGF-β suppresses the cytolytic genes and IFN-γ by a mechanism involving R-Smads and ATF1 (Thomas et al, 2005) and Eomes as well as IFN-γ and cytolytic molecules are regulated by Runx3 (Cruz-Guilloty et al, 2009), Smad4 did not regulate IFN-γ production by $CD8^+$ T cells in my model. Because Runx3 is known to cooperate with Smad3/4 to regulate target genes (Pardali et al, 2000; Zhang et al, 2000), Smad4 might be required for Runx3 to regulate IFN-γ, but not Eomes and cytolytic molecules. Recent findings revealed the melanoma-promoting effects of IFN-γ (Cho et al, 2011; Zaidi et al, 2011). Thus, the ability to upregulate CTL functions without affecting IFN-γ would prove safety and efficacy of ALK5 inhibition for anti-melanoma therapy. However, cell-specific regulatory mechanisms of IFN-γ and T-bet by TGF-β remain to be determined because TGF-β suppresses IFN-γ and T-bet via MAPK-dependent, Smad3-independent signaling in $CD4^+$ T cells (Park et al, 2007), whereas TGF-β suppresses IFN-γ and T-bet via Smad2/3/4-mediated signaling in NK cells (Tinoco et al, 2009).

Efficacy of ALK5 inhibition on a relatively immunogenic B16 melanoma model depends fully on $CD8^+$ T cells because deletion of $CD8^+$ T cells resulted in 100% loss in the efficacy of EW-7197 on tumor progression (**Fig. 51b and e**). Although NK cell deletion showed partial reduction in the efficacy of EW-7197 (**Fig. 51d and e**), ALK5 inhibition did not upregulate Eomes in NK cells (data not shown). In a relatively non-immunogenic 4T1 model, anti-TGF-β antibodies suppress metastasis via cooperative effects on multiple cellular components: $CD8^+$ T cells, NK cells, and tumor cells (Nam et al, 2008). Therefore, immunogenicity of tumors is presumably the crucial factor to affect the potency of TGF-β antagonism on the specific cellular targets in anti-tumor therapy; nevertheless enhancement of $CD8^+$ T-cell mediated anti-tumor immune response is the main outcome of TGF-β antagonism even in the non-immunogenic tumor.

TGF-β also regulates effector $CD4^+$ T cell subsets (Li et al, 2006). However, downregulation of Smad4 by neither ALK5 inhibition nor T cell-specific gene targeting affected any $CD4^+$ T cell subsets in melanoma-bearing mice. Although TGF-β inhibits T-bet (Park et al, 2007) and Eomes (Narayanan et al, 2010) in Th1 cells, Smad4 downregulation had no effect on T-bet and Eomes in $CD4^+$ T cells. Similarly with my model, systemic TGF-β antagonism by IN-1130, one of the prototype ALK5 inhibitors in the same structural family as EW-7197 ameliorates experimental autoimmune encephalomyelitis by local actions without affecting systemic peripheral immune reactions including the generation of Th17 (Luo et al, 2007). Concerning Tregs, one of the major suppressors of anti-tumor immune surveillance (Flavell et al, 2010), Smad4-independent development of Tregs in my model and Smad2/3-independent development of nTregs in vivo (Gu et al, 2012) indicate that Treg development is Smad-independent. Thus, systemic TGF-β antagonism seems to target the disease-specific major pathogenic immune effector cells in

inflammatory lesions without affecting systemic immune homeostasis. Further investigation is required to determine the distinct targets of systemic TGF-β antagonism in various diseases.

One major concern for pharmacologic Smad4 downregulation is the possibility of the gastrointestinal inflammation and spontaneous carcinogenesis that was observed in mice in which Smad4 was targeted in T cell-specific and systemic inducible routes (Hahn et al, 2011; Karlsson et al, 2007; Kim et al, 2006). However, T cell-specific Smad4 deletion by *Cd4Cre* recombinase transgene with C57BL/6 background showed a normal phenotype at least by 6 months of age in my SPF facilities. Moreover, even the complete Smad4 knockout in T cells took time to develop carcinogenesis (Hahn et al, 2011; Kim et al, 2006). Considering the short in vivo half-life of EW-7197 and maintenance of normal immune homeostasis by lifetime exposure to a soluble TGF-β antagonist (Yang et al, 2002), the risk of gastrointestinal inflammation and carcinogenesis by temporal or intermittent prescription of EW-7197 is expected to be low.

Several ALK5 inhibitors are currently at pre-clinical and clinical stages for various cancers including melanoma (Akhurst & Hata, 2012; Flavell et al, 2008; Hawinkels et al, 2011; Mohammad et al, 2011). Because orally administered EW-7197 was more efficacious than LY-2157299 (75 mg/kg bid) against melanoma at a dose as low as 2.5 mg/kg daily, EW-7197 is the good candidate as the next generation ALK5 inhibitor for anti-melanoma therapy.

Conclusion

Immune system is existed for protecting our body against diseases and disorders from enemies. It is regulated by many kinds of factors such as cytokine and chemokine. Among them, TGF-β has been characterized as a critical immune regulatory cytokine. In my doctoral dissertation, I report the novel TGF-β signaling mechanisms for Th17 differentiation in rheumatoid arthritis and for suppressing CTL responses in melanoma. First, I found the novel dynamic signaling networks of R-SMADs-STAT3-ERK in arthritogenic Th17 differentiation, which has revised the classical linear signaling cascades (Levy ED et al, 2010). Second, systemic ALK5 inhibition has a potent therapeutic efficacy against melanoma by inducing the ubiquitin-mediated degradation of Smad4, thereby relieving suppressive effect of Smad3/Smad4-mediated TGF-β signaling on Eomes in CTLs. These findings suggest that SMAD-mediated TGF-β signaling orchestrate effector T cell development and function in cell-type-specific manners.

References

Akhurst RJ, Hata A (2012) Targeting the TGFbeta signalling pathway in disease. Nat Rev Drug Discov 11**:** 790-811.

Bierie B, Moses HL (2006) Tumour microenvironment: TGFbeta: the molecular Jekyll and Hyde of cancer. Nat Rev Cancer 6**:** 506-520

Bonyadi M, Rusholme SA, Cousins FM, Su HC, Biron CA, Farrall M, Akhurst RJ (1997) Mapping of a major genetic modifier of embryonic lethality in TGF beta 1 knockout mice. Nature genetics 15: 207-11

Brown KA, Pietenpol JA, Moses HL (2007) A tale of two proteins: differential roles and regulation of Smad2 and Smad3 in TGF-beta signaling. J Cell Biochem 101**:** 9-33

Callahan JF, Burgess JL, Fornwald JA, Gaster LM, Harling JD, Harrington FP, Heer J, Kwon C, Lehr R, Mathur A et al (2002) Identification of novel inhibitors of the transforming growth factor beta1 (TGF-beta1) type 1 receptor (ALK5). J Med Chem 45**:** 999-1001

Calvo-Aller E, Baselga J, Glatt S, Claverly A, Lahn M, Arteaga CL, et al (2008) First human dose escalation study in patients with metastatic malignancies to determine safety and pharmacokinetics of LY2157299, a small molecule inhibitor of the transforming growth factor-β receptor I kinase. J Clin Oncol. 26: (suppl; abstr 14554)

Campbell IK, Hamilton JA, Wicks IP (2000) Collagen-induced arthritis in C57BL/6 (H-2b) mice: new insights into an important disease model of rheumatoid arthritis. European journal of immunology 30: 1568-75

Chang X, Liu F, Wang X, Lin A, Zhao H, Su B (2011) The kinases MEKK2 and MEKK3 regulate transforming growth factor-beta-mediated helper T cell differentiation. Immunity 34: 201-12

Cho HI, Lee YR, Celis E (2011) Interferon gamma limits the effectiveness of melanoma peptide vaccines. Blood 117**:** 135-144

Chung CD, Liao J, Liu B, Rao X, Jay P, Berta P, Shuai K (1997) Specific inhibition of Stat3 signal transduction by PIAS3. Science 278: 1803-5

Ciofani M, Madar A, Galan C, Sellars M, Mace K, Pauli F, Agarwal A, Huang W, Parkurst CN, Muratet M, Newberry KM, Meadows S, Greenfield A, Yang Y, Jain P, Kirigin FK, Birchmeier C, Wagner EF, Murphy KM, Myers RM et al. (2012) A validated regulatory network for Th17 cell specification. Cell 151: 289-303

Cruz-Guilloty F, Pipkin ME, Djuretic IM, Levanon D, Lotem J, Lichtenheld MG, Groner Y, Rao A (2009) Runx3 and T-box proteins cooperate to establish the transcriptional program of effector CTLs. J Exp Med 206**:** 51-59

DaCosta Byfield S, Major C, Laping NJ, Roberts AB (2004) SB-505124 is a selective inhibitor of transforming growth factor-beta type I receptors ALK4, ALK5, and ALK7. Molecular pharmacology 65: 744-52

Dahle O, Kumar A, Kuehn MR (2010) Nodal signaling recruits the histone demethylase Jmjd3 to counteract polycomb-mediated repression at target genes. Science signaling 3: ra48

De Boeck M, ten Dijke P (2012) Key role for ubiquitin protein modification in TGFbeta signal transduction. Ups J Med Sci 117**:** 153-165

Dong C, Davis RJ, Flavell RA (2002) MAP kinases in the immune response. Annual review of immunology 20: 55-72

Donkor MK, Sarkar A, Savage PA, Franklin RA, Johnson LK, Jungbluth AA, Allison JP, Li MO (2011) T cell surveillance of oncogene-induced prostate cancer is impeded by T cell-derived TGF-beta1 cytokine. Immunity 35**:** 123-134

Dupont S, Mamidi A, Cordenonsi M, Montagner M, Zacchigna L, Adorno M, Martello G, Stinchfield MJ, Soligo S, Morsut L et al (2009) FAM/USP9x, a deubiquitinating enzyme essential for TGFbeta signaling, controls Smad4 monoubiquitination. Cell 136**:** 123-135

Durant L, Watford WT, Ramos HL, Laurence A, Vahedi G, Wei L, Takahashi H, Sun HW, Kanno Y, Powrie F, O'Shea JJ (2010) Diverse targets of the transcription factor STAT3 contribute to T cell pathogenicity and homeostasis. Immunity 32: 605-15

Flavell RA, Sanjabi S, Wrzesinski SH, Licona-Limon P (2010) The polarization of immune cells in the tumour environment by TGFbeta. Nat Rev Immunol 10**:** 554-567

Gaarenstroom T, Hill CS (2014) TGF-beta signaling to chromatin: How Smads regulate transcription during self-renewal and differentiation. Seminars in cell & developmental biology 32C: 107-118

Ghoreschi K, Laurence A, Yang XP, Tato CM, McGeachy MJ, Konkel JE, Ramos HL, Wei L, Davidson TS, Bouladoux N, Grainger JR, Chen Q, Kanno Y, Watford WT, Sun HW, Eberl G, Shevach EM, Belkaid Y, Cua DJ, Chen W et al. (2010) Generation of pathogenic T(H)17 cells in the absence of TGF-beta signalling. Nature 467: 967-71

Glimcher LH, Townsend MJ, Sullivan BM, Lord GM (2004) Recent developments in the transcriptional regulation of cytolytic effector cells. Nat Rev Immunol 4**:** 900-911

Gorelik L, Flavell RA (2001) Immune-mediated eradication of tumors through the blockade of transforming growth factor-beta signaling in T cells. Nat Med 7**:** 1118-1122

Gu AD, Wang Y, Lin L, Zhang SS, Wan YY (2012) Requirements of transcription factor Smad-dependent and -independent TGF-beta signaling to control discrete T-cell functions. Proc Natl Acad Sci U S A 109**:** 905-910

Hasan M, Neumann B, Haupeltshofer S, Stahlke S, Fantini MC, Angstwurm K, Bodahn U, Kleiter I (2015) Activation of TGF-beta-induced non-Smad signaling pathways during Th17 differentiation. Immunol Cell Biol 93: 662-72

Hahn JN, Falck VG, Jirik FR (2011) Smad4 deficiency in T cells leads to the Th17-associated development of premalignant gastroduodenal lesions in mice. J Clin Invest 121**:** 4030-4042

Hawinkels LJ, Ten Dijke P (2011) Exploring anti-TGF-beta therapies in cancer and fibrosis. Growth Factors 29**:** 140-152

Heldin CH, Moustakas A (2012) Role of Smads in TGFbeta signaling. Cell and tissue research 347: 21-36

Hirahara K, Ghoreschi K, Laurence A, Yang XP, Kanno Y, O'Shea JJ (2010) Signal transduction pathways and transcriptional regulation in Th17 cell differentiation. Cytokine & growth factor reviews 21: 425-34

Ichiyama K, Sekiya T, Inoue N, Tamiya T, Kashiwagi I, Kimura A, Morita R, Muto G, Shichita T,

Takahashi R et al (2011) Transcription factor Smad-independent T helper 17 cell induction by transforming-growth factor-beta is mediated by suppression of eomesodermin. Immunity 34**:** 741-754

Intlekofer AM, Takemoto N, Wherry EJ, Longworth SA, Northrup JT, Palanivel VR, Mullen AC, Gasink CR, Kaech SM, Miller JD et al (2005) Effector and memory CD8+ T cell fate coupled by T-bet and eomesodermin. Nat Immunol 6**:** 1236-1244

Izzi L, Attisano L (2004) Regulation of the TGFbeta signalling pathway by ubiquitin-mediated degradation. Oncogene 23**:** 2071-2078

Isogaya K, Koinuma D, Tsutsumi S, Saito RA, Miyazawa K, Aburatani H, Miyazono K (2014) A Smad3 and TTF-1/NKX2-1 complex regulates Smad4-independent gene expression. Cell research 24: 994-1008

Iwakura Y, Ishigame H, Saijo S, Nakae S (2011) Functional specialization of interleukin-17 family members. Immunity 34: 149-62

Janknecht R, Wells NJ, Hunter T (1998) TGF-beta-stimulated cooperation of smad proteins with the coactivators CBP/p300. Genes & development 12: 2114-9

Javelaud D, Alexaki VI, Mauviel A (2008) Transforming growth factor-beta in cutaneous melanoma. Pigment Cell Melanoma Res 21**:** 123-132

Javelaud D, Delmas V, Moller M, Sextius P, Andre J, Menashi S, Larue L, Mauviel A (2005) Stable overexpression of Smad7 in human melanoma cells inhibits their tumorigenicity in vitro and in vivo. Oncogene 24**:** 7624-7629

Jin CH, Krishnaiah M, Sreenu D, Subrahmanyam VB, Rao KS, Mohan AV, et al (2011) Synthesis and biological evaluation of 1-substituted-3-(6-methylpyridin-2-yl)-4-([1,2,4]triazolo[1,5-a]pyridin-6-yl)pyra zoles as transforming growth factor-beta type 1 receptor kinase inhibitors. Bioorg Med Chem Lett. 21:6049-53

Jin CH, Krishnaiah M, Sreenu D, Subrahmanyam VB, Rao KS, Lee HJ, Park SJ, Park HJ, Lee K, Sheen YY, Kim DK (2014) Discovery of
N-((4-([1,2,4]triazolo[1,5-a]pyridin-6-yl)-5-(6-methylpyridin-2-yl)-1H-imidazol-2
-yl)methyl)-2-fluoroaniline (EW-7197): a highly potent, selective, and orally bioavailable inhibitor of

TGF-beta type I receptor kinase as cancer immunotherapeutic/antifibrotic agent. Journal of medicinal chemistry 57: 4213-38

Karlsson G, Blank U, Moody JL, Ehinger M, Singbrant S, Deng CX, Karlsson S (2007) Smad4 is critical for self-renewal of hematopoietic stem cells. J Exp Med 204**:** 467-474

Kawabata M, Imamura T, Inoue H, Hanai J, Nishihara A, Hanyu A, Takase M, Ishidou Y, Udagawa Y, Oeda E, Goto D, Yagi K, Kato M, Miyazono K (1999) Intracellular signaling of the TGF-beta superfamily by Smad proteins. Annals of the New York Academy of Sciences 886: 73-82

Kim BG, Li C, Qiao W, Mamura M, Kasprzak B, Anver M, Wolfraim L, Hong S, Mushinski E, Potter M et al (2006) Smad4 signalling in T cells is required for suppression of gastrointestinal cancer. Nature 441**:** 1015-1019

Kimura A, Kishimoto T (2010) IL-6: regulator of Treg/Th17 balance. European journal of immunology 40: 1830-5

Kim DK, Sheen YY, Jin CH, Park CY, Sreenu D, Rao KS, et al (2011) Method of treating fibrosis, cancer and vascular injuries. U.S. Pat. Appl. Publ. US 2011/0319408 A1: p 8

Kirkwood JM, Tarhini AA, Panelli MC, Moschos SJ, Zarour HM, Butterfield LH, Gogas HJ (2008) Next generation of immunotherapy for melanoma. J Clin Oncol 26**:** 3445-3455

Korn T, Bettelli E, Oukka M, Kuchroo VK (2009) IL-17 and Th17 Cells. Annual review of immunology 27: 485-517

Kretzschmar M, Doody J, Timokhina I, Massague J (1999) A mechanism of repression of TGFbeta/ Smad signaling by oncogenic Ras. Genes & development 13: 804-16

Kuhn R, Schwenk F, Aguet M, Rajewsky K (1995) Inducible gene targeting in mice. Science 269: 1427-9

Laurence A, Tato CM, Davidson TS, Kanno Y, Chen Z, Yao Z, Blank RB, Meylan F, Siegel R, Hennighausen L, Shevach EM, O'Shea J J (2007) Interleukin-2 signaling via STAT5 constrains T helper 17 cell generation. Immunity 26: 371-81

Lazarevic V, Chen X, Shim JH, Hwang ES, Jang E, Bolm AN, Oukka M, Kuchroo VK, Glimcher LH (2011) T-bet represses T(H)17 differentiation by preventing Runx1-mediated activation of the gene encoding RORgammat. Nature immunology 12: 96-104

Lee PP, Fitzpatrick DR, Beard C, Jessup HK, Lehar S, Makar KW, Perez-Melgosa M, Sweetser MT, Schlissel MS, Nguyen S et al (2001) A critical role for Dnmt1 and DNA methylation in T cell development, function, and survival. Immunity 15**:** 763-774

Levy ED, Landry CR, Michnick SW (2010) Cell signaling. Signaling through cooperation. Science 328: 983-4

Lee YS, Park JS, Kim JH, Jung SM, Lee JY, Kim SJ, Park SH (2011) Smad6-specific recruitment of Smurf E3 ligases mediates TGF-β1-induced degradation of MyD88 in TLR4 signalling. Nat Commun 2:460.

Li L, Xin H, Xu X, Huang M, Zhang X, Chen Y, Zhang S, Fu XY, Chang Z (2004) CHIP mediates degradation of Smad proteins and potentially regulates Smad-induced transcription. Mol Cell Biol 24**:** 856-864

Li MO, Wan YY, Sanjabi S, Robertson AK, Flavell RA (2006) Transforming growth factor-beta regulation of immune responses. Annu Rev Immunol 24**:** 99-146

Liu H, Yao S, Dann SM, Qin H, Elson CO, Cong Y (2013) ERK differentially regulates Th17- and Treg-cell development and contributes to the pathogenesis of colitis. European journal of immunology 43: 1716-26

Liu Y, Festing MH, Hester M, Thompson JC, Weinstein M (2004) Generation of novel conditional and hypomorphic alleles of the Smad2 gene. Genesis 40**:** 118-123

Long J, Wang G, Matsuura I, He D, Liu F (2004) Activation of Smad transcriptional activity by protein inhibitor of activated STAT3 (PIAS3). Proceedings of the National Academy of Sciences of the United States of America 101: 99-104

Lu L, Wang J, Zhang F, Chai Y, Brand D, Wang X, Horwitz DA, Shi W, Zheng SG (2010) Role of SMAD and non-SMAD signals in the development of Th17 and regulatory T cells. Journal of immunology 184: 4295-306

Luo J, Ho PP, Buckwalter MS, Hsu T, Lee LY, Zhang H, Kim DK, Kim SJ, Gambhir SS, Steinman L et al (2007) Glia-dependent TGF-beta signaling, acting independently of the TH17 pathway, is critical for initiation of murine autoimmune encephalomyelitis. J Clin Invest 117**:** 3306-3315

Malhotra N, Robertson E, Kang J (2010) SMAD2 is essential for TGF beta-mediated Th17 cell generation. The Journal of biological chemistry 285: 29044-8

Manel N, Unutmaz D, Littman DR (2008) The differentiation of human T(H)-17 cells requires transforming growth factor-beta and induction of the nuclear receptor RORgammat. Nature immunology 9: 641-9

Martinez GJ, Zhang Z, Chung Y, Reynolds JM, Lin X, Jetten AM, Feng XH, Dong C (2009) Smad3 differentially regulates the induction of regulatory and inflammatory T cell differentiation. J Biol Chem 284**:** 35283-35286

Martinez GJ, Zhang Z, Reynolds JM, Tanaka S, Chung Y, Liu T, Robertson E, Lin X, Feng XH, Dong C (2010) Smad2 positively regulates the generation of Th17 cells. J Biol Chem 285**:** 29039-29043

Massague J (2003) Integration of Smad and MAPK pathways: a link and a linker revisited. Genes & development 17: 2993-7

Massague J (2012) TGFbeta signalling in context. Nature reviews Molecular cell biology 13: 616-30

Massague J, Seoane J, Wotton D (2005) Smad transcription factors. Genes Dev 19**:** 2783-2810

Matsuzaki K (2013) Smad phospho-isoforms direct context-dependent TGF-beta signaling. Cytokine & growth factor reviews 24: 385-99

Meisel M, Hermann-Kleiter N, Hinterleitner R, Gruber T, Wachowicz K, Pfeifhofer-Obermair C, Fresser F, Leitges M, Soldani C, Viola A, Kaminski S, Baier G (2013) The kinase PKCalpha selectively upregulates interleukin-17A during Th17 cell immune responses. Immunity 38: 41-52

Mohammad KS, Javelaud D, Fournier PG, Niewolna M, McKenna CR, Peng XH, Duong V, Dunn LK, Mauviel A, Guise TA (2011) TGF-beta-RI kinase inhibitor SD-208 reduces the development and

progression of melanoma bone metastases. Cancer Res 71**:** 175-184

Moren A, Imamura T, Miyazono K, Heldin CH, Moustakas A (2005) Degradation of the tumor suppressor Smad4 by WW and HECT domain ubiquitin ligases. J Biol Chem 280**:** 22115-22123.

Morikawa M, Koinuma D, Miyazono K, Heldin CH (2013) Genome-wide mechanisms of Smad binding. Oncogene 32: 1609-15

Mullen AC, Orlando DA, Newman JJ, Loven J, Kumar RM, Bilodeau S, Reddy J, Guenther MG, DeKoter RP, Young RA (2011) Master transcription factors determine cell-type-specific responses to TGF-beta signaling. Cell 147: 565-76

Nakae S, Nambu A, Sudo K, Iwakura Y (2003) Suppression of immune induction of collagen-induced arthritis in IL-17-deficient mice. Journal of immunology 171: 6173-7

Nakashima K, Yanagisawa M, Arakawa H, Kimura N, Hisatsune T, Kawabata M, Miyazono K, Taga T (1999) Synergistic signaling in fetal brain by STAT3-Smad1 complex bridged by p300. Science 284: 479-82

Nam JS, Terabe M, Mamura M, Kang MJ, Chae H, Stuelten C, Kohn E, Tang B, Sabzevari H, Anver MR et al (2008) An anti-transforming growth factor beta antibody suppresses metastasis via cooperative effects on multiple cell compartments. Cancer Res 68**:** 3835-3843

Narayanan S, Silva R, Peruzzi G, Alvarez Y, Simhadri VR, Debell K, Coligan JE, Borrego F (2010) Human Th1 cells that express CD300a are polyfunctional and after stimulation up-regulate the T-box transcription factor eomesodermin. PLoS One 5**:** e10636

Neurath MF, Finotto S (2011) IL-6 signaling in autoimmunity, chronic inflammation and inflammation-associated cancer. Cytokine & growth factor reviews 22: 83-9

Overwijk WW, Theoret MR, Finkelstein SE, Surman DR, de Jong LA, Vyth-Dreese FA, Dellemijn TA, Antony PA, Spiess PJ, Palmer DC et al (2003) Tumor regression and autoimmunity after reversal of a functionally tolerant state of self-reactive CD8+ T cells. J Exp Med 198**:** 569-580

Pardali E, Xie XQ, Tsapogas P, Itoh S, Arvanitidis K, Heldin CH, ten Dijke P, Grundström T, Sideras P (2000) Smad and AML proteins synergistically confer transforming growth factor beta1 responsiveness to human germ-line IgA genes. J Biol Chem 275: 3552-3560.

Paolino M, Penninger JM (2009) E3 ubiquitin ligases in T-cell tolerance. Eur J Immunol 39**:** 2337-2344

Park IK, Letterio JJ, Gorham JD (2007) TGF-beta 1 inhibition of IFN-gamma-induced signaling and Th1 gene expression in CD4+ T cells is Smad3 independent but MAP kinase dependent. Mol Immunol 44**:** 3283-3290

Pearce EL, Mullen AC, Martins GA, Krawczyk CM, Hutchins AS, Zediak VP, Banica M, DiCioccio CB, Gross DA, Mao CA et al (2003) Control of effector CD8+ T cell function by the transcription factor Eomesodermin. Science 302**:** 1041-1043

Pedroza-Gonzalez A, Xu K, Wu TC, Aspord C, Tindle S, Marches F, Gallegos M, Burton EC, Savino D, Hori T et al (2011) Thymic stromal lymphopoietin fosters human breast tumor growth by promoting type 2 inflammation. J Exp Med 208**:** 479-490

Pellegrini M, Calzascia T, Elford AR, Shahinian A, Lin AE, Dissanayake D, Dhanji S, Nguyen LT, Gronski MA, Morre M et al (2009) Adjuvant IL-7 antagonizes multiple cellular and molecular inhibitory networks to enhance immunotherapies. Nat Med 15: 528-536

Peng SL, Townsend MJ, Hecht JL, White IA, Glimcher LH (2004) T-bet regulates metastasis rate in a murine model of primary prostate cancer. Cancer Res 64**:** 452-455

Russell JH, Ley TJ (2002) Lymphocyte-mediated cytotoxicity. Annu Rev Immunol 20**:** 323-370

Sakuma M, Hatsushika K, Koyama K, Katoh R, Ando T, Watanabe Y, Wako M, Kanzaki M, Takano S, Sugiyama H, Hamada Y, Ogawa H, Okumura K, Nakao A (2007) TGF-beta type I receptor kinase inhibitor down-regulates rheumatoid synoviocytes and prevents the arthritis induced by type II collagen antibody. International immunology 19: 117-26

Schraml BU, Hildner K, Ise W, Lee WL, Smith WA, Solomon B, Sahota G, Sim J, Mukasa R, Cemerski S, Hatton RD, Stormo GD, Weaver CT, Russell JH, Murphy TL, Murphy KM (2009) The AP-1 transcription factor Batf controls T(H)17 differentiation. Nature 460: 405-9

Sekimoto G, Matsuzaki K, Yoshida K, Mori S, Murata M, Seki T, Matsui H, Fujisawa J, Okazaki K (2007) Reversible Smad-dependent signaling between tumor suppression and oncogenesis. Cancer research 67: 5090-6

Takimoto T, Wakabayashi Y, Sekiya T, Inoue N, Morita R, Ichiyama K, Takahashi R, Asakawa M, Muto G, et al (2010) Smad2 and Smad3 are redundantly essential for the TGF-beta-mediated regulation of regulatory T plasticity and Th1 development. J Immunol 185**:** 842-55

Thomas DA, Massague J (2005) TGF-beta directly targets cytotoxic T cell functions during tumor evasion of immune surveillance. Cancer Cell 8**:** 369-380

Thomson TM, Real FX, Murakami S, Cordon-Cardo C, Old LJ, Houghton AN (1988) Differentiation antigens of melanocytes and melanoma: analysis of melanosome and cell surface markers of human pigmented cells with monoclonal antibodies. J Invest Dermatol 90**:** 459-466

Tinoco R, Alcalde V, Yang Y, Sauer K, Zuniga EI (2009) Cell-intrinsic transforming growth factor-beta signaling mediates virus-specific CD8+ T cell deletion and viral persistence in vivo. Immunity 31**:** 145-157

Travis MA, Sheppard D (2014) TGF-beta activation and function in immunity. Annual review of immunology 32: 51-82

Rosloniec EF, Cremer M, Kang AH, Myers LK, Brand DD (2010) Collagen-induced arthritis. Current protocols in immunology / edited by John E Coligan [et al] Chapter 15: Unit 15 5 1-25

Ulloa L, Doody J, Massague J (1999) Inhibition of transforming growth factor-beta/SMAD signalling by the interferon-gamma/STAT pathway. Nature 397: 710-3

Veldhoen M, Hocking RJ, Atkins CJ, Locksley RM, Stockinger B (2006) TGFbeta in the context of an inflammatory cytokine milieu supports de novo differentiation of IL-17-producing T cells. Immunity 24: 179-89

Wan M, Cao X, Wu Y, Bai S, Wu L, Shi X, Wang N (2002) Jab1 antagonizes TGF-beta signaling by inducing Smad4 degradation. EMBO Rep 3**:** 171-176

Wan M, Tang Y, Tytler EM, Lu C, Jin B, Vickers SM, Yang L, Shi X, Cao X (2004) Smad4 protein stability is regulated by ubiquitin ligase SCF beta-TrCP1. J Biol Chem 279**:** 14484-14487

Watkins SK, Zhu Z, Watkins KE, Hurwitz AA (2012) Isolation of immune cells from primary tumors. J Vis Exp 64: e3952

Wrighton KH, Lin X, Feng XH (2009) Phospho-control of TGF-beta superfamily signaling. Cell research 19: 8-20

Xiao S, Jin H, Korn T, Liu SM, Oukka M, Lim B, Kuchroo VK (2008) Retinoic acid increases Foxp3+ regulatory T cells and inhibits development of Th17 cells by enhancing TGF-beta-driven Smad3 signaling and inhibiting IL-6 and IL-23 receptor expression. Journal of immunology 181: 2277-84

Yamamoto T, Matsuda T, Muraguchi A, Miyazono K, Kawabata M (2001) Cross-talk between IL-6 and TGF-beta signaling in hepatoma cells. FEBS letters 492: 247-53

Yang X, Chen L, Xu X, Li C, Huang C, Deng CX (2001) TGF-beta/Smad3 signals repress chondrocyte hypertrophic differentiation and are required for maintaining articular cartilage. The Journal of cell biology 153: 35-46

Yang X, Letterio JJ, Lechleider RJ, Chen L, Hayman R, Gu H, Roberts AB, Deng C (1999) Targeted disruption of SMAD3 results in impaired mucosal immunity and diminished T cell responsiveness to TGF-beta. EMBO J 18**:** 1280-1291

Yang XP, Ghoreschi K, Steward-Tharp SM, Rodriguez-Canales J, Zhu J, Grainger JR, Hirahara K, Sun HW, Wei L, Vahedi G, Kanno Y, O'Shea JJ, Laurence A (2011) Opposing regulation of the locus encoding IL-17 through direct, reciprocal actions of STAT3 and STAT5. Nature immunology 12: 247-54

Yang YA, Dukhanina O, Tang B, Mamura M, Letterio JJ, MacGregor J, Patel SC, Khozin S, Liu ZY, Green J et al (2002) Lifetime exposure to a soluble TGF-beta antagonist protects mice against metastasis without adverse side effects. J Clin Invest 109**:** 1607-1615

Yoon JH, Jung SM, Park SH, Kato M, Yamashita T, Lee IK, Sudo K, Nakae S, Han JS, Kim OH, Oh BC, Sumida T, Kuroda M, Ju JH, Jung KC, Park SH, Kim DK, Mamura M (2013) Activin receptor-like kinase5 inhibition suppresses mouse melanoma by ubiquitin degradation of Smad4, thereby derepressing eomesodermin in cytotoxic T lymphocytes. EMBO molecular medicine 5: 1720-3

Zaidi MR, Davis S, Noonan FP, Graff-Cherry C, Hawley TS, Walker RL, Feigenbaum L, Fuchs E, Lyakh L, Young HA et al (2011) Interferon-gamma links ultraviolet radiation to melanomagenesis in mice. Nature 469**:** 548-553

Zhang Q, Yang X, Pins M, Javonovic B, Kuzel T, Kim SJ, Parijs LV, Greenberg NM, Liu V, Guo Y et al (2005) Adoptive transfer of tumor-reactive transforming growth factor-beta-insensitive CD8+ T cells: eradication of autologous mouse prostate cancer. Cancer Res 65**:** 1761-1769

Zhang Y, Feng XH, Derynck R (1998) Smad3 and Smad4 cooperate with c-Jun/c-Fos to mediate TGF-beta-induced transcription. Nature 394: 909-913

Zhang Y, Derynck R (2000) Transcriptional regulation of the transforming growth factor-beta -inducible mouse germ line Ig alpha constant region gene by functional cooperation of Smad, CREB, and AML family members.J Biol Chem 275:16979-16985.

Zhu Y, Ju S, Chen E, Dai S, Li C, Morel P, Liu L, Zhang X, Lu B (2010) T-bet and eomesodermin are required for T cell-mediated antitumor immune responses. J Immunol 185**:** 3174-3183